OSMR SIGNALING INDUCES TAMP-SPECIFIC BBB DYSFUNCTION FOLLOWING AUTOIMMUNE-MEDIATED NEUTROPHIL RECRUITMENT

by

Travis Scott Wertz

A dissertation

submitted in partial fulfillment

of the requirements for the degree of

Doctor of Philosophy in Biomolecular Sciences

Boise State University

December 2021

BOISE STATE UNIVERSITY GRADUATE COLLEGE

DEFENSE COMMITTEE AND FINAL READING APPROVALS

of the dissertation submitted by

Travis Scott Wertz

Dissertation Title: OSMR Signaling Induces TAMP-Specific BBB Dysfunction Following Autoimmune-Mediated Neutrophil Recruitment

Date of Final Oral Examination: 05 November 2021

The following individuals read and discussed the dissertation submitted by student Travis Scott Wertz, and they evaluated the student's presentation and response to questions during the final oral examination. They found that the student passed the final oral examination.

Richard S. Beard Jr., Ph.D.	Co-Chair, Supervisory Committee
Cheryl L. Jorcyk, Ph.D.	Co-Chair, Supervisory Committee
Daniel Fologea, Ph.D.	Member, Supervisory Committee

The final reading approval of the dissertation was granted by Richard S. Beard Jr., Ph.D., and Cheryl L. Jorcyk, Ph.D., Co-Chairs of the Supervisory Committee. The dissertation was approved by the Graduate College.

DEDICATION

To my mom, Tammy Wertz. I'm glad I've made you proud.

ACKNOLEDGMENTS

It would be truly impossible to undertake such work without the support of countless people. First, gratitude to my mentor, Dr. Richard Beard, who encouraged not only scientific growth, but in growth in leadership; to Dr. Cheryl Jorcyk, who co-chaired my defense committee, and always encouraged me to do my best work possible; and to Dr. Daniel Fologea, an amazing advocate, and brilliant biophysicist.

Beth Gee, Program Manager of the Biomolecular Sciences Graduate Program, knew just what I needed, often before I even mentioned it. The Biomolecular Research Center, namely Tracy Yarnell, Rhiannon Wood, Barb Gibben, Diane Smith, and Dr. Cindy Keller-Peck gave academic, scientific, and personal support over many years. The Office of Research Compliance assisted daily in each of the complex animal experiments. Thank you to Bev Montgomery, Chelsea Garrison, Aspen Foote, and Matt Lundgren for your exceptional support.

Finally, my long-time lab mates, Brian Hoettels, Kristina Chapman, Des Self and Sacora Sanders, along with a host of undergraduates Jessica McCallister, Heidi Henderson, Emily Lawrence, Colton Brodock, Ofeira Faapouli, Steven Pilarski, Alex Lanza, and Erica Korbel. You are all rock stars and helped in a million ways – especially in keeping my sanity through the long days.

ABSTRACT

Integrity of the brain microvessels that form the blood-brain barrier (BBB) is maintained through fine-tuned regulation of endothelial tight junction proteins, chiefly represented by claudin 5 and the tight junction-associated MARVEL protein (TAMP) occludin. Under proinflammatory conditions in autoimmune-mediated multiple sclerosis (MS), autoreactive effector T cells are activated in white matter regions of the brain and spinal cord and release cytokines to recruit circulating neutrophils that, in turn, release neurotoxic substances. Lack of tight junctions in peripheral blood vessels allows neutrophils to exit blood vessels unhindered, but BBB tight junctions must first be downregulated before neutrophils can transmigrate into the brain. The resulting loss of BBB integrity initiates a pathogenic feedback loop propagating the inflammatory injury. Understanding the established relationship between neutrophilia and BBB dysfunction in neuroinflammation, I set out to better define the cellular contributions behind this pathology. Early on, I identified increased circulating levels of the cytokine oncostatin M (OSM) concomitant with a pathogenic increase in OSM+ neutrophil counts during the effector phase of experimental autoimmune encephalomyelitis (EAE), a mouse model of MS. Next, I found that BBB endothelial cells selectively downregulate occludin, but not claudin 5, after stimulation with OSM. To dissect the mechanisms responsible, I identified that fewer neutrophils are able to cross BBB endothelial monolayers lacking OSMRβ, the cognate OSM receptor. Finally, in OSMRβ-knockout mice, I found a rescue in symptoms, BBB permeability to small molecules, and occludin expression during the

effector phase of EAE. Overall, this work identifies a novel role for OSM as an inflammatory cytokine released by neutrophils that specifically regulates BBB TAMPs during autoimmune-mediated neuroinflammation.

TABLE OF CONTENTS

LIST OF TABLES

LIST OF FIGURES

LIST OF ABBREVIATIONS

Ai14	B6.Cg-Gt(ROSA)26Sor$^{tm14(CAG-tdTomato)Hze}$/J
AT-EAE	Adoptive Transfer Experimental Autoimmune Encephalomyelitis
BBB	Blood-brain barrier
BBB^{Cre}	Tg(Slco1c1-icre/ERT2)1Mrks mice
BBB^{Reporter}	Tg(Slco1c1-icre/ERT2)1Mrks x B6.Cg-Gt(ROSA)26Sor$^{tm14(CAG-tdTomato)Hze}$/J
Bgn	Biglycan
BMVEC	Brain microvascular endothelial cell
CLDN5	Claudin 5
CNS	Central Nervous System
DMEM	Dulbecco's Modified Eagle Medium
DPI	Days post induction
EAE	Experimental Autoimmune Encephalomyelitis
EC^{Cre}	B6.Cg-Tg(Tek-cre/ERT2)1Arnd/ArndCnrm
EC^{Reporter}	B6.Cg-Tg(Tek-cre/ERT2)1Arnd/ArndCnrm) x B6.Cg-Gt(ROSA)26Sor$^{tm14(CAG-tdTomato)Hze}$/J
ECIS	Electric Cell-substrate Impedance Sensing
ECIS-TEER	Electric Cell-substrate Impedance Sensing Trans-Endothelial Electrical Resistance
FBS	Fetal Bovine Serum

FMO	Fluorescence minus one
GM-CSF	Granulocyte-Monocyte-Colony Stimulating Factor
HBSS	Hank's Balanced Salt Solution
ICAM-1	Intercellular Adhesion Molecule-1
IFN-γ	Interferon-γ
IL-1β	Interleukin-1β
IL-17	Interleukin-17
IL-6	Interleukin-6
IP	Intraperitoneal injection
LIF	Leukemia Inhibitory Factor
MCP-1	Monocyte Chemoattractant Protein-1
MOG_{35-55}	Myelin Oligodendrocyte Glycoprotein amino acids 35-55
MS	Multiple Sclerosis
NaFl	Sodium Fluorescein
NLR	Neutrophil-to-Lymphocyte Ratio
NVU	Neurovascular Unit
OCLN	Occludin
OSM	Oncostatin M
OSMR	Oncostatin M Receptor β
$OSMR^{fl/fl}$	Oncostatin M Receptor Conditional Knockout
$OSMR^{KO}$	Oncostatin M Receptor Global Knockout
PBS	Phosphate Buffered Saline
PBSTC	PBS + 0.1% Triton + 2 mM Ca^{2+} + 10% donkey serum

PIL	Perivenular Inflammatory Lesion
STAT	Signal transduction and activator of transcription
TAMP	Tight junction associated MARVEL protein
TCR	T-cell receptor
TEER	Trans-endothelial Electric Resistance
Tg	Transgenic
WT	Wild type

CHAPTER ONE: THE BLOOD-BRAIN BARRIER DURING HOMEOSTASIS AND DISEASE: A REVIEW

Introduction

The blood-brain barrier (BBB) is the specialized series of blood vessels that supplies nutrients and removes waste from the brain. Under normal conditions, the endothelium lining these vessels maintains a barrier against water, solutes, toxins, and pathogens (Daneman & Prat, 2015; Yuan & Rigor, 2010). During inflammation, however, this barrier can be breached, leading to demyelination, neural injury, or even death (Frischer et al., 2009; Hong et al., 2016). One inflammatory cytokine, oncostatin M (OSM) has been found in multiple diseases, however it's source and actions are poorly understood (Alikhani et al., 2014; Brilot et al., 2019; Janssens et al., 2015). This review discusses the current literature surrounding blood-brain barrier functioning and interactions with the immune system, highlighting the pathophysiology of the BBB during diseases like multiple sclerosis.

Common Diseases Involving the Blood-Brain Barrier

The blood-brain barrier has been implicated in many diseases including stroke, Alzheimer's, and multiple sclerosis. In each of these, the endothelial cells forming the barrier protect the cells of the parenchyma from damage caused by circulating immune cells, neurotoxic substances, and fluctuating nutrient concentrations (de Vries et al., 1997; Profaci et al., 2020; Sweeney et al., 2018).

Multiple Sclerosis

Multiple sclerosis (MS) is a pervasive, chronic disease that effects an estimated 623,437 people (288.2 per 100,000) in the United States (Wilkins, 2019). With the estimated cost of treatment at $95,632 per year per patient (Nicholas et al., 2020) , and a significant loss in quality of life (Valentine et al., 2021), studies into the effective prevention and treatment of MS are needed.

In the clinic, MS presents with patients having weakness, spasticity, numbness, and neuropathies. As the disease progresses, cognitive decline and other psychiatric issues are common, along with painful cramps, seizure disorders, and dysfunctions of the bowel and bladder (Javalkar et al., 2016). Physiologically, chronic inflammatory processes cause blood-brain barrier and blood-spinal cord barrier to be breached, allowing autoreactive T cells to form, and neutrophils to invade, leading to demyelination and neuronal death (Cassan & Liblau, 2007; De Bondt et al., 2020; Ortiz et al., 2014). The specific mechanisms, however, remain unknown.

OSM has been found both in lesions and in increased concentrations in serum of MS patients, (Huang et al., 2020; Ruprecht et al., 2001). When found with increased concentrations of hepatocyte growth factor, it may be a strong bioindicator of MS (Huang et al., 2020).

One murine model of MS is experimental autoimmune encephalomyelitis (EAE). In this process, autoreactive T cells are formed through a vaccination process against myelin oligodendrocyte glycoprotein amino acids 35-55 (MOG_{35-55}). Coinjection of pertussis toxin encourages immune surveillance, which results in both symptomatic and physiologic properties similar to that of MS (Constantinescu et al., 2011; S. D. Miller &

Karpus, 2007). Wildtype C57BL/6 mice that have EAE exhibit ascending flaccid paralysis beginning at the tail. It is rare that the disease course moves beyond weakness of the forelimbs (Stromnes & Goverman, 2006a). Histologic examination of mouse brain tissues reveal similar features to MS: neutrophils in the brain parenchyma near blood vessels, surrounded by fibrinogen leakage (Aubé et al., 2014).

Properties of the Blood-Brain Barrier

Physiology and Function of Vasculature

Oxygen is crucial for tissue functioning. It is delivered by red blood cells through blood vessels. The BBB is a specialized region of the vascular system that protects the brain from external components: leukocytes, bacteria, viruses, toxins, and even ions, while still maintaining adequate nutritional supply to the demanding neural tissues (Daneman & Prat, 2015).

Cellular Composition

Beyond the endothelial cells that create the BBB and the neurons that they support, the brain also contains astrocytes and pericytes. The neurovascular unit (NVU), then, describes the relationship between the blood supply, neuron, and the supporting cells (Muoio et al., 2014). (**Figure 1.1**). In fact, it is estimated that every neuron is supported by its own capillary, highlighting the importance of the blood supply to brain function (Schlageter et al., 1999).

Sharing the basement membrane of the endothelial cells, pericytes support the arterioles, venules, and capillaries within the central nervous system (Bell et al., 2010). Pericytes contain gap junctions with endothelial cells, providing quick avenues of regulation (Cuevas et al., 1984). It is thought that the presence of pericytes provides some

of the necessary signaling to encourage CNS-localized endothelial cells to form the intensified barriers of the BBB (Sweeney et al., 2016; Winkler et al., 2012).

Astrocytic end-feet form an additional ring around the endothelial/pericyte structure termed the glia limitans (Horng et al., 2017). During homeostasis, these cells provide additional support to the endothelial tight junctions; during inflammatory processes, astrocytes gain immune functions and signal to infiltrating leukocytes (Priego & Valiente, 2019).

Differences to Peripheral Vasculature

At rest, the brain requires nearly 20% of all blood flow to maintain its highly active metabolic state (Clarke & Sokoloff, 1999). Compared to the periphery, the brain maintains a high rate of perfusion. In periods of higher neuronal activity, the local endothelium responds to the increased concentrations of cations by releasing nitric oxide, a potent vasodilator to the precapillary arterioles (Chen et al., 2008; Faraci & Heistad, 1990). Interestingly, while it is relatively common for peripheral capillaries to contain smooth muscle cells to constrict blood flow, the CNS capillaries completely lack smooth muscle, highlighting the tremendous nutrient supply required by neural tissue (Cipolla, 2009).

Physical Properties of the Blood-Brain Barrier

The brain endothelium meets the tremendous nutrient demands of the brain while maintaining a strict barrier through active transport and transcytosis (Yazdani et al., 2019). Importantly, BBB endothelial cells express an insulin-independent carrier for glucose – glucose transporter 1 – to maintain high levels of available energy (Lee & Klip, 2012; Zheng et al., 2010). Small lipids are generally thought to enter via passive

diffusion, whereas amino acids require multiple transporters (Lacombe et al., 2018; Oldendorf, 1973).

Under homeostasis, the BBB broadly restricts the movement of leukocytes into the parenchyma of the brain (Engelhardt & Coisne, 2011). When required, as in infection or neural tissue death, endothelial cells capture surveilling leukocytes through express of various cell adhesion molecules (L. Yang et al., 2005). The halted leukocyte becomes activated, and begins releasing various inflammatory molecules (see *Cytokines*, below) (L. Yang et al., 2005). In response, the endothelium will modulate its barriers, and the cell passes through, a process called diapedesis (Pan et al., 2011).

Tight Junction Proteins

Blood-brain barrier endothelial cells maintain the tight regulation of water, ions, and nutrients through the expression of multiple tight junction proteins. The prototypical tight junction protein is claudin 5 (CLDN5), a member of the claudin family (H.-C. Bauer et al., 2014). Likely the most important tight junction molecule, *CLDN5* ablation in mice causes death within 48 hours after birth, while knockdown in otherwise-healthy mice causes a schizophrenia-like phenotype (Greene et al., 2017). In MS lesions, claudin 5 at endothelial junctions is lost; we have similarly found that claudin 5 is lost in brain microvessels of mice with EAE (Beard Jr. et al., 2018; van Horssen et al., 2007).

Occludin (OCLN) is a member of the tight junction associated MARVEL protein (TAMP) family. In mice, *OCLN* knockout results in sterility, however no other gross phenotypical aberrations were noted (Saitou et al., 2000). In humans, occludin mutations can cause brain malformation and microcephaly (Bendriem et al., 2019). Using serum from patients with multiple sclerosis, Minagar et al found that occludin was

downregulated in *in vitro* endothelial culture (Minagar et al., 2003). Similarly, occludin staining was lost in lesions from mice with EAE (Errede et al., 2012).

Immune System Interactions with the Blood Brain Barrier

T Cells

T cells are critical to the regular functions of the immune system. Expressing T-cell receptors (TCR), individual T cells recognize specific antigens, and then direct the immune response based upon that identification (Fink & Hendricks, 2011). T cells that attempt self-antigens are removed from circulation by the thymus (Jordan et al., 2001). During multiple sclerosis, however, T are likely identifying neurovascular components as foreign invaders, and thus mount a response against them (Frischer et al., 2009).

After activation with specific antigen, T cells can differentiate into a variety of T helper cells that have different effects, among them T_H1 cells, which are important for host defense, and T_H17 cells, which process inflammation and wound healing (Zhang et al., 2013). T_H1 cells are required for various multiple sclerosis subtypes, where they release interferon-γ, which regulates over 200 genes in other cell types (Arellano et al., 2017; Boehm et al., 1997). Similarly, T_H17 cells are required to produce interleukin-17 (IL-17), which signal resident neurovascular cells to begin inflammatory processes (Kebir et al., 2007). These roles appear to be mirrored in experimental autoimmune encephalomyelitis; T_H17 cells cross the blood-brain barrier first through endothelial-mediated tight-junction reorganization, followed by T_H1 cells, with caveolae-mediated extravasation (Hohlfeld & Steinman, 2017; Lutz et al., 2017).

Clinically, T cells are targeted in patients with MS, through various modalities, including immunosuppressants and monoclonal antibody therapy (O'Brien et al., 2010).

Neutrophils

Neutrophils, the most numerous of all the leukocytes, play an important role in the generation of neuroinflammatory injury, a condition associated with a decrease in BBB integrity (Dixon, 1997; Liu et al., 2018; Stock et al., 2018). Neutrophils contain a host of cytotoxic and otherwise inflammatory granules, ready in their cytoplasm for near-immediate response (Sheshachalam et al., 2014). Neutrophils are widely regarded as the first-line defense mechanism of innate immunity, as they phagocytize, release multiple signaling compounds, and form extracellular traps for circulating pathogens and bioactive compounds (Mantovani et al., 2011). During neuroinflammatory injury, however, these processes can worsen disease progress and outcome.

A high neutrophil-to-lymphocyte ratio is a strong predictor of poor disease course and outcome of chronic diseases, including MS (D'Amico et al., 2019; Demirci et al., 2016; Song et al., 2021). Neutrophil presence in MS lesions is correlated with BBB leakage (Aubé et al., 2014). These relationships are also found in EAE: when neutrophils are depleted with anti-Ly6G antibodies, disease is both delayed and significantly reduced (Aubé et al., 2014; Wu et al., 2010). Finally, several FDA-approved drugs have targeted T cells with varying success, however modulating the neutrophil response has yet to fully explored (Woodberry et al., 2018).

Other Leukocytes' Contribution

While this dissertation focuses mainly on the roles of T cells and neutrophils, other leukocytes have a function in the initiation and recovery of both EAE and MS.

B Lymphocytes

Antibody-producing B cells may be required for the initial induction of both EAE and MS, however the literature is unclear (Mann et al., 2012). Significantly, when using recombinant human MOG for induction of EAE in mice, B cells were required, however when using recombinant rat MOG for induction, they are not (Oliver et al., 2003). Similarly, MOG-reactive B lymphocytes alone are not sufficient to induce EAE (Litzenburger et al., 1998). Finally, there is some evidence that B cells are required for the recovery of EAE through producing interleukin-10 to signal resolution (Mann et al., 2007). Because these medications do not cross the blood-brain barrier, however, they are most effective in the treatment of early-stage disease, and have the potential side effect of delaying the anti-inflammatory processes of B cells (Cross et al., 2006).

In multiple sclerosis, B cells are similarly thought to be involved in both the initiation and resolution of the disease (Cencioni et al., 2021). Significantly, there have been two FDA-approved treatments involving B cell depletion for the treatment of MS (Greenfield & Hauser, 2018).

B cells enter the CNS through so-called backdoors – that is, not directly through the BBB, but through the associated vasculature that do not express as-tight of junctions (Takeshita & Ransohoff, 2012). The cells then follow the chemokine gradients produced by other immune cells (Takeshita & Ransohoff, 2012).

Together, there is no data to suggest that B cells have significant direct interactions with the BBB. B lymphocytes play a role in onset and recovery of MS and EAE but lack any known function during acute disease.

Macrophages

Macrophages act as antigen presenters, and have roles in both the initiation and recovery EAE (Jiang et al., 2014). During the early stages of inflammation, these cells appear as the inflammatory M1 phenotype, increasing their antigen-presenting capacity and cytokine output (Chu et al., 2018). During the repair process, separate macrophages and microglia polarize to the anti-inflammatory M2 phenotype, reducing inflammation and encouraging tissue remodeling (Chu et al., 2018).

In patients with multiple sclerosis, similar effects are found. Macrophages are found to accumulate near oligodendrocytes, and provide signals for neutrophil invasion (Tsutsui et al., 2018). They are also found, to a lesser degree, as anti-inflammatory M2 macrophages in healing lesions (Vogel et al., 2013).

While no conclusive evidence can be found, it appears that macrophages do not directly challenge or modify endothelial barrier function during early inflammation, but rather are recruited through chemokine gradients and selectively allowed across the endothelium (Corraliza, 2014).

Eosinophils

In addition to pathogenic infection, eosinophils are generally thought to play a role in many inflammatory diseases (Ramirez et al., 2018). While they are found in the spinal cord of mice with EAE, they are neither sufficient nor required for the disease process, and have no influence on the progression or severity of the disease (Ruppova et al., 2021). In general, and mostly due to the cells' principal role as an anti-parasitic, eosinophils are only thought to interact with the BBB during specific types of

meningoencephalitis, where they release matrix metalloproteinases to overcome the claudin 5-strengthened barrier (Chiu & Lai, 2014).

Basophils

Basophils are the least abundant cells of the immune system, and play a role in various inflammatory processes (Siracusa et al., 2013). While they may aid in the transition of T cells into T_H17 inflammatory cells through production of IL-6, they have a redundant role and are not required for EAE (Yuk et al., 2017). To date, no literature could be found indicating basophils interact with the blood-brain barrier.

Cytokines

Interleukin-1β

Interleukin-1β (IL-1β) is a proinflammatory cytokine that is responsible for some forms of BBB disruption, fever, and immune system activation (C.-C. Lin & Edelson, 2017). During multiple sclerosis, mRNA transcripts have been found in brain tissues, however the specific sources of such are unclear (C.-C. Lin & Edelson, 2017). IL-1β has been found to increase the fraction of T_H17 cells, expanding inflammatory injury (Duhen & Campbell, 2014).

IL-1β causes significant hyperpermeability when stimulating BBB-ECs *in vitro* (Beard et al., 2014). During EAE, IL-1β has been found to promote neutrophil-endothelial adhesion, an important step in the initiation of the disease (Aubé et al., 2014). In mice with BBB-specific IL-1β receptor knockout, EAE severity was significantly reduced, highlighting the importance of barrier integrity to the amelioration of neuroinflammatory disease processes (Hauptmann et al., 2020).

IL-17

Interleukin-17 (IL-17) is a cytokine produced by multiple immune cells, including T_H17 cells, neutrophils, and mast cells (A. M. Lin et al., 2011). When stimulated with IL-17, immortalized mouse brain endothelial cells downregulate and reorganize their tight junctions, causing increased permeability and neutrophil transmigration (Huppert et al., 2010). IL-17 also has a role in priming neutrophils for mobilization (McGinley et al., 2020). Mice deficient in IL-17A are resistant to EAE, however T cells from *Il17a*-knockout mice produce adoptive transfer EAE in WT mice that is no different than that induced from WT T cells (McGinley et al., 2020). This additionally highlights the importance of neutrophils to the neuroinflammatory process. In multiple sclerosis patients, increased concentrations of IL-17 has been found in the serum (Schofield et al., 2016). This increased concentration has been correlated with increased number of lesions measured by MRI (Hedegaard et al., 2008).

In sum, IL-17 plays an important role in the pathogenesis of EAE and MS, including overcoming the blood-brain barrier, indicating a potential during acute inflammatory injury.

Oncostatin M

Oncostatin M is a cytokine with diverse effects. Belonging to the interleukin-6 (IL-6) family of cytokines, OSM signals through a heterodimer of oncostatin M receptor β (OSMR) and gp130 (Heinrich et al., 2003; Thoma et al., 1994). Intercellularly, OSM can use various pathways, including JAK/STAT and AKT, to activate 54 different post-translational modifications, and modulate the expression of 322 genes, depending on the cell type (Dey et al., 2013). OSM has been found to be a consequential cytokine in

multiple diseases, including the atherosclerosis, ischemic heart disease, and multiple cancers (Albasanz-Puig et al., 2011; Linsley et al., 1990; Richards, 2013; Ryan et al., 2015; Tawara et al., 2019).

On human microvascular endothelial cells, OSM upregulated intercellular adhesion molecule-1 (ICAM-1), a protein used to halt surveilling leukocytes; monocyte chemoattractant protein-1 (MCP-1), a C-C chemokine known for monocyte recruitment; and interleukin-6, which stimulates the production of neutrophils and growth of T and B cells (Fielding et al., 2008; Ruprecht et al., 2001). Importantly, Ruprecht et al. found OSM in the inflamed lesions of MS patients, where none was found in the parenchyma of health patients. These lesions were noted to have near-complete loss of myelin and leukocyte infiltration. Finally, there is some data to suggest that in rat brain endothelial cells, OSM causes an increase in electrical permeability concomitant with reorganization of the tight junction protein claudin 5, however the experiments were completed with immature monolayers that lack the characteristically-robust tight junctions of fully developed monolayers (Beard Jr. et al., 2018; Takata et al., 2008).

Conversely, OSM could be important for the repair of demyelination. When astrocytes are exposed to oncostatin M, they upregulate TIMP metallopeptidase inhibitor 1 (TIMP-1), an important mediator for the transition from inflammation to wound healing processes in tissues (Houben et al., 2020). Houben notes that OSM signaling is important for remyelination in a cuprizone-mediated model of demyelination. Utilizing Luxol fast blue staining, global OSMR knockout mice do not repair demyelination at the same rate as wildtype mice. Overexpression of OSMR in neurons also provides cerebroprotective benefits during stroke, further exemplifying the dual-nature of this cytokine (Guo et al.,

2015). Significantly, in both inflammatory and anti-inflammatory contexts, the source of oncostatin m is not clear, and potentially from multiple sources.

Finally, oncostatin M has been found in the blood plasma of patients with relapsing-remitting multiple sclerosis, however no correlations between disease severity or state and concentrations of OSM were made (Alikhani et al., 2014).

Together, oncostatin M remains a relevant target for analysis during inflammatory processes. More specifically, OSM appears to have a role in both the pathogenesis and recovery of multiple sclerosis and related neuroinflammatory diseases. Because oncostatin M causes endothelial cells to signal to circulating inflammatory leukocytes, and leukocytes are then found in the brain parenchyma, the source and effect of OSM on endothelial barrier function requires further elucidation.

Conclusions

In summary, the blood-brain barrier provides a multitude of novel targets for investigation during neuroinflammation. Under homeostasis, the endothelium supports a well-regulated environment for optimal neuronal functioning. In early stages of inflammation, leukocyte-mediated blood-brain barrier breakdown likely allows for infiltration and further activation of surveilling immune cells. While the literature is unsettled about its specific role and source, oncostatin M is a likely agent during inflammation. Finally, the endothelia l response to OSM is unclear, and requires further investigation. As a whole, this dissertation undertakes the analysis of neutrophil-derived oncostatin M as a potent mediator of the endothelial tight junction protein occludin during the neuroinflammatory disease experimental autoimmune encephalomyelitis as a physiologically relevant model of multiple sclerosis.

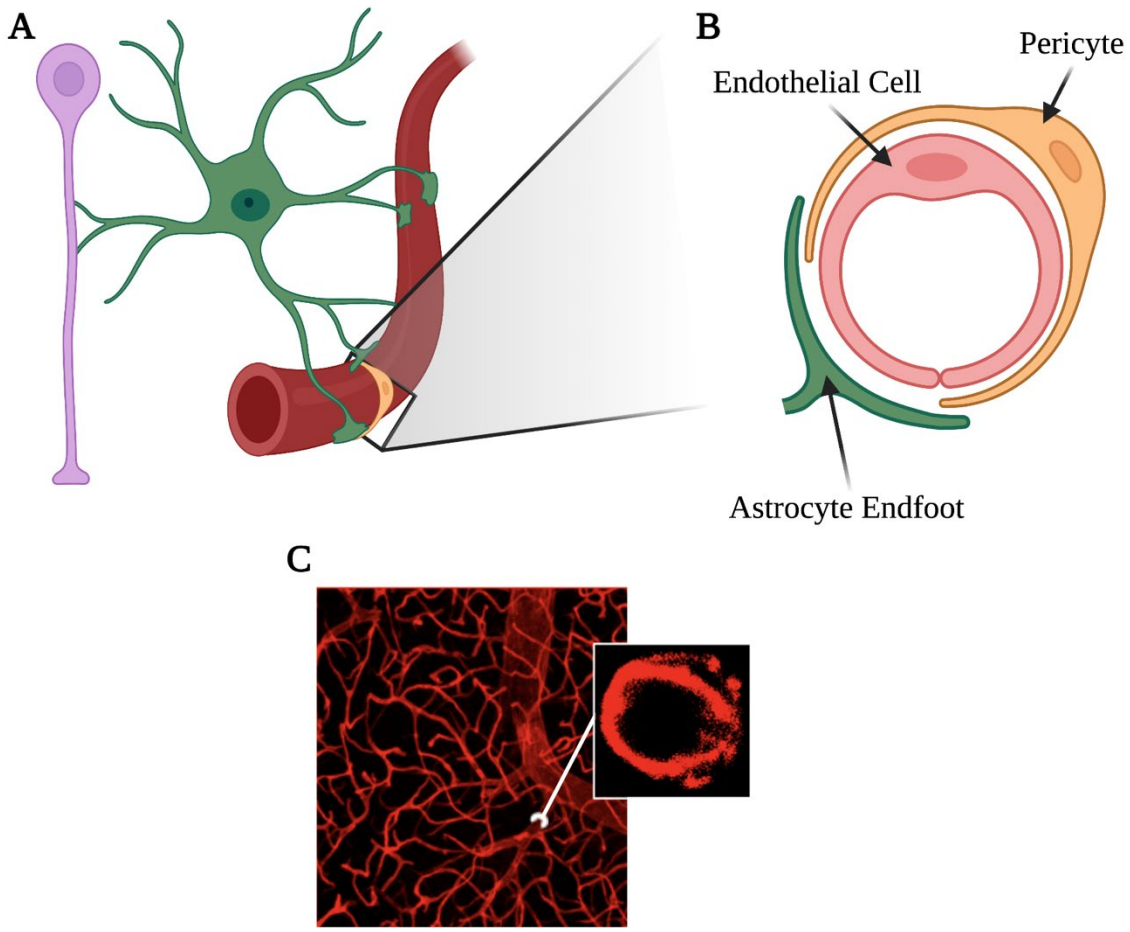

Figure 1.1 The Neurovascular Unit.

A) The neurovascular unit contains the neuron (purple), astrocyte (green), pericyte (yellow), and endothelial cell (pink) of the capillary (red). **B)** The pericyte and endothelial cell are closely associated, sharing a basement membrane. **C)** Representative confocal micrograph of murine brain tissue perfused with tomato lectin (red), a strong endothelial glycocalyx marker. Inset is a transverse section of a 5 μm capillary. Created with Biorender.com

References

Albasanz-Puig, A., Murray, J., Preusch, M., Coan, D., Namekata, M., Patel, Y., Dong, Z. M., Rosenfeld, M. E., & Wijelath, E. S. (2011). Oncostatin M is expressed in atherosclerotic lesions: A role for Oncostatin M in the pathogenesis of atherosclerosis. *Atherosclerosis*, *216*(2), 292–298. https://doi.org/10/c3jvg4

Alikhani, P., Alsahebfosoul, F., & Shajarian, M. (2014). Investigation of Oncostatin M protein expression in Iranian relapsing remitting multiple sclerosis patients. *Multiple Sclerosis and Related Disorders*, *3*(6), 747. https://doi.org/10.1016/j.msard.2014.09.172

Arellano, G., Acuña, E., Reyes, L. I., Ottum, P. A., De Sarno, P., Villarroel, L., Ciampi, E., Uribe-San Martín, R., Cárcamo, C., & Naves, R. (2017). Th1 and Th17 Cells and Associated Cytokines Discriminate among Clinically Isolated Syndrome and Multiple Sclerosis Phenotypes. *Frontiers in Immunology*, *8*, 753. https://doi.org/10/gbnc5m

Aubé, B., Lévesque, S. A., Paré, A., Chamma, É., Kébir, H., Gorina, R., Lécuyer, M.-A., Alvarez, J. I., De Koninck, Y., Engelhardt, B., Prat, A., Côté, D., & Lacroix, S. (2014). Neutrophils Mediate Blood–Spinal Cord Barrier Disruption in Demyelinating Neuroinflammatory Diseases. *The Journal of Immunology*, *193*(5), 2438–2454. https://doi.org/10.4049/jimmunol.1400401

Bauer, H.-C., Krizbai, I. A., Bauer, H., & Traweger, A. (2014). "You Shall Not Pass"-tight junctions of the blood brain barrier. *Frontiers in Neuroscience*, *8*, 392. https://doi.org/10.3389/fnins.2014.00392

Beard Jr., R. S., Hoettels, B. A., Meegan, J. E., Wertz, T. S., Cha, B. J., Yang, X., Oxford, J. T., Wu, M. H., & Yuan, S. Y. (2018). AKT2 maintains brain endothelial claudin-5 expression and selective activation of IR/AKT2/FOXO1-signaling reverses barrier dysfunction. *Journal of Cerebral Blood Flow & Metabolism*, 0271678X1881751. https://doi.org/10.1177/0271678X18817512

Beard, R. S., Haines, R. J., Wu, K. Y., Reynolds, J. J., Davis, S. M., Elliott, J. E., Malinin, N. L., Chatterjee, V., Cha, B. J., Wu, M. H., & Yuan, S. Y. (2014). Non-muscle Mlck is required for -catenin- and FoxO1-dependent downregulation of Cldn5 in IL-1 -mediated barrier dysfunction in brain endothelial cells. *Journal of Cell Science*, *127*(8), 1840–1853. https://doi.org/10.1242/jcs.144550

Bell, R. D., Winkler, E. A., Sagare, A. P., Singh, I., LaRue, B., Deane, R., & Zlokovic, B. V. (2010). Pericytes control key neurovascular functions and neuronal phenotype in the adult brain and during brain aging. *Neuron*, *68*(3), 409–427. https://doi.org/10/c9kwmq

Bendriem, R. M., Singh, S., Aleem, A. A., Antonetti, D. A., & Ross, M. E. (2019). Tight junction protein occludin regulates progenitor Self-Renewal and survival in developing cortex. *ELife*, *8*, e49376. https://doi.org/10/gjj3k2

Boehm, U., Klamp, T., Groot, M., & Howard, J. C. (1997). CELLULAR RESPONSES TO INTERFERON-γ. *Annual Review of Immunology*, *15*(1), 749–795. https://doi.org/10/b6w7zx

Cassan, C., & Liblau, R. S. (2007). Immune tolerance and control of CNS autoimmunity: From animal models to MS patients. *Journal of Neurochemistry*, *100*(4), 883–892. https://doi.org/10/dckfg6

Cencioni, M. T., Mattoscio, M., Magliozzi, R., Bar-Or, A., & Muraro, P. A. (2021). B cells in multiple sclerosis—From targeted depletion to immune reconstitution therapies. *Nature Reviews Neurology*, *17*(7), 399–414. https://doi.org/10/gkbsnd

Chen, K., Pittman, R. N., & Popel, A. S. (2008). Nitric Oxide in the Vasculature: Where Does It Come From and Where Does It Go? A Quantitative Perspective. *Antioxidants & Redox Signaling*, *10*(7), 1185–1198. https://doi.org/10/dp7vnk

Chiu, P.-S., & Lai, S.-C. (2014). Matrix metalloproteinase-9 leads to blood–brain barrier leakage in mice with eosinophilic meningoencephalitis caused by Angiostrongylus cantonensis. *Acta Tropica*, *140*, 141–150. https://doi.org/10/f6rjkk

Cipolla, M. J. (2009). Anatomy and Ultrastructure. In *The Cerebral Circulation*. Morgan & Claypool Life Sciences. https://www.ncbi.nlm.nih.gov/books/NBK53086/

Clarke, D. D., & Sokoloff, L. (1999). Circulation and Energy Metabolism of the Brain. *Basic Neurochemistry: Molecular, Cellular and Medical Aspects. 6th Edition*. https://www.ncbi.nlm.nih.gov/books/NBK20413/

Constantinescu, C. S., Farooqi, N., O'Brien, K., & Gran, B. (2011). Experimental autoimmune encephalomyelitis (EAE) as a model for multiple sclerosis (MS). *British Journal of Pharmacology*, *164*(4), 1079–1106. https://doi.org/10/djfqzc

Corraliza, I. (2014). Recruiting specialized macrophages across the borders to restore brain functions. *Frontiers in Cellular Neuroscience*, *8*, 262. https://doi.org/10/gmx8q4

Cross, A. H., Stark, J. L., Lauber, J., Ramsbottom, M. J., & Lyons, J.-A. (2006). Rituximab reduces B cells and T cells in cerebrospinal fluid of multiple sclerosis patients. *Journal of Neuroimmunology*, *180*(1–2), 63–70. https://doi.org/10/bs4s5z

Cuevas, P., Gutierrez-Diaz, J. A., Reimers, D., Dujovny, M., Diaz, F. G., & Ausman, J. I. (1984). Pericyte endothelial gap junctions in human cerebral capillaries. *Anatomy and Embryology*, *170*(2), 155–159. https://doi.org/10/c79w87

D'Amico, E., Zanghì, A., Romano, A., Sciandra, M., Palumbo, G. A. M., & Patti, F. (2019). The Neutrophil-to-Lymphocyte Ratio is Related to Disease Activity in Relapsing Remitting Multiple Sclerosis. *Cells*, *8*(10), 1114. https://doi.org/10/ggc2vj

Daneman, R., & Prat, A. (2015). The Blood–Brain Barrier. *Cold Spring Harbor Perspectives in Biology*, *7*(1), a020412. https://doi.org/10.1101/cshperspect.a020412

De Bondt, M., Hellings, N., Opdenakker, G., & Struyf, S. (2020). Neutrophils: Underestimated Players in the Pathogenesis of Multiple Sclerosis (MS). *International Journal of Molecular Sciences*, *21*(12), 4558. https://doi.org/10/gksp7p

de Vries, H. E., Kuiper, J., Boer, A. G. de, Berkel, T. J. C. V., & Breimer, D. D. (1997). The Blood-Brain Barrier in Neuroinflammatory Diseases. *Pharmacological Reviews*, *49*(2), 143–156.

Demirci, S., Demirci, S., Kutluhan, S., Koyuncuoglu, H. R., & Yurekli, V. A. (2016). The clinical significance of the neutrophil-to-lymphocyte ratio in multiple sclerosis. *The International Journal of Neuroscience*, *126*(8), 700–706. https://doi.org/10/ggc2vr

Dixon, L. R. (1997). The complete blood count: Physiologic basis and clinical usage. *The Journal of Perinatal & Neonatal Nursing*, *11*(3), 1–18. https://doi.org/10/gmx9xm

Duhen, T., & Campbell, D. J. (2014). IL-1β promotes the differentiation of polyfunctional human CCR6+CXCR3+ Th1/17 cells that are specific for pathogenic and commensal microbes. *Journal of Immunology (Baltimore, Md.: 1950)*, *193*(1), 120–129. https://doi.org/10/gkspzs

Engelhardt, B., & Coisne, C. (2011). Fluids and barriers of the CNS establish immune privilege by confining immune surveillance to a two-walled castle moat surrounding the CNS castle. *Fluids and Barriers of the CNS*, *8*, 4. https://doi.org/10/fbs9t6

Errede, M., Girolamo, F., Ferrara, G., Strippoli, M., Morando, S., Boldrin, V., Rizzi, M., Uccelli, A., Perris, R., Bendotti, C., Salmona, M., Roncali, L., & Virgintino, D. (2012). Blood-Brain Barrier Alterations in the Cerebral Cortex in Experimental Autoimmune Encephalomyelitis. *Journal of Neuropathology & Experimental Neurology*, *71*(10), 840–854. https://doi.org/10/gjv6ns

Faraci, F. M., & Heistad, D. D. (1990). Regulation of large cerebral arteries and cerebral microvascular pressure. *Circulation Research*, *66*(1), 8–17. https://doi.org/10/gmzm2f

Fielding, C. A., McLoughlin, R. M., McLeod, L., Colmont, C. S., Najdovska, M., Grail, D., Ernst, M., Jones, S. A., Topley, N., & Jenkins, B. J. (2008). IL-6 Regulates Neutrophil Trafficking during Acute Inflammation via STAT3. *The Journal of Immunology*, *181*(3), 2189–2195. https://doi.org/10/f3v2xb

Fink, P. J., & Hendricks, D. W. (2011). Post-thymic maturation: Young T cells assert their individuality. *Nature Reviews. Immunology*, *11*(8), 544–549. https://doi.org/10/bnr8qx

Frischer, J. M., Bramow, S., Dal-Bianco, A., Lucchinetti, C. F., Rauschka, H., Schmidbauer, M., Laursen, H., Sorensen, P. S., & Lassmann, H. (2009). The relation between inflammation and neurodegeneration in multiple sclerosis brains. *Brain: A Journal of Neurology*, *132*(Pt 5), 1175–1189. https://doi.org/10/b8c5wv

Greene, C., Kealy, J., Humphries, M. M., Gong, Y., Hou, J., Hudson, N., Cassidy, L. M., Martiniano, R., Shashi, V., Hooper, S. R., Grant, G. A., Kenna, P. F., Norris, K., Callaghan, C. K., Islam, M. dN, O'Mara, S. M., Najda, Z., Campbell, S. G., Pachter, J. S., … Campbell, M. (2017). Dose-dependent expression of claudin-5 is a modifying factor in schizophrenia. *Molecular Psychiatry*. https://doi.org/10.1038/mp.2017.156

Greenfield, A. L., & Hauser, S. L. (2018). B Cell Therapy for Multiple Sclerosis: Entering an Era. *Annals of Neurology*, *83*(1), 13–26. https://doi.org/10/gcv79h

Guo, S., Li, Z.-Z., Gong, J., Xiang, M., Zhang, P., Zhao, G.-N., Li, M., Zheng, A., Zhu, X., Lei, H., Minoru, T., & Li, H. (2015). Oncostatin M Confers Neuroprotection against Ischemic Stroke. *Journal of Neuroscience*, *35*(34), 12047–12062. https://doi.org/10/f7thhq

Hauptmann, J., Johann, L., Marini, F., Kitic, M., Colombo, E., Mufazalov, I. A., Krueger, M., Karram, K., Moos, S., Wanke, F., Kurschus, F. C., Klein, M., Cardoso, S., Strauß, J., Bolisetty, S., Lühder, F., Schwaninger, M., Binder, H., Bechman, I., … Waisman, A. (2020). Interleukin-1 promotes autoimmune neuroinflammation by suppressing endothelial heme oxygenase-1 at the blood–brain barrier. *Acta Neuropathologica*, *140*(4), 549–567. https://doi.org/10/ghs462

Hedegaard, C. J., Krakauer, M., Bendtzen, K., Lund, H., Sellebjerg, F., & Nielsen, C. H. (2008). T helper cell type 1 (Th1), Th2 and Th17 responses to myelin basic protein and disease activity in multiple sclerosis. *Immunology*, *125*(2), 161–169. https://doi.org/10/cwxwr6

Heinrich, P. C., Behrmann, I., Haan, S., Hermanns, H. M., Müller-Newen, G., & Schaper, F. (2003). Principles of interleukin (IL)-6-type cytokine signalling and its regulation. *The Biochemical Journal*, *374*(Pt 1), 1–20. https://doi.org/10/fbzv77

Hohlfeld, R., & Steinman, L. (2017). T Cell–Transfer Experimental Autoimmune Encephalomyelitis: Pillar of Multiple Sclerosis and Autoimmunity. *The Journal of Immunology*, *198*(9), 3381–3383. https://doi.org/10/gmzfnz

Hong, H., Kim, B. S., & Im, H.-I. (2016). Pathophysiological Role of Neuroinflammation in Neurodegenerative Diseases and Psychiatric Disorders. *International Neurourology Journal*, *20*(Suppl 1), S2-7. https://doi.org/10.5213/inj.1632604.302

Horng, S., Therattil, A., Moyon, S., Gordon, A., Kim, K., Argaw, A. T., Hara, Y., Mariani, J. N., Sawai, S., Flodby, P., Crandall, E. D., Borok, Z., Sofroniew, M. V., Chapouly, C., & John, G. R. (2017). Astrocytic tight junctions control inflammatory CNS lesion pathogenesis. *The Journal of Clinical Investigation*, *127*(8), 3136–3151. https://doi.org/10/gbrgc5

Houben, E., Janssens, K., Hermans, D., Vandooren, J., Haute, C. V. den, Schepers, M., Vanmierlo, T., Lambrichts, I., Horssen, J. van, Baekelandt, V., Opdenakker, G., Baron, W., Broux, B., Slaets, H., & Hellings, N. (2020). Oncostatin M-induced astrocytic tissue inhibitor of metalloproteinases-1 drives remyelination. *Proceedings of the National Academy of Sciences*, *117*(9), 5028–5038. https://doi.org/10/gmx8hv

Huang, J., Khademi, M., Fugger, L., Lindhe, Ö., Novakova, L., Axelsson, M., Malmeström, C., Constantinescu, C., Lycke, J., Piehl, F., Olsson, T., & Kockum, I. (2020). Inflammation-related plasma and CSF biomarkers for multiple sclerosis. *Proceedings of the National Academy of Sciences*, *117*(23), 12952–12960. https://doi.org/10/ghs4ms

Huppert, J., Closhen, D., Croxford, A., White, R., Kulig, P., Pietrowski, E., Bechmann, I., Becher, B., Luhmann, H. J., Waisman, A., & Kuhlmann, C. R. W. (2010). Cellular mechanisms of IL-17-induced blood-brain barrier disruption. *The FASEB Journal*, *24*(4), 1023–1034. https://doi.org/10/btcf6j

Janssens, K., Maheshwari, A., Van den Haute, C., Baekelandt, V., Stinissen, P., Hendriks, J. J. A., Slaets, H., & Hellings, N. (2015). Oncostatin M protects against demyelination by inducing a protective microglial phenotype. *GLIA*, *63*(10), 1729–1737. https://doi.org/10.1002/glia.22840

Javalkar, V., McGee, J., & Minagar, A. (2016). Chapter 1 - Clinical Manifestations of Multiple Sclerosis: An Overview. In A. Minagar (Ed.), *Multiple Sclerosis* (pp. 1–12). Academic Press. https://doi.org/10.1016/B978-0-12-800763-1.00001-4

Jiang, Z., Jiang, J. X., & Zhang, G.-X. (2014). Macrophages: A double-edged sword in experimental autoimmune encephalomyelitis. *Immunology Letters*, *160*(1), 17–22. https://doi.org/10/f55n86

Jordan, M. S., Boesteanu, A., Reed, A. J., Petrone, A. L., Holenbeck, A. E., Lerman, M. A., Naji, A., & Caton, A. J. (2001). Thymic selection of CD4+CD25+ regulatory T cells induced by an agonist self-peptide. *Nature Immunology*, *2*(4), 301–306. https://doi.org/10/br2p42

Kebir, H., Kreymborg, K., Ifergan, I., Dodelet-Devillers, A., Cayrol, R., Bernard, M., Giuliani, F., Arbour, N., Becher, B., & Prat, A. (2007). Human TH17 lymphocytes promote blood-brain barrier disruption and central nervous system inflammation. *Nature Medicine*, *13*(10), 1173–1175. https://doi.org/10/dznt6p

Lacombe, R. J. S., Chouinard-Watkins, R., & Bazinet, R. P. (2018). Brain docosahexaenoic acid uptake and metabolism. *Molecular Aspects of Medicine*, *64*, 109–134. https://doi.org/10/gmzm5s

Lee, W. L., & Klip, A. (2012). Shuttling glucose across brain microvessels, with a little help from GLUT1 and AMP kinase. Focus on "AMP kinase regulation of sugar transport in brain capillary endothelial cells during acute metabolic stress." *American Journal of Physiology - Cell Physiology*, *303*(8), C803–C805. https://doi.org/10/gmzm3b

Lin, A. M., Rubin, C. J., Khandpur, R., Wang, J. Y., Riblett, M., Yalavarthi, S., Villanueva, E. C., Shah, P., Kaplan, M. J., & Bruce, A. T. (2011). Mast Cells and Neutrophils Release IL-17 through Extracellular Trap Formation in Psoriasis. *The Journal of Immunology*, *187*(1), 490–500. https://doi.org/10/d7s589

Lin, C.-C., & Edelson, B. T. (2017). New Insights into the Role of IL-1β in Experimental Autoimmune Encephalomyelitis and Multiple Sclerosis. *The Journal of Immunology*, *198*(12), 4553–4560. https://doi.org/10/gbpscj

Linsley, P. S., Kallestad, J., Ochs, V., & Neubauer, M. (1990). Cleavage of a hydrophilic C-terminal domain increases growth-inhibitory activity of oncostatin M. *Molecular and Cellular Biology*, *10*(5), 1882–1890.

Litzenburger, T., Fässler, R., Bauer, J., Lassmann, H., Linington, C., Wekerle, H., & Iglesias, A. (1998). B lymphocytes producing demyelinating autoantibodies: Development and function in gene-targeted transgenic mice. *The Journal of Experimental Medicine*, *188*(1), 169–180. https://doi.org/10/d69mz9

Liu, Y.-W., Li, S., & Dai, S.-S. (2018). Neutrophils in traumatic brain injury (TBI): Friend or foe? *Journal of Neuroinflammation*, *15*(1), 146. https://doi.org/10/ghgmsp

Lutz, S. E., Smith, J. R., Kim, D. H., Olson, C. V. L., Ellefsen, K., Bates, J. M., Gandhi, S. P., & Agalliu, D. (2017). Caveolin1 Is Required for Th1 Cell Infiltration, but Not Tight Junction Remodeling, at the Blood-Brain Barrier in Autoimmune Neuroinflammation. *Cell Reports*, *21*(8), 2104–2117. https://doi.org/10/ghvvrp

Mann, M. K., Maresz, K., Shriver, L. P., Tan, Y., & Dittel, B. N. (2007). B cell regulation of CD4+CD25+ T regulatory cells and IL-10 via B7 is essential for recovery from experimental autoimmune encephalomyelitis. *Journal of Immunology (Baltimore, Md.: 1950)*, *178*(6), 3447–3456. https://doi.org/10/f3vq68

Mann, M. K., Ray, A., Basu, S., Karp, C. L., & Dittel, B. N. (2012). Pathogenic and regulatory roles for B cells in experimental autoimmune encephalomyelitis. *Autoimmunity*, *45*(5), 388–399. https://doi.org/10/gmwgjg

Mantovani, A., Cassatella, M. A., Costantini, C., & Jaillon, S. (2011). Neutrophils in the activation and regulation of innate and adaptive immunity. *Nature Reviews Immunology*, *11*(8), 519–531. https://doi.org/10/d3pgsp

McGinley, A. M., Sutton, C. E., Edwards, S. C., Leane, C. M., DeCourcey, J., Teijeiro, A., Hamilton, J. A., Boon, L., Djouder, N., & Mills, K. H. G. (2020). Interleukin-17A Serves a Priming Role in Autoimmunity by Recruiting IL-1β-Producing Myeloid Cells that Promote Pathogenic T Cells. *Immunity*, *52*(2), 342-356.e6. https://doi.org/10/ghz29d

Miller, S. D., & Karpus, W. J. (2007). Experimental autoimmune encephalomyelitis in the mouse. *Current Protocols in Immunology*, *Chapter 15*, Unit 15.1. https://doi.org/10/b36256

Minagar, A., Ostanin, D., Long, A. C., Jennings, M., Kelley, R. E., Sasaki, M., & Alexander, J. S. (2003). Serum from patients with multiple sclerosis downregulates occludin and VE-cadherin expression in cultured endothelial cells. *Multiple Sclerosis (Houndmills, Basingstoke, England)*, *9*(3), 235–238. https://doi.org/10/d2pm64

Muoio, V., Persson, P. B., & Sendeski, M. M. (2014). The neurovascular unit—Concept review. *Acta Physiologica (Oxford, England)*, *210*(4), 790–798. https://doi.org/10/f5vx44

Nicholas, J., Halpern, R., Ziehn, M., Peterson-Brandt, J., Leszko, M., & Deshpande, C. (2020). Real-world cost of treatment for multiple sclerosis patients initiating and receiving infused disease-modifying therapies per recommended label in the United States. *Journal of Medical Economics*, *23*(8), 885–893. https://doi.org/10/gksdsk

O'Brien, K., Gran, B., & Rostami, A. (2010). T-cell based immunotherapy in experimental autoimmune encephalomyelitis and multiple sclerosis. *Immunotherapy*, *2*(1), 99–115.

Oldendorf, W. (1973). Stereospecificity of blood-brain barrier permeability to amino acids. *American Journal of Physiology-Legacy Content*, *224*(4), 967–969. https://doi.org/10/gmzm5v

Oliver, A. R., Lyon, G. M., & Ruddle, N. H. (2003). Rat and human myelin oligodendrocyte glycoproteins induce experimental autoimmune encephalomyelitis by different mechanisms in C57BL/6 mice. *Journal of Immunology (Baltimore, Md.: 1950)*, *171*(1), 462–468. https://doi.org/10/gmwgjq

Ortiz, G. G., Pacheco-Moisés, F. P., Macías-Islas, M. Á., Flores-Alvarado, L. J., Mireles-Ramírez, M. A., González-Renovato, E. D., Hernández-Navarro, V. E., Sánchez-López, A. L., & Alatorre-Jiménez, M. A. (2014). Role of the Blood–Brain Barrier in Multiple Sclerosis. *Archives of Medical Research*, *45*(8), 687–697. https://doi.org/10/f62rp8

Pan, W., Stone, K. P., Hsuchou, H., Manda, V. K., Zhang, Y., & Kastin, A. J. (2011). Cytokine Signaling Modulates Blood-Brain Barrier Function. *Current Pharmaceutical Design*, *17*(33), 3729–3740.

Priego, N., & Valiente, M. (2019). The Potential of Astrocytes as Immune Modulators in Brain Tumors. *Frontiers in Immunology*, *10*, 1314. https://doi.org/10/gmzf9g

Profaci, C. P., Munji, R. N., Pulido, R. S., & Daneman, R. (2020). The blood–brain barrier in health and disease: Important unanswered questions. *Journal of Experimental Medicine*, *217*(4). https://doi.org/10/gjfrn8

Ramirez, G. A., Yacoub, M.-R., Ripa, M., Mannina, D., Cariddi, A., Saporiti, N., Ciceri, F., Castagna, A., Colombo, G., & Dagna, L. (2018). Eosinophils from Physiology to Disease: A Comprehensive Review. *BioMed Research International*, *2018*, 9095275. https://doi.org/10/gc86qz

Richards, C. D. (2013). The enigmatic cytokine oncostatin m and roles in disease. *ISRN Inflammation*, *2013*, 512103. https://doi.org/10.1155/2013/512103

Ruppova, K., Lim, J.-H., Fodelianaki, G., August, A., & Neuwirth, A. (2021). Eosinophils are dispensable for development of MOG35–55-induced experimental autoimmune encephalomyelitis in mice. *Immunology Letters*, *239*, 72–76. https://doi.org/10/gmwhq4

Ruprecht, K., Kuhlmann, T., Seif, F., Hummel, V., Kruse, N., Br Ck, W., & Rieckmann, P. (2001). Effects of Oncostatin M on Human Cerebral Endothelial Cells and Expression in Inflammatory Brain Lesions. *Journal of Neuropathology and Experimental Neurology*, *60*(11).

Ryan, R. E., Martin, B., Mellor, L., Jacob, R. B., Tawara, K., McDougal, O. M., Oxford, J. T., & Jorcyk, C. L. (2015). Oncostatin M binds to extracellular matrix in a bioactive conformation: Implications for inflammation and metastasis. *Cytokine*, *72*(1), 71–85. https://doi.org/10.1016/j.cyto.2014.11.007

Saitou, M., Furuse, M., Sasaki, H., Schulzke, J.-D., Fromm, M., Takano, H., Noda, T., & Tsukita, S. (2000). Complex Phenotype of Mice Lacking Occludin, a Component of Tight Junction Strands. *Molecular Biology of the Cell*, *11*(12), 4131–4142.

Schlageter, K. E., Molnar, P., Lapin, G. D., & Groothuis, D. R. (1999). Microvessel Organization and Structure in Experimental Brain Tumors: Microvessel Populations with Distinctive Structural and Functional Properties. *Microvascular Research*, *58*(3), 312–328. https://doi.org/10/dcvr55

Schofield, C., Fischer, S. K., Townsend, M. J., Mosesova, S., Peng, K., Setiadi, A. F., Song, A., & Baruch, A. (2016). Characterization of IL-17AA and IL-17FF in rheumatoid arthritis and multiple sclerosis. *Bioanalysis*, *8*(22), 2317–2327. https://doi.org/10/f9jr4m

Sheshachalam, A., Srivastava, N., Mitchell, T., Lacy, P., & Eitzen, G. (2014). Granule Protein Processing and Regulated Secretion in Neutrophils. *Frontiers in Immunology*, *5*, 448. https://doi.org/10/gmzd3p

Siracusa, M. C., Kim, B. S., Spergel, J. M., & Artis, D. (2013). Basophils and allergic inflammation. *The Journal of Allergy and Clinical Immunology*, *132*(4), 789–788. https://doi.org/10/f2mdk4

Song, M., Graubard, B. I., Rabkin, C. S., & Engels, E. A. (2021). Neutrophil-to-lymphocyte ratio and mortality in the United States general population. *Scientific Reports*, *11*(1), 464. https://doi.org/10/gk8g5z

Stock, A. J., Kasus-Jacobi, A., & Pereira, H. A. (2018). The role of neutrophil granule proteins in neuroinflammation and Alzheimer's disease. *Journal of Neuroinflammation*, *15*(1), 240. https://doi.org/10/gd6t9h

Stromnes, I. M., & Goverman, J. M. (2006). Active induction of experimental allergic encephalomyelitis. *Nature Protocols*, *1*(4), 1810–1819. https://doi.org/10/fhgg3p

Sweeney, M. D., Ayyadurai, S., & Zlokovic, B. V. (2016). Pericytes of the neurovascular unit: Key functions and signaling pathways. *Nature Neuroscience*, *19*(6), 771–783. https://doi.org/10/gghv6n

Sweeney, M. D., Sagare, A. P., & Zlokovic, B. V. (2018). Blood–brain barrier breakdown in Alzheimer disease and other neurodegenerative disorders. *Nature Reviews Neurology*, *14*(3), 133–150. https://doi.org/10/gcwswg

Takata, F., Sumi, N., Nishioku, T., Harada, E., Wakigawa, T., Shuto, H., Yamauchi, A., & Kataoka, Y. (2008). Oncostatin M induces functional and structural impairment of blood-brain barriers comprised of rat brain capillary endothelial cells. *Neuroscience Letters*, *441*(2), 163–166. https://doi.org/10.1016/j.neulet.2008.06.030

Takeshita, Y., & Ransohoff, R. M. (2012). Inflammatory cell trafficking across the blood–brain barrier: Chemokine regulation and in vitro models. *Immunological Reviews*, *248*(1), 228–239. https://doi.org/10/f33gkm

Tawara, K., Scott, H., Emathinger, J., Wolf, C., LaJoie, D., Hedeen, D., Bond, L., Montgomery, P., & Jorcyk, C. (2019). HIGH expression of OSM and IL-6 are associated with decreased breast cancer survival: Synergistic induction of IL-6 secretion by OSM and IL-1β *Oncotarget*, *10*(21), 2068–2085. https://doi.org/10/gmx8k2

Thoma, B., Bird, T. A., Friend, D. J., Gearing, D. P., & Dower, S. K. (1994). Oncostatin M and leukemia inhibitory factor trigger overlapping and different signals through partially shared receptor complexes. *The Journal of Biological Chemistry*, *269*(8), 6215–6222.

Tsutsui, M., Hirase, R., Miyamura, S., Nagayasu, K., Nakagawa, T., Mori, Y., Shirakawa, H., & Kaneko, S. (2018). TRPM2 Exacerbates Central Nervous System Inflammation in Experimental Autoimmune Encephalomyelitis by Increasing Production of CXCL2 Chemokines. *Journal of Neuroscience*, *38*(39), 8484–8495. https://doi.org/10/gfcj4j

Valentine, T. R., Alschuler, K. N., Ehde, D. M., & Kratz, A. L. (2021). Prevalence, co-occurrence, and trajectories of pain, fatigue, depression, and anxiety in the year following multiple sclerosis diagnosis. *Multiple Sclerosis Journal*, 13524585211023352. https://doi.org/10/gksdsw

van Horssen, J., Brink, B. P., de Vries, H. E., van der Valk, P., & Bø, L. (2007). The blood-brain barrier in cortical multiple sclerosis lesions. *Journal of Neuropathology and Experimental Neurology*, *66*(4), 321–328. https://doi.org/10/bcqxfc

Vogel, D. Y., Vereyken, E. J., Glim, J. E., Heijnen, P. D., Moeton, M., van der Valk, P., Amor, S., Teunissen, C. E., van Horssen, J., & Dijkstra, C. D. (2013). Macrophages in inflammatory multiple sclerosis lesions have an intermediate activation status. *Journal of Neuroinflammation*, *10*, 35. https://doi.org/10/gmwscn

Wilkins, L. W. &. (2019). The prevalence of MS in the United States: A population-based estimate using health claims data. *Neurology*, *93*(15), 688–688. https://doi.org/10/gksdn8

Winkler, E. A., Sengillo, J. D., Bell, R. D., Wang, J., & Zlokovic, B. V. (2012). Blood–Spinal Cord Barrier Pericyte Reductions Contribute to Increased Capillary Permeability. *Journal of Cerebral Blood Flow & Metabolism*, *32*(10), 1841–1852. https://doi.org/10/gmx8qh

Woodberry, T., Bouffler, S. E., Wilson, A. S., Buckland, R. L., & Brüstle, A. (2018). The Emerging Role of Neutrophil Granulocytes in Multiple Sclerosis. *Journal of Clinical Medicine*, *7*(12), 511. https://doi.org/10/gk8g56

Wu, F., Cao, W., Yang, Y., & Liu, A. (2010). Extensive infiltration of neutrophils in the acute phase of experimental autoimmune encephalomyelitis in C57BL/6 mice. *Histochemistry and Cell Biology*, *133*(3), 313–322. https://doi.org/10.1007/s00418-009-0673-2

Yang, L., Froio, R. M., Sciuto, T. E., Dvorak, A. M., Alon, R., & Luscinskas, F. W. (2005). ICAM-1 regulates neutrophil adhesion and transcellular migration of TNF-α-activated vascular endothelium under flow. *Blood*, *106*(2), 584. https://doi.org/10.1182/BLOOD-2004-12-4942

Yazdani, S., Jaldin-Fincati, J. R., Pereira, R. V. S., & Klip, A. (2019). Endothelial cell barriers: Transport of molecules between blood and tissues. *Traffic*, *20*(6), 390–403. https://doi.org/10/ghvvp8

Yuk, C. M., Park, H. J., Kwon, B.-I., Lah, S. J., Chang, J., Kim, J.-Y., Lee, K.-M., Park, S.-H., Hong, S., & Lee, S.-H. (2017). Basophil-derived IL-6 regulates TH17 cell differentiation and CD4 T cell immunity. *Scientific Reports*, *7*(1), 41744. https://doi.org/10/f9nt2c

Zhang, X., Ing, S., Fraser, A., Chen, M., Khan, O., Zakem, J., Davis, W., & Quinet, R. (2013). Follicular helper T cells: New insights into mechanisms of autoimmune diseases. *The Ochsner Journal*, *13*(1), 131–139.

Zheng, P.-P., Romme, E., van der Spek, P. J., Dirven, C. M. F., Willemsen, R., & Kros, J. M. (2010). Glut1/SLC2A1 is crucial for the development of the blood-brain barrier in vivo. *Annals of Neurology*, *68*(6), 835–844. https://doi.org/10/cpb2n3

CHAPTER TWO: ONCOSTATIN M RECEPTOR KNOCKOUT AS A MODEL FOR STUDYING AUTOIMMUNE-MEDIATED BLOOD-BRAIN BARRIER DISRUPTION

Introduction

Given the complex and multi-system nature of blood-brain barrier disruption, multiple experimental modalities were employed to demonstrate the role of oncostatin M (OSM) during disease. By utilizing genetic manipulations and experimental autoimmune encephalomyelitis (EAE), a murine model of neuroinflammation, we were able to decipher cell-level biochemical responses to stimuli. By taking advantage of the physical properties of fluorescent molecules, we identified lesions and cell populations, and quantified inflammation. Finally, we extended our research to ex vivo analysis of highly purified transgenic blood-brain barrier endothelial cells, allowing for thorough cell-type specific analysis and identification of the main cellular players of neuroinflammatory-mediated blood-brain barrier disruption.

Transgenic Animals

All animal work was approved by the Boise State University Institutional Animal Care and Use Committee under protocols 006-AC16-011, AC19-013, AC19-014, and AC19-015. All experimental mice were genotyped by Transnetyx (Cordova, TN).

Oncostatin M Receptor Complete and Conditional Knockout

After initial experiments identified OSM as an endothelial pro-inflammatory mediator, we obtained oncostatin M receptor (OSMR) knockout ($OSMR^{KO}$) mice (B6.129S-Osmr<tm1Mtan>), a kind gift from Dr. Cheryl Jorcyk. While these mice have

altered hematopoiesis, by adulthood they show comparable peripheral leukocyte counts to wildtype C57BL/6 mice (Tanaka et al., 2003). Genotype of breeding mice were confirmed through polymerase chain reaction by Transnetyx (Cordova, TN).

Because OSMR is expressed by multiple cell types (T. J. Brown et al., 1987; Grenier et al., 1999; Hurst et al., 2002), we also obtained oncostatin M receptor floxed ($OSMR^{fl/fl}$) mice (Osmr<tm1.1Nat>/J) from The Jackson Laboratory (Stock #011081; Bar Harbor, ME) for future studies in tissue-specific targeted disruption OSMR.

Cre Drivers for Tissue Specific Knockout

Initially, a pan endothelial inducible Cre driver (EC^{Cre}, B6.Cg-Tg(Tek-cre/ERT2)1Arnd/ArndCnrm) was crossed to the reporter mouse line Ai14 (B6.Cg-Gt(ROSA)26Sor$^{tm14(CAG-tdTomato)Hze}$/J, The Jackson Laboratory Stock #007914), resulting in $EC^{Reporter}$ mice. After administration of tamoxifen, cells that express Cre will have a bright tdTomato fluorescent signal (**Figure 2.1**).

Because of Cre expression concerns, blood-brain barrier-specific inducible Cre mice (BBB^{Cre}, Tg(Slco1c1-icre/ERT2)1Mrks) were obtained, a kind gift of Dr. Markus Schwaninger of the Institute of Experimental and Clinical Pharmacology and Toxicology at the University of Lübeck, Germany. Breeding plans were designed so that Cre was passed on to approximately 50% of offspring, allowing for littermate experiments. These mice were also crossed with the Ai14 line, creating $BBB^{Reporter}$ mice. Breeding plans were designed so that Cre was passed on to approximately 50% of offspring, allowing for littermate experiments.

Cre(+) and Cre(-) littermates were aged to 30 days. Mice received twice-daily intraperitoneal injections of tamoxifen (20 mg/mL in 10% absolute ethanol USP, 90%

corn oil USP) at 20 mg/kg bodyweight for 5 days, for a total of 10 injections. After resting for 14 days, the mice were deeply anesthetized, and perfused with normal saline transcardially to remove all blood. The brain was sectioned into 100 μm slices with a vibratome. Slices from each genotype were post-stained with tomato lectin labeled with DyLight649 overnight, then washed 6 times for one hour each. Sections were then mounted in VECTASHIELD and imaged using the Zeiss 510 meta or Leica Stellaris 5 confocal microscope.

Confirmation of Inducible Knockout

To additionally quantify inducible tissue-specific knockout, mice from an adjacent research project were used: biglycan-floxed ($Bgn^{tm1.1Debi}$) mice were crossed with both EC^{Cre} and BBB^{Cre} lines. The resultant Cre(+) and Cre(-) mice were aged to 30 days. Mice received twice-daily intraperitoneal injections of tamoxifen (20 mg/mL in 10% absolute ethanol USP, 90% corn oil USP) at 50 mg/kg bodyweight for 5 days, for a total of 10 injections. After resting for 14 days, the mice were deeply anesthetized, and perfused with normal saline transcardially to remove all blood. The brain was processed to extract microvessels containing the BBB-ECs by homogenization with a dounce and centrifugation over a layer of 32% 70 kD *Leuconostoc* dextran (Sigma-Aldrich 313900) in HBSS. See *Microvessel Isolation*, below.

Microvessel DNA was isolated through hot sodium hydroxide lysis and neutralized with Tris hydrochloride (Truett et al., 2000). The crude DNA was then purified using a purification column (New England Biolabs T1030S), then quantified using a NanoDrop and normalized. The region around the excised portion of *bgn* was

amplified using DreamTaq according to manufacturer's directions, using the protocol in **Table 2.1** with the primers listed in **Table 2.2**.

Results

$EC^{Reporter}$ mice have very low Cre expression in the brain, approximately 10%, when comparing green reporter area to red microvessel area (**Figure 2.2 A**). By PCR, even less excision is noted when looking at *bgn* (**Figure 2.2 C**). Comparatively, $BBB^{Reporter}$ mice show high reporter signal are compared to red microvessel area (**Figure 2.2 B**). By PCR, knockout efficiency was found to be ~75% of *bgn* (**Figure 2.2 C**).

Importantly, Cre was found to be active only in those cells that were also stained with tomato lectin, a strong endothelial glycocalyx marker (Robertson et al., 2015) (**Figure 2.2 C**). Together, these data indicate that $OSMR^{fl/fl}$ mice will be a good candidate blood-brain barrier-specific OSMR-knockout experiments.

Experimental Autoimmune Encephalomyelitis

To provide relevant inflammatory processes, we employ experimental autoimmune encephalomyelitis (EAE). This model relies on Freund's adjuvant complete with killed mycobacterium tuberculosis, pertussis toxin, and myelin oligodendrocyte glycoprotein amino acids 35-55 (MOG_{35-55}) to provide a robust, reproducible inflammatory condition (S. D. Miller & Karpus, 2007). The disease is generally separated into multiple symptomatic stages: preclinical (days 0 – 7), where mice show no outward disease symptoms, but have significant immune activation; onset (days 7 – 12), where mice begin showing weakness at the tail, with infiltration increasing; acute (days 12 – 14), where paralysis is evident, and plateau, where the disease course has peaked, but resolution is not yet occurred. C57BL/6 mice exhibit a chronic model of EAE, where

mice only partially recover, and can remain symptomatic until euthanasia (**Table 2.3, Figure 2.3 A**) (Stromnes & Goverman, 2006a).

Cellularly, there are two major disease phases: the induction phase, where myelin specific $CD4^+$ T cells are created and primed, and the effector phase, where the immune compliment is activated, the blood-brain barrier is breached, and demyelination occurs (S. D. Miller & Karpus, 2007). Because of the potential for a knockout to modulate either phase, we examined each independently.

Adoptive transfer experimental autoimmune encephalomyelitis (AT-EAE) utilizes C57BL/6 mice to generate myelin specific $CD4^+$ T cells, forgoing the potential of genetic manipulations from modulating the induction phase. In brief, wildtype mice are induced with active EAE as above. At day 11 post induction, splenocytes are isolated and are cultured *ex vivo* with MOG_{35-55} to provide additional antigen, interleukin-12 to stimulate growth and activation, and anti-interferon gamma to further enhance proliferation (Stromnes & Goverman, 2006b; Thakker et al., 2007). The cells are then injected into mice with various genetic manipulations (**Figure 2.4**). Wildtype C57BL/6 mice present a similar experimental course to that of active EAE induction (**Figure 2.3 B**) (Stromnes & Goverman, 2006b).

Challenges Regarding Experimental Autoimmune Encephalomyelitis

Sex Variability in Incidence and Severity

Experimental autoimmune encephalomyelitis has variable incidence and severity based upon many factors, including murine strain and sex. Depending on the strain used, either sex exhibits greater incidence of the disease, however in C57BL/6 mice, there is no difference (Papenfuss et al., 2004). Female C57BL/6 mice appear to have greater severity

of EAE, including behavioral changes indicating pain (Rahn et al., 2014). As multiple sclerosis is noted to effect more women than men, using female mice for EAE studies is well supported (Duquette et al., 1992).

Stress and Immunomodulation

Mice experiencing stress have modulated immune responses, preventing the expected course of EAE from happening (Fournier et al., 2020; Pérez-Nievas et al., 2010). Generally, stress causes reduced symptoms, however there are some reports of mild stress worsening the EAE clinical course (Gerrard et al., 2017). There appears to be some differences based upon the type of EAE administered, the species used, or even the genetic background of the animal, however this is not well studied. No matter the reason, stressors must be well-controlled to prevent variability, including limited enrichment, unpredictable noises, and others (Fournier et al., 2020; Leigh et al., 2015; Wolf et al., 2018).

Non-Invasive Blood-Brain Barrier Permeability Assay

While the blood-brain barrier is normally impermeable to solutes, inflammation causes endothelial modulation of barrier function. Quantification of leak is achieved through the injection of fluorescent molecules. Serum and brain homogenate is collected from the mice, and the fluorescent concentration is measured by a standard plate reader to determine the permeability surface-area product, P_S (mg/mL), as in **Equation 2.1**, where C_b is the concentration of tracer in the brain per gram of brain weight, ${}_0\int^t$ is the integrated serum concentration per milliliter, and t is the time between injection and sample harvest (Bell et al., 2010; Mackic et al., 1998).

Equation 2.1

$$P_S = \frac{C_b}{\int_0^t C_p \times t}$$

This measurement is further enhanced using sized tracers. By conjugating fluorescent dye with large, inert molecules, the effective hydrodynamic radius is increased (Choi et al., 2010). When using tracers with distinct spectra, the relative size of perforations can be estimated (Bell et al., 2010; Saunders et al., 2015) (**Table 2.4**). Molecules that are small enough to pass through will be found readily in brain homogenate, where those that are too large will only be found in the serum (**Figure 2.5**).

Perivenular Inflammatory Lesion Analysis

During inflammatory injury, like experimental autoimmune encephalomyelitis and multiple sclerosis, activated leukocytes overcome the blood-brain barrier, and infiltrate into the brain parenchyma (Stromnes & Goverman, 2006b). This injury, called a perivenular inflammatory lesion (PIL), happens in the venules over the white matter in the cerebellum during early disease, however in advanced cases lesions can also be found in the vasculature of the white matter of the brain, the hippocampus, and the brainstem (Popescu et al., 2013; van Horssen et al., 2007). These PILs contain neutrophils, T cells, B cells, macrophages, and myelin fragments (De Bondt et al., 2020; Lassmann, 2018).

The number of lesions found is directly correlated with symptom severity and outcomes of the diseases: the more lesions a person has indicates the worse symptoms they will experience and the worse overall prognosis they have (Davda et al., 2019; Khoury & Weiner, 1998). The endothelium near the lesion likely remains leaky for months after the onset of the disease, highlighting the power of this measure (Trip & Miller, 2005). Therefore, the analysis of PILs as an outcome of genetic or pharmacologic intervention is well supported.

General Protocol

Mice are subjected to experimental autoimmune encephalomyelitis and allowed to age until the appropriate endpoint. After a surgical depth of anesthesia is reached, the mouse is immobilized in a supine position, and a transverse incision is made across the abdomen. After removing the diaphragm, 100 μL of Alexa fluor-conjugated tomato lectin is injected transcardially. The right atrium is removed, and a line containing 20 mL of sulfo-NHS biotin (0.3 mg/mL in PBS) is introduced at the same site and injected using a syringe pump to maintain consistent flow, followed by 20 mL of 4% paraformaldehyde in PBS. The brains are removed, sectioned, and counterstained with Texas red-conjugated streptavidin, and mounted as above.

Outcomes and Results

Brain sections imaged by confocal microscopy demonstrate consistent and thorough staining with tomato lectin, even in animals with EAE. Texas red signal, however, appears only over white matter regions that contain large (80 – 100 μm) vessels that are fed by smaller (10 – 30 μm) post-capillary venules. These lesions have low tomato lectin staining, indicating the potential loss of the endothelial glycocalyx. Similarly, the Texas red signal appears around the vasculature, and not in it, indicating the leak of the small molecule out of the vessel (**Figure 2.6**).

Microvessel and Brain Endothelial Cell Isolation

Purpose

Isolating the components of the neurovascular unit provides additional opportunities to establish the different cellular contributions to neuroinflammatory processes. Utilizing primary brain endothelial cells allows for the extension of *in vivo*

genetic manipulations to further analyze the signaling pathways and function of the blood-brain barrier.

Comparison of Primary Blood-Brain Barrier Endothelial Cells to Immortalized Blood-Brain Barrier Endothelial Cells

There are many commercially available BBB endothelial cell lines, including bEnd.3, cEND, hBEC-5i, and hBMEC, providing various systems for study. Because of their immortalization, however, these cells create additional challenges when analyzing tight junctions. bEnd.3, for example, are a mouse brain endothelial line derived from a benign endothelioma (Hallmann et al., 2000). While they express high levels of claudin 5, occludin staining is not localized to cell borders, but is rather found throughout the cytoplasm (R. C. Brown et al., 2007). The human hBEC-5i cell line was created by mixing pieces of cerebral cortex from deceased patients, and culturing the outgrowth; these cells do not exhibit contact inhibition, and will grow in layers on top of each other (Puech et al., 2018).

Immortalized cells have the advantage of being excellent candidates for genetic manipulations, with multiple manufacturers offering cell-line specific products for both electroporation-mediated transfection and liposome-mediated transfection. With the variety of genetically modified mice available, however, inducible manipulations using the Cre/Lox system via exogenous TAT-Cre are becoming more common (Kang et al., 2018; Sgolastra et al., 2018).

Need for Endothelial Cell Enrichment

As the endothelial cells lining the blood vessels contain tight interactions with both pericytes and astrocytes, the resultant cell pellet from the below protocol likely has a

mixture of cell types. Brain endothelial cells are unique in the neurovascular unit in that they express the P-glycoprotein efflux pump, providing them multidrug resistance to drugs like puromycin (Hamilton et al., 2001; Tatsuta et al., 1992). Therefore, positive selection may be carried out to create a highly-purified brain endothelial population (Watson et al., 2013).

General Protocol

This protocol is modified from Watson et al (2013). Mice are selected from pups between 7 and 10 days old, of the correct genotype. 10 pups produce enough endothelial cells to cover 25 cm^2. After decapitation, the heads of mice are sprayed with ethanol and moved into a biosafety cabinet. The skull is opened, and the meninges are cleared with a Kimwipe. The brains are removed with forceps and placed in 25 mL of sterile ice-cold isolation buffer (Hank's balanced salt solution (HBSS) with metal ions, 10 mM HEPES, 0.1% bovine serum albumin). Using a loose-fitting dounce (Kimble Chase KONTES, catalog 885300-0040), the suspension is ground until an even homogenate is formed, approximately 6 – 10 times. The homogenate is then transferred to a fresh 50 mL conical, and additional buffer is used to rinse the dounce.

After centrifuging the homogenate for 5 minutes at 500 RCF and 4 °C, the supernatant is removed. The pellet is then washed in 6 mL of phenol-free Dulbecco's modified Eagle medium (DMEM). After centrifuging for 5 minutes at 500 RCF and 4 °C, the supernatant is again removed. The pellet is then resuspended in prewarmed digestion buffer (2 mg/mL collagenase/dispase; 20 µg/mL DNAse I; in phenol-free DMEM), at an approximate 1:1 volume ratio, and slowly rotated for 30 minutes at 37 °C.

The homogenate is the centrifuged for 5 minutes at 500 RCF and 4 °C, and the supernatant is removed. 5 mL of prewarmed 22% bovine serum albumin (w/v in HBSS) is mixed with the pellet. After centrifugation for 7 minutes at 3000 RCF the supernatant with top cell layer is placed into a fresh 15 mL conical. The pellet is resuspended in 1 mL warm DMEM. The resulting supernatant can be centrifuged an additional two times using this method to increase yield, with pellets being combined into DMEM.

The conical containing the combined pellets is then filled with additional DMEM and centrifuged for 5 minutes at 500 RCF and 37 °C. After supernatant removal, 500 µL of warm digestion buffer is added, and the n incubated at 37 °C for 25 minutes. The cells are then centrifuged for 5 minutes at 500 RCF and 37 °C, and the supernatant removed. The pellet is resuspended in 5 mL of complete primary endothelial cell media (CellBiologics M1168) with 3 µM puromycin to select against any non-endothelial cells remaining (Perrière et al., 2005; Watson et al., 2013). The cells are then plated into collagen IV-coated (1 µg/cm^2) cultureware. For the first three days post-seeding, the cells are carefully washed with warm HBSS during the media change. Puromycin is maintained a for the first 7 days, then is no longer included. The endothelial cells are allowed to mature for 7 – 10 days before experimentation.

Outcomes and Results

The resultant cell monolayers express high levels of tight junction proteins claudin 5 and occludin (Beard Jr. et al., 2018; Watson et al., 2013). They also exhibit low permeability to small molecules, providing a physiologically relevant *in* vitro blood-brain barrier model (Watson et al., 2013).

ECIS-TEER

Electric Cell-Substrate Impedance Sensing

Electric Cell-Substrate Impedance Sensing (ECIS) allows for the real-time and continuous monitoring of barrier function of cell monolayers (Szulcek et al., 2014). Because monolayers that form tight junctions restrict ion movement, the function of the barrier can be assessed through the measurement of AC current flow at 4000 Hz (Anderson & Van Itallie, 2009) (**Figure 2.7 A**).

ECIS is used extensively in the analysis of blood-brain barrier function. Our lab has previously utilized this tool to measure the effects of various siRNAs, inflammatory cytokines, hormones, and pharmacologic interventions on endothelial function (Beard Jr. et al., 2018).

General Protocol

ECIS arrays are washed with 10 mM L-cysteine in water to stabilize the gold electrodes (Szulcek et al., 2014). The array is then coated with collagen IV (1 $\mu g/cm^2$). Brain microvascular endothelial cells are seeded at confluence and allowed to sit at room temperature for 15 minutes to for even seeding. The cells are allowed to mature for 7 – 10 days before experimentation (Beard Jr. et al., 2018).

Outcomes and Results

Because ECIS allows continuous monitoring, a tracing is generated, granting the correlation of time to all measurements (**Figure 2.7 B**). This especially gives insight into the determination of regulatory mechanisms: is barrier function reduced due to tight junction protein rearrangement – a relatively fast and transient method – or

through expression modifications, which is decidedly slower (A. T. Bauer et al., 2010; Beard Jr. et al., 2018; Beard et al., 2014).

Table 2.1 Thermocycling Protocol

Step	Temperature	Time
1.	95 ℃	3 minutes
2.	95 ℃	30 seconds
3.	60 ℃	60 seconds
4.	72 ℃	1 minute
5.	Repeat steps 2 – 4 x 25	
6.	72 ℃	5 minutes

Table 2.2 bgn Excision Primers

Gene	Sequence (5' to 3')	Size (bp)
Bgn Floxed	GTG TGC CTC AGA ATG TTC CA CTC AGT CCA GTC GGT GTC CT	Floxed: 248 Wildtype: 179
Bgn Excised	GAG CCA GGA GGA GTT TGA TG CTC AGT CCA GTC GGT GTC CT	Floxed: 1195 Wildtype: 978 Excised: 414

Table 2.3 Modified Experimental Autoimmune Encephalomyelitis Scoring (Stromnes & Goverman, 2006a)

Score	Observation
0	No Symptoms
1	Tail paralysis
2	Tail paralysis and hind limb weakness
3	Tail paralysis and hind limb paralysis
4	Tail paralysis, hind limb paralysis, front limb weakness
5	Found dead

Table 2.4 Commonly Used Tracers

Tracer	Radius (nm)	Spectrum (Ex/Em)	Citation
AF-647-Dextran 10 kD	~3.0	650/668	(Zeini et al., 2021)
Evans Blue	1.3*	620/680	(Bohne et al., 2003)
FITC-Dextran 4 kD	~1.4	495/519	(Shi, Zeng, et al., 2014)
Sodium Fluorescein	0.502	490/525	(Mustafa et al., 1993)
TRITC-Dextran 155 kD	~8.5	544/570	(Shi, Palacio-Mancheno, et al., 2014)

* There is some discussion on the appropriateness of Evans blue, and its potential to bind albumin, causing a major shift in the hydrodynamic radius of the molecule (Saunders et al., 2015).

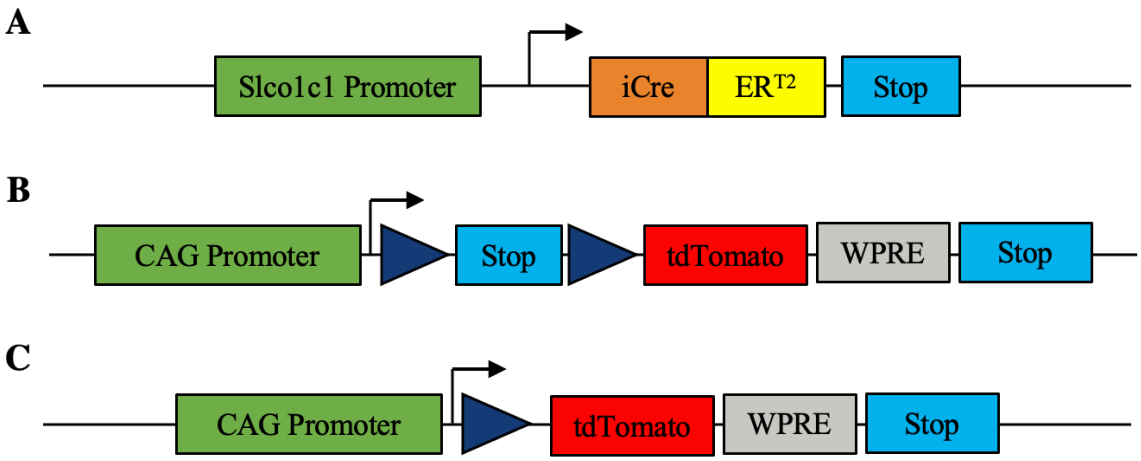

Figure 2.1 B6.Cg-Gt(ROSA)26Sor$^{tm14(CAG-tdTomato)Hze}$/J Gene Plan.

A) Cre is randomly inserted in the mouse genome under the control of the Slco1c1 promoter (green). Because Cre (orange) is bound to an estrogen type II (yellow) receptor, it is bound in the nuclear envelope. Upon administration of tamoxifen, a synthetic estrogen, Cre translocates into the nucleus and acts to remove the sequence between two *lox* sites. **B)** A cassette containing the synthetic CAG promoter (green), a lox-stop-lox sequence (dark blue, blue, dark blue), the coding for tdTomato (red) and the WPRE enhancer (gray) was placed in the ROSA26 locus. Under normal conditions, tdTomato is not expressed. **C)** After tamoxifen administration the stop codons and one lox site are removed, allowing the CAG promoter (green) to act upon tdTomato (red), producing a bright fluorescent signal in those cells where Cre was produced. Adapted from (Madisen et al., 2010).

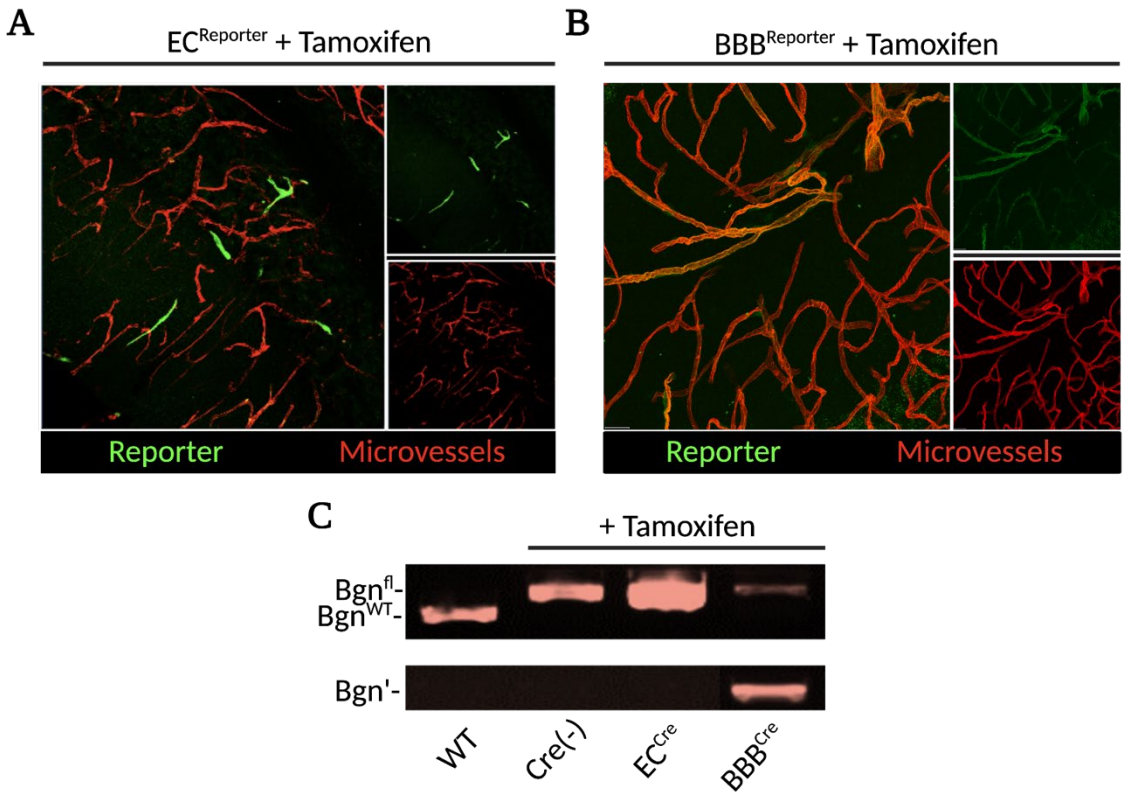

Figure 2.2 Efficiency of Cre recombinase in Endothelial-Specific and Blood-Brain Barrier-Specific Mouse Lines.

All mice received twice-daily intraperitoneal injections of tamoxifen (20 mg/mL in 10% absolute ethanol USP, 90% corn oil USP) at 20 mg/kg bodyweight for 5 days, for a total of 10 injections. **A)** $EC^{Reporter}$ mice show recombination-positive tdTomato (green) signal in approximately 10% of tomato lectin (red) brain capillaries as analyzed by confocal imaging. In contrast, **B)** $BBB^{Reporter}$ mice show tdTomato (green) in nearly 100% of tomato lectin (red) brain capillaries. **C)** Similarly, when analyzing PCR products from isolated microvessels from mice, WT mice show no recombination. Cre(-) Biglycan(fl/fl) mice show no recombination (Bgn`); pan-endothelial Cre(+) Biglycan(fl/fl) mice have undetectable recombination; and blood-brain barrier endothelial Cre(+) Biglycan(fl/fl) mice have approximately 75% recombination. Created with Biorender.com

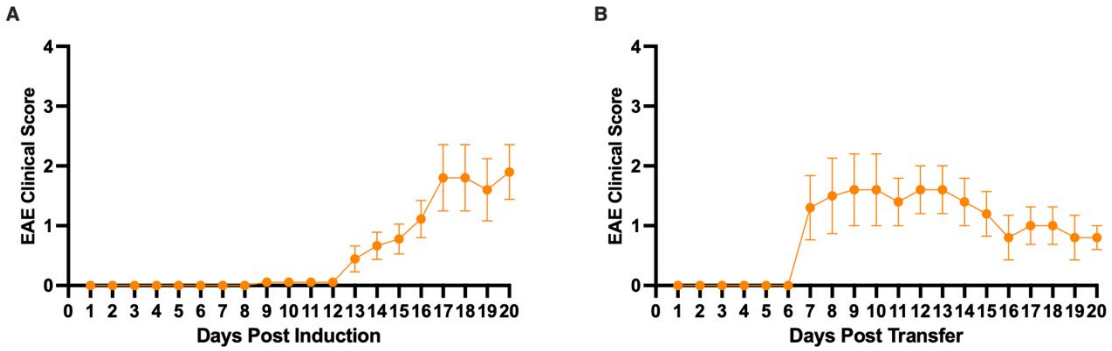

Figure 2.3 Normal presentation of active and adoptive transfer experimental autoimmune encephalomyelitis in wildtype C57BL/6 Mice.

A) In wild type mice with active experimental autoimmune encephalomyelitis, symptom onset begins days 7 – 12. Acute phase occurs during the steep incline and leads to peak symptoms. The clinical score levels, but generally does not return to lower scores. Data is representative of 5 mice ± standard deviation. **B)** In adoptive transfer EAE, mice generally get symptoms earlier. Pre-onset happens during days 6 – 10, and mice reach peak scores within approximately 24 hours. Mice have a reduction in symptoms over the next 14 days, but do not fully recover. Data is representative of mean score of 5 mice ± standard error of the mean.

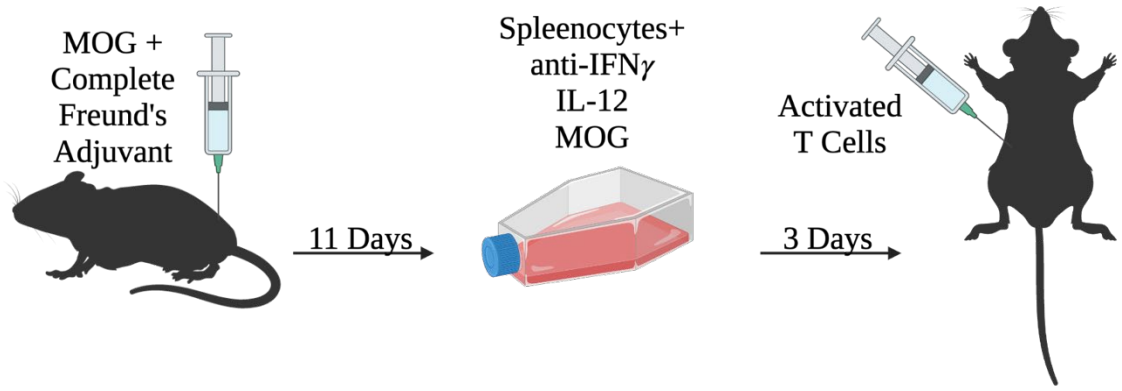

Figure 2.4 Experimental preparation of adoptive transfer experimental autoimmune encephalomyelitis.

Wildtype mice are injected with MOG_{35-55} in complete Freund's adjuvant. After 11 days, spleen cells are isolated and cultured with additional MOG_{35-55}, IL-12, and anti-IFNγ. After 3 days of activation, the cells are then injected intraperitoneally into mice with the genotype of interest. Created with Biorender.com

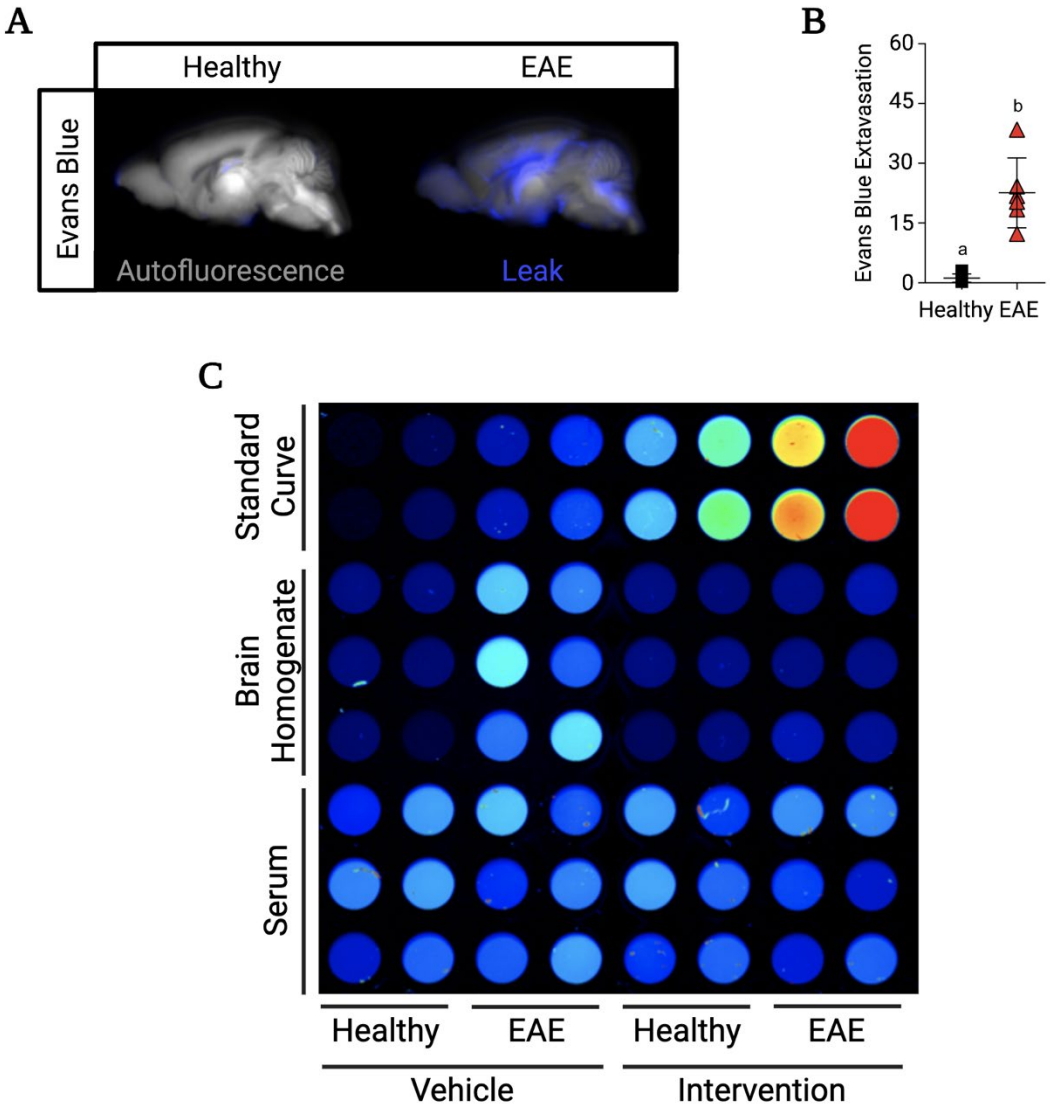

Figure 2.5 Quantification of Blood-Brain Barrier Solute Permeability during Experimental Autoimmune Encephalomyelitis.

A) Qualitative comparison of plasma protein leakage by Evans blue assay in healthy mock-EAE right hemisphere and EAE right hemisphere. Measured using LI-COR Odyssey CLx; Evans blue at 700 nm is pseudo colored blue, myelin autofluorescence at 800 nm is pseudo colored gray. Adapted from (Beard Jr. et al., 2018). **B)** Quantitative results of Evans blue permeability assay. Mice with active EAE (n = 6) at 8 days post injection have significantly increased permeability to Evans blue compared to healthy (n = 5) animals. Graph is represented as dot plot with mean ± standard deviation.

Adapted from (Beard Jr. et al., 2018). **C)** Representative standard curve, serum samples, and brain homogenates (n=6 per group) of Evans blue permeability assay measured by LI-COR Odyssey CLx at 700 nm at 8 days post injection. Healthy animals show low concentrations of Evans blue in brain homogenate compared to vehicle-treated mice with EAE, who show high permeability. Administration of DMAQ-B1, an AKT2-dependant claudin-5 modulator, rescues blood-brain barrier permeability (Beard Jr. et al., 2018). Created with BioRender.com

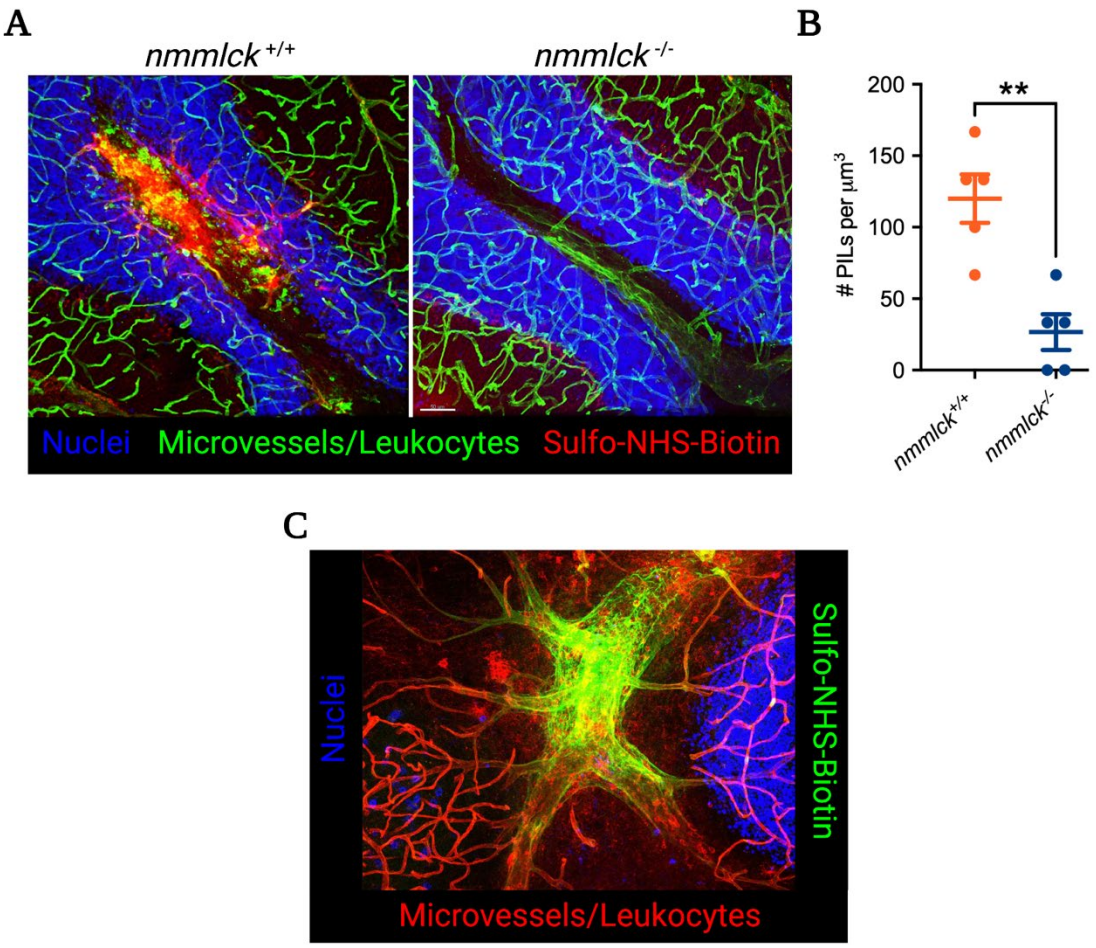

Figure 2.6 Analysis of Perivenular Inflammatory Lesions

A) Perivenular inflammatory lesions (PILs) appear as sulfo-NHS-biotin (red) positive regions in the venules (green) supporting white matter when assessed via confocal microscopy. **B)** Wild type mice get significantly more PILs during the effector phase of experimental autoimmune encephalomyelitis compared to *nmmlck*$^{-/-}$ mice, a related model that our lab uses. PILs are counted via confocal microscopy, where the surface area of brain sections is quantified. **C)** Zooming in on an individual PIL shows loss of tomato lectin microvessel staining (red), and a diffuse ring around the venule of sulfo-NHS-biotin (green), highlighting the leak outside of the vessel. PIL count

represented as mean ± standard deviation of midsagittal brain slice of 5 mice per genotype. ** = $p < 0.05$ by Mann-Whitney test. Created with Biorender.com

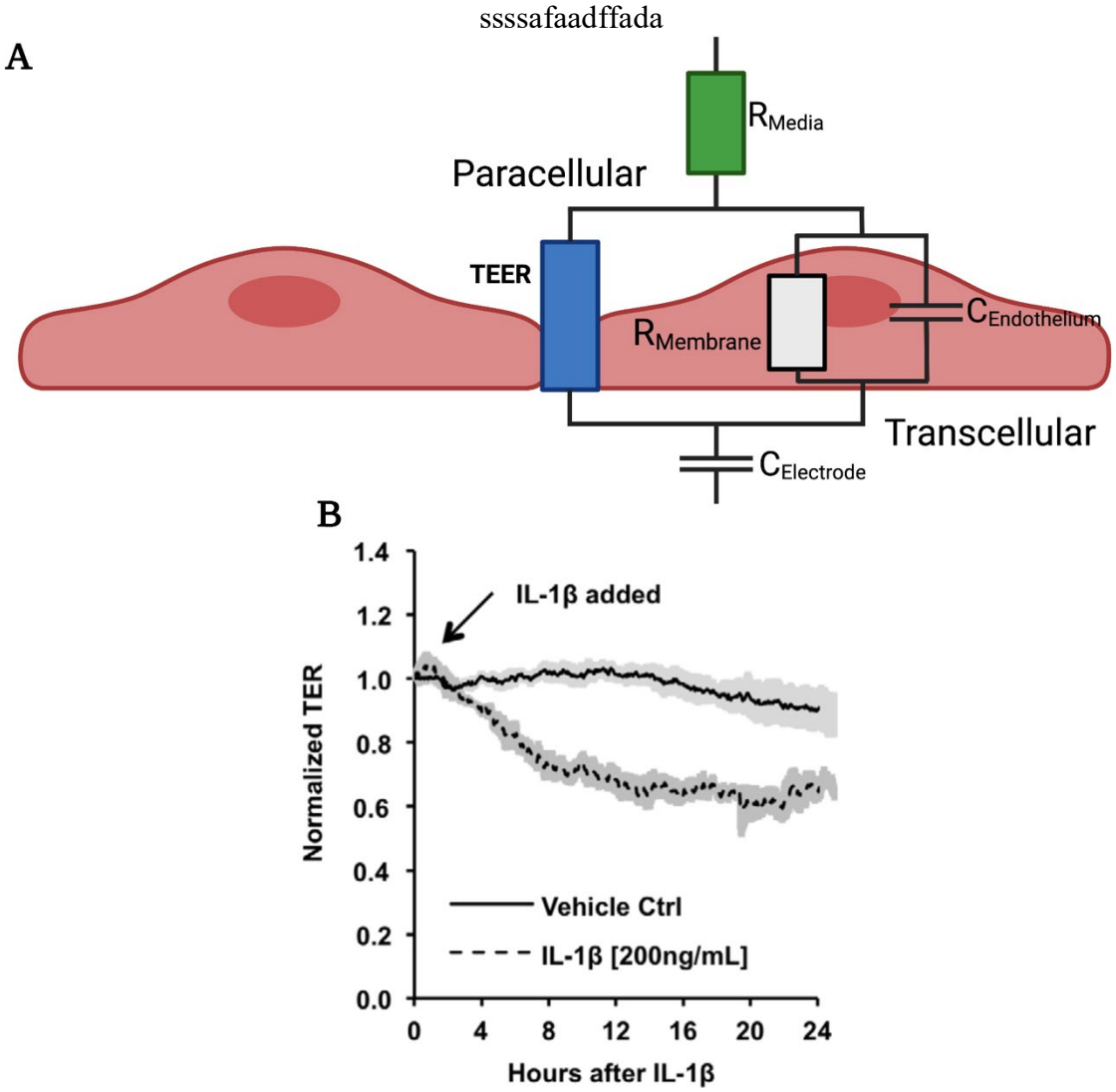

Figure 2.7 Electronic Cell-Substrate Impedance Sensing (ECIS) as a Measure of Endothelial Barrier Function.

A) A generalized circuit diagram of resistance pathways in endothelial monolayers. Tight junctions modulate trans-endothelial electrical resistance (TEER, blue) through paracellular routes; however, the media (green) can further affect this measure. Similarly, the resistance of the transcellular pathway is modulated by the composition of

the membrane, including lipids and ion channels (gray). The ECIS software tunes the frequency of the device to separate out the paracellular from the transcellular routes, where low frequencies of alternating current (approximately 4000 Hz) test paracellular impedance and higher frequencies (up to 25,000 Hz) assess transcellular impedance. Finally, using software modeling, the capacitance is removed, providing a measure of barrier function as resistance (Giaever & Keese, 1991). Adapted from (Benson et al., 2013). **B)** TEER, and therefore barrier function, is lost over 24 hours after the addition of interleukin-1β, a commonly used positive control for endothelial barrier dysfunction. Tracing is the mean resistance normalized to time 0. Shading indicates the standard error of the mean. Figure adapted from (Beard et al., 2014). Created with Biorender.com

References

Anderson, J. M., & Van Itallie, C. M. (2009). Physiology and Function of the Tight Junction. Cold Spring Harbor Perspectives in Biology, 1(2), a002584. https://doi.org/10/db696x

Bauer, A. T., Bürgers, H. F., Rabie, T., & Marti, H. H. (2010). Matrix metalloproteinase-9 mediates hypoxia-induced vascular leakage in the brain via tight junction rearrangement. *Journal of Cerebral Blood Flow and Metabolism: Official Journal of the International Society of Cerebral Blood Flow and Metabolism*, *30*(4), 837–848. https://doi.org/10/ckmwvp

Beard Jr., R. S., Hoettels, B. A., Meegan, J. E., Wertz, T. S., Cha, B. J., Yang, X., Oxford, J. T., Wu, M. H., & Yuan, S. Y. (2018). AKT2 maintains brain endothelial claudin-5 expression and selective activation of IR/AKT2/FOXO1-signaling reverses barrier dysfunction. *Journal of Cerebral Blood Flow & Metabolism*, 0271678X1881751. https://doi.org/10.1177/0271678X18817512

Beard, R. S., Haines, R. J., Wu, K. Y., Reynolds, J. J., Davis, S. M., Elliott, J. E., Malinin, N. L., Chatterjee, V., Cha, B. J., Wu, M. H., & Yuan, S. Y. (2014). Non-muscle Mlck is required for -catenin- and FoxO1-dependent downregulation of Cldn5 in IL-1 -mediated barrier dysfunction in brain endothelial cells. *Journal of Cell Science*, *127*(8), 1840–1853. https://doi.org/10.1242/jcs.144550

Bell, R. D., Winkler, E. A., Sagare, A. P., Singh, I., LaRue, B., Deane, R., & Zlokovic, B. V. (2010). Pericytes control key neurovascular functions and neuronal phenotype in the adult brain and during brain aging. *Neuron*, *68*(3), 409–427. https://doi.org/10/c9kwmq

Benson, K., Cramer, S., & Galla, H.-J. (2013). Impedance-based cell monitoring: Barrier properties and beyond. *Fluids and Barriers of the CNS*, *10*(1), 5. https://doi.org/10/f4j8p3

Brown, T. J., Lioubin, M. N., & Marquardt, H. (1987). Purification and characterization of cytostatic lymphokines produced by activated human T lymphocytes. Synergistic antiproliferative activity of transforming growth factor beta 1, interferon-gamma, and oncostatin M for human melanoma cells. *Journal of Immunology (Baltimore, Md.: 1950)*, *139*(9), 2977–2983.

Davda, N., Tallantyre, E., & Robertson, N. P. (2019). Early MRI predictors of prognosis in multiple sclerosis. *Journal of Neurology*, *266*(12), 3171–3173. https://doi.org/10/gmz628

De Bondt, M., Hellings, N., Opdenakker, G., & Struyf, S. (2020). Neutrophils: Underestimated Players in the Pathogenesis of Multiple Sclerosis (MS). *International Journal of Molecular Sciences*, *21*(12), 4558. https://doi.org/10/gksp7p

de Vries, H. E., Kuiper, J., Boer, A. G. de, Berkel, T. J. C. V., & Breimer, D. D. (1997). The Blood-Brain Barrier in Neuroinflammatory Diseases. *Pharmacological Reviews*, *49*(2), 143–156.

Duquette, P., Pleines, J., Girard, M., Charest, L., Senecal-Quevillon, M., & Masse, C. (1992). The Increased Susceptibility of Women to Multiple Sclerosis. *Canadian Journal of Neurological Sciences*, *19*(4), 466–471. https://doi.org/10/gmqhtm

Fournier, A. P., Baudron, E., Wagnon, I., Aubert, P., Vivien, D., Neunlist, M., Bardou, I., & Docagne, F. (2020). Environmental enrichment alleviates the deleterious effects of stress in experimental autoimmune encephalomyelitis. *Multiple Sclerosis Journal - Experimental, Translational and Clinical*, *6*(4), 2055217320959806. https://doi.org/10/gmqhsz

Gerrard, B., Singh, V., Babenko, O., Gauthier, I., Wee Yong, V., Kovalchuk, I., Luczak, A., & Metz, G. A. S. (2017). Chronic mild stress exacerbates severity of experimental autoimmune encephalomyelitis in association with altered non-coding RNA and metabolic biomarkers. *Neuroscience*, *359*, 299–307. https://doi.org/10/gbt6t8

Giaever, I., & Keese, C. R. (1991). Micromotion of mammalian cells measured electrically. *Proceedings of the National Academy of Sciences*, *88*(17), 7896–7900. https://doi.org/10/fxgwbx

Grenier, A., Dehoux, M., Boutten, A., Arce-Vicioso, M., Durand, G., Gougerot-Pocidalo, M. A., & Chollet-Martin, S. (1999). Oncostatin M production and regulation by human polymorphonuclear neutrophils. *Blood*, *93*(4), 1413–1421.

Hallmann, R., Savigni, D. L., Morgan, E. H., & Baker, E. (2000). Characterization of iron uptake from transferrin by murine endothelial cells. *Endothelium: Journal of Endothelial Cell Research*, *7*(2), 135–147. https://doi.org/10/gmztzs

Hamilton, K. O., Backstrom, G., Yazdanian, M. A., & Audus, K. L. (2001). P-glycoprotein efflux pump expression and activity in Calu-3 cells. *Journal of Pharmaceutical Sciences*, *90*(5), 647–658. https://doi.org/10/fq82dg

Hurst, S. M., McLoughlin, R. M., Monslow, J., Owens, S., Morgan, L., Fuller, G. M., Topley, N., & Jones, S. A. (2002). Secretion of oncostatin M by infiltrating neutrophils: Regulation of IL-6 and chemokine expression in human mesothelial cells. *Journal of Immunology (Baltimore, Md.: 1950)*, *169*(9), 5244–5251. https://doi.org/10/gkm6mb

Kang, Q., Sun, Z., Zou, Z., Wang, M., Li, Q., Hu, X., & Li, N. (2018). Cell-penetrating peptide-driven Cre recombination in porcine primary cells and generation of marker-free pigs. *PLOS ONE*, *13*(1), e0190690. https://doi.org/10/gcsr2j

Khoury, S. J., & Weiner, H. L. (1998). Multiple Sclerosis: What Have We Learned From Magnetic Resonance Imaging Studies? *Archives of Internal Medicine*, *158*(6), 565–573. https://doi.org/10/dc74bh

Lassmann, H. (2018). Multiple Sclerosis Pathology. *Cold Spring Harbor Perspectives in Medicine*, *8*(3), a028936. https://doi.org/10/gcv3hm

Leigh, N. D., Kokolus, K. M., O'Neill, R. E., Du, W., Eng, J. W.-L., Qiu, J., Chen, G. L., McCarthy, P. L., Farrar, J. D., Cao, X., & Repasky, E. A. (2015). Housing Temperature-Induced Stress Is Suppressing Murine Graft-versus-Host Disease through β2-Adrenergic Receptor Signaling. *Journal of Immunology (Baltimore, Md. : 1950)*, *195*(10), 5045–5054. https://doi.org/10.4049/jimmunol.1500700

Mackic, J. B., Weiss, M. H., Miao, W., Kirkman, E., Ghiso, J., Calero, M., Bading, J., Frangione, B., & Zlokovic, B. V. (1998). Cerebrovascular Accumulation and Increased Blood-Brain Barrier Permeability to Circulating Alzheimer's Amyloid β Peptide in Aged Squirrel Monkey with Cerebral Amyloid Angiopathy. *Journal of Neurochemistry*, *70*(1), 210–215. https://doi.org/10/c9j93s

Madisen, L., Zwingman, T. A., Sunkin, S. M., Oh, S. W., Zariwala, H. A., Gu, H., Ng, L. L., Palmiter, R. D., Hawrylycz, M. J., Jones, A. R., Lein, E. S., & Zeng, H. (2010). A robust and high-throughput Cre reporting and characterization system for the whole mouse brain. *Nature Neuroscience*, *13*(1), 133–140. https://doi.org/10.1038/nn.2467

Miller, S. D., & Karpus, W. J. (2007). Experimental autoimmune encephalomyelitis in the mouse. *Current Protocols in Immunology*, *Chapter 15*, Unit 15.1. https://doi.org/10/b36256

Papenfuss, T. L., Rogers, C. J., Gienapp, I., Yurrita, M., McClain, M., Damico, N., Valo, J., Song, F., & Whitacre, C. C. (2004). Sex differences in experimental autoimmune encephalomyelitis in multiple murine strains. *Journal of Neuroimmunology*, *150*(1–2), 59–69. https://doi.org/10/c4d477

Pérez-Nievas, B. G., García-Bueno, B., Madrigal, J. L., & Leza, J. C. (2010). Chronic immobilisation stress ameliorates clinical score and neuroinflammation in a MOG-induced EAE in Dark Agouti rats: Mechanisms implicated. *Journal of Neuroinflammation*, *7*(1), 60. https://doi.org/10/fnvb8f

Perrière, N., Demeuse, P., Garcia, E., Regina, A., Debray, Andreux, J., Couvreur, P., Scherrmann, J., Temsamani, J., Couraud, P., Deli, M., & Roux, F. (2005). Puromycin-based purification of rat brain capillary endothelial cell cultures. Effect on the expression of blood-brain barrier-specific properties. *Journal of Neurochemistry*, *93*(2). https://doi.org/10.1111/j.1471-4159.2004.03020.x

Popescu, B. F. Gh., Pirko, I., & Lucchinetti, C. F. (2013). Pathology of Multiple Sclerosis: Where Do We Stand? *Continuum : Lifelong Learning in Neurology*, *19*(4 Multiple Sclerosis), 901–921. https://doi.org/10/ggn57t

Puech, C., Hodin, S., Forest, V., He, Z., Mismetti, P., Delavenne, X., & Perek, N. (2018). Assessment of HBEC-5i endothelial cell line cultivated in astrocyte conditioned medium as a human blood-brain barrier model for ABC drug transport studies. *International Journal of Pharmaceutics*, *551*(1–2), 281–289. https://doi.org/10/gfdmz7

Rahn, E. J., Iannitti, T., Donahue, R. R., & Taylor, B. K. (2014). Sex differences in a mouse model of multiple sclerosis: Neuropathic pain behavior in females but not males and protection from neurological deficits during proestrus. *Biology of Sex Differences*, *5*, 4. https://doi.org/10/gb9g3j

Robertson, R. T., Levine, S. T., Haynes, S. M., Gutierrez, P., Baratta, J. L., Tan, Z., & Longmuir, K. J. (2015). Use of labeled tomato lectin for imaging vasculature structures. *Histochemistry and Cell Biology*, *143*(2), 225–234. https://doi.org/10/f6w596

Saunders, N. R., Dziegielewska, K. M., Møllgård, K., & Habgood, M. D. (2015). Markers for blood-brain barrier integrity: How appropriate is Evans blue in the twenty-first century and what are the alternatives? *Frontiers in Neuroscience*, *9*. https://doi.org/10/gj3vq8

Sgolastra, F., Kuksin, C. A., Gonzalez-Perez, G., Minter, L. M., & Tew, G. N. (2018). Enhanced TAT-Cre Protein Transduction for Efficient Gene Recombination in T cells. *ACS Applied Bio Materials*, *1*(2), 444–451. https://doi.org/10/gmzt2s

Stromnes, I. M., & Goverman, J. M. (2006a). Active induction of experimental allergic encephalomyelitis. *Nature Protocols*, *1*(4), 1810–1819. https://doi.org/10/fhgg3p

Stromnes, I. M., & Goverman, J. M. (2006b). Passive induction of experimental allergic encephalomyelitis. *Nature Protocols*, *1*(4), 1952–1960. https://doi.org/10/b48w6x

Szulcek, R., Bogaard, H. J., & van Nieuw Amerongen, G. P. (2014). Electric Cell-substrate Impedance Sensing for the Quantification of Endothelial Proliferation, Barrier Function, and Motility. *Journal of Visualized Experiments : JoVE*, *85*, 51300. https://doi.org/10/gk4qsj

Tanaka, M., Hirabayashi, Y., Sekiguchi, T., Inoue, T., Katsuki, M., & Miyajima, A. (2003). Targeted disruption of oncostatin M receptor results in altered hematopoiesis. *Blood*, *102*(9), 3154–3162. https://doi.org/10.1182/blood-2003-02-0367

Tatsuta, T., Naito, M., Oh-hara, T., Sugawara, I., & Tsuruo, T. (1992). Functional involvement of P-glycoprotein in blood-brain barrier. *The Journal of Biological Chemistry*, *267*(28), 20383–20391.

Thakker, P., Leach, M. W., Kuang, W., Benoit, S. E., Leonard, J. P., & Marusic, S. (2007). IL-23 Is Critical in the Induction but Not in the Effector Phase of Experimental Autoimmune Encephalomyelitis. *The Journal of Immunology*, *178*(4), 2589–2598. https://doi.org/10.4049/jimmunol.178.4.2589

Trip, S. A., & Miller, D. H. (2005). Imaging in multiple sclerosis. *Journal of Neurology, Neurosurgery & Psychiatry*, *76*(suppl 3), iii11–iii18. https://doi.org/10/dtw46f

Truett, G. E., Heeger, P., Mynatt, R. L., Truett, A. A., Walker, J. A., & Warman, M. L. (2000). Preparation of PCR-quality mouse genomic DNA with hot sodium hydroxide and tris (HotSHOT). *BioTechniques*, *29*(1), 52, 54. https://doi.org/10/gfkmx7

van Horssen, J., Brink, B. P., de Vries, H. E., van der Valk, P., & Bø, L. (2007). The blood-brain barrier in cortical multiple sclerosis lesions. *Journal of Neuropathology and Experimental Neurology*, *66*(4), 321–328. https://doi.org/10/bcqxfc

Watson, P. M. D., Paterson, J. C., Thom, G., Ginman, U., Lundquist, S., & Webster, C. I. (2013). Modelling the endothelial blood-CNS barriers: A method for the production of robust in vitro models of the rat blood-brain barrier and blood-spinal cord barrier. *BMC Neuroscience*, *14*, 59. https://doi.org/10/gb5hvd

Wolf, G., Lifschytz, T., Ben-Ari, H., Tatarskyy, P., Merzel, T. K., Lotan, A., & Lerer, B. (2018). Effect of chronic unpredictable stress on mice with developmental under-expression of the Ahi1 gene: Behavioral manifestations and neurobiological correlates. *Translational Psychiatry*, *8*(1), 1–11. https://doi.org/10/gdt8kt

Yuan, S. Y., & Rigor, R. R. (2010). *Regulation of Endothelial Barrier Function*. Morgan & Claypool Life Sciences. https://doi.org/10.4199/C00025ED1V01Y201101ISP013

Zeini, D., Glover, J. C., Knudsen, K. D., & Nyström, B. (2021). Influence of Lysine and TRITC Conjugation on the Size and Structure of Dextran Nanoconjugates with Potential for Biomolecule Delivery to Neurons. *ACS Applied Bio Materials*. https://doi.org/10/gms2t5

CHAPTER THREE: THE CONTRIBUTION OF NEUTROPHIL-DERIVED ONCOSTATIN M TO BLOOD-BRAIN BARRIER DYSFUNCTION

Abstract

Background

Blood-brain barrier (BBB) dysfunction is correlated with many pervasive diseases, including multiple sclerosis (MS). This study characterizes the role of oncostatin M (OSM), a pluripotent cytokine, during the effector phase of experimental autoimmune encephalomyelitis (EAE), a murine model of neuroinflammation.

Methods

The progression of EAE was compared using wildtype and transgenic *osmr*$\beta^{-/-}$ mice, measuring BBB solute extravasation, and microvessel tight junction mRNA changes. *In vitro*, cell culture studies were utilized to assess the role of OSM in decreasing tight junction expression, inducing permeability, and leukocyte extravasation. Electric cell-substrate impedance sensing was completed to determine the dose-response and temporal relationship of primary cultured brain microvascular endothelial cells to OSM.

Results

We found that OSM signaling through the OSMR receptor on BBB endothelial cells selectively causes downregulation of the tight junction protein occludin- without modulating claudin 5- causing increases in permeability both *in vivo* and *in vitro*. This BBB

dysfunction allows neutrophil transmigration, with subsequent demyelination and neurological deficits.

Conclusions

Together, our findings define a physiologically relevant role of oncostatin M in blood-brain barrier dysfunction and neutrophil transmigration during the effector phase of EAE.

Introduction

Barrier integrity of the brain vasculature is maintained through complex regulation of endothelial cell-cell tight junction proteins (Yuan & Rigor, 2010). These proteins – namely the claudin and tight junction associated MARVEL protein (TAMP) families, among others, allow the endothelium to precisely control the extra-vascular environment, including solutes, pathogens, and leukocytes (Anderson & Van Itallie, 2009; Daneman & Prat, 2015; Yazdani et al., 2019). Pathologies of the blood-brain barrier precede many neurodegenerative disorders including Alzheimer's, stroke, traumatic brain injury, and multiple sclerosis (Campos-Bedolla et al., 2014; Davda et al., 2019; Rosenberg, 2012).

During inflammation, BBB protein expression can be altered, allowing leakage of potentially neurotoxic substances (Beard Jr. et al., 2018; Errede et al., 2012). Specifically, in neuroinflammatory diseases such as multiple sclerosis (MS), a host of barrier-diminishing factors are responsible for this change (Ortiz et al., 2014; Petermann & Korn, 2011). One potential agent is the cytokine oncostatin M (OSM), which has been found in increased concentrations in MS patients' plasma; similarly, MS brain lesions have shown

OSM reactivity (Alikhani et al., 2014; Ruprecht et al., 2001). The source of OSM, however, has thus far remained elusive (Alikhani et al., 2014; Janssens et al., 2015).

Leukocytosis – a condition in where the total number of circulating leukocytes increases to pathological levels – has been considered a sign of multiple sclerosis since at least 1930 (McKenna, 1930). A host of factors cause this increase, with neutrophils having the most marked expansion (Caravagna et al., 2018; D'Amico et al., 2019). Neutrophils are well known producers of oncostatin M, and thus present as a promising source of the cytokine (Elbjeirami et al., 2011; Setiadi et al., 2019).

Neutrophils are activated by a host of immunomodulators, like granulocyte-monocyte-colony stimulating factor (GM-CSF), which has recently been found to be significantly upregulated during neuroinflammatory disease (Monaghan & Wan, 2020; Woodberry et al., 2018). GM-CSF, likely released from the inflamed endothelium, causes a rapid neutrophil-maturation from bone marrow stem cells, and upregulation of granule-bound inflammatory factors in circulating neutrophils. (Elbjeirami et al., 2011).

Experimental autoimmune encephalomyelitis (EAE), a murine model of multiple sclerosis, recapitulates this multi-tissue inflammatory cascade (Aubé et al., 2014; S. D. Miller & Karpus, 2007; Siffrin et al., 2010). Infiltration of neutrophils into the central nervous system (CNS) parenchyma has been found to be important for the pathogenesis of early stages of EAE: before external symptoms are present, leukocyte transmigration and blood-brain barrier leakage are colocalized (Aubé et al., 2014; Beard Jr. et al., 2018; Wu et al., 2010). This injury, termed by our lab a "perivenular inflammatory lesion" (PIL), happens in the post-capillary venules over the white matter tracts in the cerebellum, and are a direct cause of the muscle weakness and motor deficiencies

encountered in MS patients (Popescu et al., 2013; van Horssen et al., 2007). Understanding how neutrophils cross the endothelium, however, is not well understood.

Under homeostasis, brain microvascular endothelial cells (BMVECs) have high expression of multiple tight junctional proteins, including claudin 5, and tight junction-associated MARVEL-domain-containing proteins (TAMP) occludin and tricellulin. (Beard Jr. et al., 2018; Beard et al., 2014; Yuan & Rigor, 2010) By restricting passive pericellular flux, the endothelium itself controls passage of all solutes through highly-regulated transport mechanism. (Daneman & Prat, 2015; D. W. Miller, 1999; Yuan & Rigor, 2010). Similarly, leukocyte transmigration is strictly controlled (Larochelle et al., 2011; Phillipson & Kubes, 2011). During inflammation, however, leukocytes become pathogenic by releasing multiple factors that change how the blood-brain barrier functions: tight junctions are downregulated, intercellular adhesion is weakened, and leakage of solutes and water into the CNS occurs (H.-C. Bauer et al., 2014; Dejana, 2004; Taddei et al., 2008). Based upon each of these factors, it is our lab's hypothesis that the regulation of endothelial tight junctions in the face of the inflammatory milieu is both sufficient and necessary for the prevention of neuroinflammatory disease.

In these studies, the temporal relationship between neutrophil recruitment, oncostatin M release, and blood brain barrier dysfunction are defined. Through *in vitro* mechanistic studies, the role of neutrophil-derived OSM was confirmed, leading to decreases in the TAMP occludin, but not claudin 5, resulting in barrier dysfunction. *In vivo* analyses reveal the loss of OSM signaling rescues EAE-induced blood-brain barrier dysfunction and neutrophil extravasation in the critical pre-onset stage, leading to the

significant reduction of neurologic deficiencies. Collectively, these studies demonstrate the critical role of tight junctions in the impedance of neuroinflammatory disease.

Methods

Reagents and Supplies

A complete list of reagents and supplies including vendor and catalog number can be found in **Table 3.1** and **Table 3.2**.

Animal Model and Husbandry

All animal use was approved by the Boise State University Institutional Animal Care and Use Committee under protocols AC16-011, AC19-013, AC19-014, and AC19-015. Animals were maintained under a 12-hour light/dark cycle with food and water ad libitum. Female wild type (*osmrβ*$^{+/+}$) and *osmrβ*$^{-/-}$ (OSMR^{KO}) mice on a C57BL/6 background, aged 10 to 12 weeks, were used in these studies. C57BL/6 background was chosen for genetic homology and their historical use in the inflammatory model experimental autoimmune encephalomyelitis.

Neuroinflammatory Model: Induction of EAE and Clinical Scoring

Animals were injected with Freund's complete adjuvant with inactivated Mycobacterium tuberculosis H37Ra (CFA), myelin oligodendrocyte glycoprotein (amino acids 35-55), and pertussis toxin according to manufacturer's protocol. Briefly, 100 µL of CFA was injected subcutaneously at both the shoulders and base of tail. Pertussis toxin in PBS was administered via intraperitoneal injection (IP) twice, 24 hours apart. Mice were then returned to their cages and evaluated daily to determine progression of the disease. Scoring was completed as follows: 0 = no signs of paralysis, 1 = tail paralysis, 2 =

unsteady gait/hind-limb weakness, 3 = hind-limb paralysis, 4 = hindlimb and forelimb paralysis, and 5 = death.

Adoptive transfer experimental autoimmune encephalomyelitis (AT-EAE), also known as passive EAE, was used to determine the effects of $OSMR^{KO}$ on the effector phase specifically. Utilizing the Hooke AT-EAE protocol, 100 µL of CFA with MOG_{35-55} was injected subcutaneously at both the shoulders and base of tail of four 10-week-old female C57BL/6J (Jax #000664) mice. At day 11 post injection, mice were deeply anesthetized, and euthanized via cervical dislocation. The spleens were harvested aseptically, and ground with a loose-fitting dounce to form a homogenate in RPMI with 2% fetal bovine serum (FBS) and 10 mM HEPES, then passed across 70 µm strainer. After rinsing out the dounce, the cells were centrifuged for 10 minutes at 300 RCF at 4 °C. The supernatant was removed, and the cells were washed with additional media, filtered, and centrifuged two additional times. The resultant cell pellet was suspended in T cell culture media (RPMI 1640, 2 mM L-glutamine, 100 IU/mL penicillin, 0.1 mg/mL streptomycin, 1x MEM non-essential amino acids, 1 mM sodium pyruvate, $5.5x10^{-5}$ M 2-mercaptoethanol, 10 mM HEPES) on ice during counting. Counting was completed using Molecular Probes NucRed and NucGreen stains on an BD Accuri C6 flow cytometer. Cells were diluted to 3.5 x 10^6 cell/mL, plated to T175s, then stimulated with 20 µg/mL MOG_{35-55}, 20 ng/mL IL-12, and 10 µg/mL anti-interferon γ antibodies. Cells were incubated at 37 °C, at 5% CO2 in a humidified incubator for 70 hours.

Following stimulation, cells suspensions were centrifuged for 10 minutes at 300 RCF at 4 °C. The supernatant was discarded, and cell pellets were combined in HBSS. After counting again, cells were diluted to 1.5 x 10^8 cell/mL. 10 10-week-old female

mice (5 wildtype, 5 $OSMR^{KO}$) were injected with 20 million cells IP each, and returned to their cage, and evaluated using the same metrics as above.

Histology

Under deep anesthesia, mice were exsanguinated via transcardial perfusion with PBS, followed by perfusion fixation with 2% paraformaldehyde in PBS. Brains and spinal cords were harvested and post-fixed with 2% paraformaldehyde in PBS overnight at 4 °C, then rinsed and stored in PBS with sodium azide. Sectioning was completed with agarose-mounted organs on a vibratome set to 100 microns.

Immunohistopathology:

Immunohistopathology was completed according to standard protocols on tissues harvested as above. After slicing, brain sections were incubated overnight in PBSTC (PBS + 0.1% Triton + 2 mM Ca^{2+} + 10% donkey serum) with appropriate sera and primary antibodies. Sections were washed in TBSTC hourly six times, then incubated in secondary antibodies overnight at 4 °C. Sections again were washed hourly six times before being mounted in VECTASHIELD mounting medium and stored at -20 °C. All steps were carried out at 4 °C. Imaging was completed on either a Zeiss Meta 510 LSM or Leica Stellaris 5. Specific antibodies and working concentrations can be found in **Table 3.2**.

Blood-Brain Barrier Integrity: *In vivo* Solute Extravasation Assays

Sodium fluorescein (NaFl) solute extravasation assays in experimental animals (EAE, 8 d.p.i) were used to assess small solute permeability of the spinal cord and brain. Mice were given i.p. injections (10 uL/g of 5% w/v NaFl in 0.9% saline). 2 hours post-injection, serum and brain sections were collected and analyzed as previously described.

(Beard et al., 2016) In brief, trichloroacetic acid was added to samples to precipitate protein. Samples were then diluted with a sodium borate buffer and compared to a standard curve for quantitative assessment of NaFl concentration. The permeability surface-area product, P_S (mg/mL) was calculated as follows: C_b is the concentration of tracer in the brain per gram of brain weight, ${}_0\int^t$ is the integrated serum concentration per milliliter, and t is the time between injection and sample harvest (Bell et al., 2010; Mackic et al., 1998).

$$P_S = \frac{C_b}{\int_0^t C_p \times t}$$

Leukocyte Counts: Flow Cytometry

Whole blood was collected via cardiac puncture from deeply anesthetized mice at the appropriate endpoint. Using the eBioscience 1-Step Fix/Lyse and Permeabilization kits, leukocytes were stained with listed antibodies (**Table 3.2**) according to manufacturer's directions. Resultant suspensions were analyzed with a BD Accuri C6 flow cytometer. First, single-antibody and fluorescence minus one (FMO) controls were ran to establish gates and compensation. Then, each sample was individually ran to collect 1.0 x 10^4 CD45+ cells to capture neutrophil to leukocyte ratio; 1.0 x 10^4 Ly6G+ cells to capture OSM+ neutrophils; and 1.0 x 10^4 CD4+ cells to capture OSM+ CD4 T cells. Data was analyzed using FlowJo.

BBB-EC Isolation: Primary Mouse BBB Endothelial Cells

As we have described previously, (Beard Jr. et al., 2018) primary brain microvascular endothelial cells were obtained from C57BL/6 mice aged P7-P10. Cells were plated at confluence and grown on collagen IV-coated (10 μg/cm^2) tissue culture plasticware using endothelial growth medium at 37 °C in a humidified, 5% CO2

incubator. After plating, cells from the initial plating or the first passage were matured for 7 days before experiments.

In Vitro Inflammatory Model: Neutrophil Transendothelial Migration Assays

Primary BMVECs (both wild type and $OSMR^{KO}$) were grown as in *BBB-EC Isolation* and passaged onto transwell plates (Corning collagen IV pre-coated 12 well plates). Primary astrocytes were grown in the abluminal chamber. Encephalitogenic T cells were grown as above for adoptive transfer experimental autoimmune encephalomyelitis, then 1.0×10^5 cells were placed in the bottom side. Neutrophils were isolated from C57BL/6 mice as outlined above and were labeled with CellTracker™ in line with manufacturer instructions and used within two hours of isolation. Following abluminal stimulation with MOG, 1.0×10^5 neutrophils were immediately added to luminal side. Neutrophils that had transmigrated were counted at 2 and 4 hours after addition by fluorescent microscopy. Control T cells- generated from EAE-naïve mice- were handled in the same manner.

Blood-Brain Barrier Function Analysis: Real-Time TEER

Electric cell-substrate impedance sensor (ECIS) arrays were used to demonstrate TEER of BBB-EC during inflammatory challenge as previously described. (Beard Jr. et al., 2018; Beard et al., 2016) BBB-ECs were prepared as above were grown on cysteine-reduced Col-IV coated 8W10E+ arrays. Neutrophil conditioned media was prepared as above. TEER was measured continuously after the addition of inflammatory challenge and presented as normalized TEER, with peak changed quantified for statistical analysis.

Immunoblotting

Two-color near-infrared immunoblotting was used to determine protein expression according to standard protocols and quantified using LI-COR Odyssey CLx and LI-COR ImageStudio. Specific antibodies and working concentrations can be found in **Table 3.2**.

Statistics

Statistical analysis was completed using GraphPad Prism (version 9.2.0). *A priori* power analysis was administered to determine appropriate animal group size. Unless otherwise stated within figure legends, data is presented as the mean ± standard deviation.

Results

Oncostatin M has a Role in the Pathogenesis of the Neuroinflammatory Disease Experimental Autoimmune Encephalomyelitis

Leukocytosis, or the pathogenic increase in leukocyte counts, has been a consistent pathology of neuroinflammatory disease for nearly 100 years (Iovino et al., 2019; McKenna, 1930). Neutrophils, the first-line defense mechanism of innate immunity, are chief among these; they phagocytize, release multiple signaling compounds, and form extracellular traps for circulating pathogens and bioactive compounds (Mantovani et al., 2011). The cytokine oncostatin M is produced by neutrophils during inflammation, and has a multitude of effects depending the context of its release (Brilot et al., 2019; Dey et al., 2013; Pothoven et al., 2016). In patients with multiple sclerosis, increased serum concentrations of OSM have been found (Alikhani et

al., 2014). Lastly, a high neutrophil-to-lymphocyte ratio is a strong predictor of poor disease course and outcomes (Demirci et al., 2016; Song et al., 2021).

We analyzed these findings in the context of a murine model of neuroinflammation, experimental autoimmune encephalomyelitis. At 8 days post-induction (DPI) of EAE, wild type (WT) mice exhibited a significant increase in serum OSM, compared to unimmunized healthy controls (**Figure 3.1 A**). Flow cytometry analysis confirms an increase in neutrophil-to-lymphocyte ratio, from 0.5 ± 0.07 in healthy mice to 3.4 ± 0.99 in mice with EAE (**Figure 3.1 B**). While total CD4 percentage of CD45+ leukocytes do not change, Ly6G+ neutrophils increase from 5.5% ± 1.0 to 32.6% ± 5.05 in animals with disease (**Figure 3.1 C**). Nearly all neutrophils and CD4 cells contain OSM in both healthy and diseased mice, however the OSM+ neutrophils increase to 32.9% ± 4.1 in EAE mice (**Figure 3.1 D**), with no change in OSM+ CD4 counts (**Figure 3.1 E**).

Neutrophils Extravasate Across the Blood-Brain Barrier Endothelial During Inflammatory Stimuli

During neurogenic inflammation, neutrophils cross the blood-brain barrier where they exert the first-line innate defense of phagocytosis and cytokine release (Muller, 2013; Takeshita & Ransohoff, 2012). Utilizing flow cytometry on brain homogenates taken from mice during the effector phase of EAE, we identified a significant increase in neutrophils in the brain parenchyma, with no change in CD4+ T cells (**Figure 3.2 A**). Confocal microscopy confirms this observation (**Figure 3.2 B**). Consistent with our findings of all neutrophils containing OSM, confocal microscopy shows OSM colocalized to Ly6G+ neutrophils (**Figure 3.2 C**). To further clarify the endothelial

contributions to neutrophil transmigration, we created a novel *in vitro* model of inflammation. Utilizing a transwell system, primary BBB endothelial cell monolayers are grown in the upper chamber. In the bottom chamber astrocytes are grown. At maturity, encephalitogenic or naïve T cells and myelin oligodendrocyte glycoprotein was added to the bottom well, and neutrophils to the top. Neutrophils transmigrated toward immunized T_H17 cells at a rate of 3.2% per hour, compared to 0.37% per hour towards naïve T_H0 cells (**Figure 3.2 D**).

Oncostatin M Causes Downregulation of Endothelial Occludin, but not Claudin 5, Decreasing Barrier Integrity

Cell culture studies were completed to better understand the role of OSM on endothelial function. First, human primary brain microvascular endothelial cells (BMVECs) were challenged with increasing concentrations of recombinant human oncostatin M. Over 20 hours, barrier function as measured by trans-endothelial electric resistance (TEER) using electronic cell-substrate impedance sensing (ECIS) at 4000 Hz; peak dysfunction was achieved with 250 ng/ml (**Figure 3.3 A**). Concomitantly, occludin proteins were found decreased over 24 hours, with no change in claudin 5 expression (**Figure 3.3 B**). RNA analysis was completed to establish the transcriptional control of occludin **(Figure 3.3 C)**.

Preventing Oncostatin M Signaling Rescues Endothelial Barrier Dysfunction

The cognate receptor oncostatin M is oncostatin M receptor β (OSMR), of which knockout mice are available (Heinrich et al., 2003; Tanaka et al., 2003). Analysis of the oncostatin M signaling pathway was completed with OSMR knockout ($OSMR^{KO}$) endothelial monolayers *in vitro*. After challenge with 100 ng/mL oncostatin M, WT

monolayers exhibit marked barrier dysfunction over 24 hours, whereas $OSMR^{KO}$ monolayers do not (**Figure 3.4 A**). Similarly, $OSMR^{KO}$ monolayers are resistant to neutrophil transendothelial migration, showing a marked decrease in neutrophils found in the abluminal chamber (**Figure 3.4 B**).

OSMR-Knockout Rescues Two Models of Experimental Autoimmune Encephalomyelitis

We lastly sought to determine the effect of attenuated oncostatin M signaling upon the course of experimental autoimmune encephalomyelitis. With active EAE induction, OSMR knockout significantly lessens severity of disease, but does not change day of onset, number of days with symptoms, or maximal clinical score (**Figure 3.5 A**). Because global oncostatin M knockout could be modulating either the inductor stage of EAE, preventing the generation of myelin-specific CD4 cells or the effector phase, where blood-brain barrier dysfunction and demyelination occur, adoptive transfer EAE was undertaken. In this model, effector T cells are generated in wildtype mice, and then transferred into experimental mice (Stromnes & Goverman, 2006b). Here, OSMR knockout significantly decreased severity and number of days with symptoms but did not change day of onset or maximal clinical score (**Figure 3.5 B**). To confirm barrier integrity was indeed maintained, permeability of the small molecule fluorescein was measured. $OSMR^{KO}$ significantly reduces BBB permeability during active EAE (**Figure 3.5 C**). Finally, RNA from isolated brain microvessels was analyzed to confirm that $OSMR^{KO}$ prevents loss of occludin. Here, our hypothesis was confirmed, and EAE-induced loss of occludin was restored with OSMR knockout (**Figure 3.5 D**).

Discussion

The fundamental conclusion from these studies is that oncostatin M drives occludin-dependent barrier dysfunction during neuroinflammatory disease. We completed an incremental approach to demonstrate the relationship between oncostatin M signaling and occludin downregulation, followed by increased blood-brain barrier permeability. First, we identified oncostatin M as a relevant inflammatory mediator in experimental autoimmune encephalomyelitis. Second, we found that neutrophils are a likely source of OSM, and that in an inflammatory response, will cross BBB monolayers. Third, we established that by preventing oncostatin M signaling in endothelial monolayers, OSM-induced TEER loss is rescued, and neutrophil transmigration is significantly reduced. Finally, we determined that OSM is an important mediator in the effector phase of experimental autoimmune encephalomyelitis; by preventing the oncostatin M cascade EAE symptoms are significantly reduced.

Historically, blood-brain barrier dysfunction has long been considered a pathology of neuroinflammatory disorders like multiple sclerosis and experimental autoimmune encephalomyelitis (Aubé et al., 2014; Beard Jr. et al., 2018; Beard et al., 2014; Kermode et al., 1990; Rodrigues & Granger, 2015). Preventing this dysfunction, then, could be key in the larger fight against neuroinflammatory disease. While it is likely that many signaling molecules have responsibility in this process, we have demonstrated that oncostatin M has a profound effect on occludin expression specifically.

Previous studies have identified that both rat and human endothelial cells produce less occludin during stimulation with OSM, however Takata et al. (2008) found that OSM additionally caused altered ZO-1 localization and decreased claudin 5 expression

(Ruprecht et al., 2001; Takata et al., 2008, 2018). In our *in vitro* human studies, we confirmed decreased concentration of occludin, but our results contradict those of Takata et al.; we identified no change in claudin 5 expression. Endothelial maturity is a potential factor. We have previously found that claudin 5 expression is low in immature endothelial cells, and therefore could be more sensitive to inflammatory stimuli (Beard Jr. et al., 2018). When utilizing only fully mature endothelial monolayers, claudin 5 maintained high expression throughout our OSM-only studies. Significantly, claudin 5 expression was not rescued in EAE trials with $OSMR^{KO}$, providing further support of oncostatin M not regulating claudin 5. Additionally, neutrophils contain other inflammatory factors in their granules, many of which have claudin 5 effects (Grenier et al., 1999; Mantovani et al., 2011; Woodberry et al., 2018). It is likely, then, that the claudin and TAMP families are regulated through differing processes.

In the literature, oncostatin M is almost always referred to as a pleiotropic cytokine, a fact which is well-reflected within the CNS. While OSM causes blood-brain barrier dysfunction, it has neuroprotective effects in other cell types. Janssens et al demonstrate a protective microglial phenotype and limited oligodendrocyte death in a cuprizone-mediated model of demyelination; mice stereotactically injected with lentivirus encoding for OSM have less demyelination than controls (Janssens et al., 2015). Similarly, oncostatin M prevents glutamate-mediated neural excitotoxicity (Moidunny et al., 2010). In a review, Brilot et al reports that only one study reports neurotoxic effects (Brilot et al., 2019).

Experimental autoimmune encephalomyelitis has two phases: the induction phase, where myelin specific $CD4^+$ T cells are created and primed, and the effector phase, where

the immune compliment is activated, the blood-brain barrier is breached, and demyelination occurs (S. D. Miller & Karpus, 2007). Initial studies were completed using active EAE; because OSM signaling has some effects in T_H17 regulation, analysis of the effector phase was required, indicating that the disease amelioration observed may have been because the induction phase was prevented (Son et al., 2017). Adoptive transfer experimental autoimmune encephalomyelitis (AT-EAE), also known as passive EAE, was employed to decouple the induction phase by initiating the disease in wildtype mice (Falk et al., 1969; Stromnes & Goverman, 2006b). In this study, encephalitogenic T cells were created from wildtype animals, then injected into $OSMR^{KO}$ mice. Because $OSMR^{KO}$ mice still exhibited decreased clinical scoring, our analysis concluded that the effector phase is of EAE is modulated through oncostatin M signaling. As experimental autoimmune encephalomyelitis, and indeed multiple sclerosis, have hosts of circulating inflammatory factors like IL-1β and IL-17 that cause barrier dysfunction, the incomplete amelioration of disease found in $OSMR^{KO}$ mice is unsurprising (Jahan-Abad et al., 2020). Finally, when further analyzed in the context of our *in vitro* studies, we conclude that the prevention of OSM signaling at the blood-brain barrier prevents the dysfunctions generated by experimental autoimmune encephalomyelitis.

In summary, these studies identify that neutrophil-derived oncostatin M signaling at the blood-brain barrier causes occludin-dependent barrier dysfunction, potentiating leukocyte transmigration and neuroinflammatory injury.

Funding

These studies were funded by American Heart Association 20119990670; National Institutes of Health 1R01NS110934-01A1, P20GM103408, P20GM109095;

Sigma Xi Grants in Aid of Research G2018100198254939; National Science Foundation 0619793 and 0923535; the MJ Murdock Charitable Trust; and the Idaho State Board of Education.

Acknowledgements

We greatly appreciate the support of the Biomolecular Research Center and the Biomedical Research Vivarium at Boise State University.

Author Contributions

TSW completed and interpreted most of these experiments. BAH participated in cell culture experiments of figures 2, 3, and 4. DAS participated in flow cytometry experiments. KC participated in animal husbandry, and primary endothelial isolations in figures 2, 3, and 4. SYY provided guidance throughout these studies. JTO provided guidance throughout these studies. CLJ provided guidance throughout these studies. RSBJ initiated, directed, and sponsored the work through all levels of development as primary investigator. All authors have discussed the results and approved this manuscript.

Disclosures and Conflict of Interest

The authors declare no potential conflicts of interest.

Table 3.1 Reagents Used

Reagents	Company	Catalog Number
1-Step Fix/Lyse Solution	eBioscience	00533354
4–20% Mini-PROTEAN TGX Precast Protein Gels	Bio-Rad	4561094
Anti-Interferon-γ Blocking Antibody	BioLegend	75833-044
Bovine Serum Albumin	Sigma-Aldrich	A1470
CellTracker Green CMFDA	Thermo Scientific	C7025
CellTracker Orange CMRA	Thermo Scientific	C34551
Collagenase/Dispase	Sigma-Aldrich	11097113001
Collagen IV	R&D Systems	341001002
DMEM (phenol free)	Gibco	31-053-028
DNAse I	Spectrum	D348910MG
ECIS Array	Applied Biophysics	8W10E+PC
Fetal Bovine Serum	Atlanta Biologicals	S115500
Fetal Bovine Serum, Heat Inactivated	Fisher Scientific	A3840001
Human Complete Endothelial Cell Medium	Cell Biologics	H1168
Human Primary Brain Microvascular Endothelial Cells	Cell Biologics	H-6023
iScript cDNA Synthesis Kit	Bio-Rad	1708891

Reagents	Company	Catalog Number
MOG_{35-55}/CFA Emulsion with PTX	Hooke Laboratories	EK-2110
MOG_{35-55} in Tissue Culture Media	Hooke Laboratories	DS-0111
Mouse Complete Astrocyte Medium	Cell Biologics	M2266
Mouse Complete Endothelial Cell Medium	Cell Biologics	M1168
Mouse IL-12 (recombinant)	BioLegend	577002
Mouse Oncostatin M DuoSet ELISA	R&D Systems	DY495-05
Mouse (C57BL/6) Primary Astrocytes	Cell Biologics	C57-6285
Odyssey Blocking Buffer (TBS)	LI-COR	927-50000
Oncostatin M (recombinant human)	R&D Systems	295-OM-010
Oncostatin M (recombinant mouse)	R&D Systems	495-MO-025
Permeabilization Buffer	eBioscience	00833356
Phosphate Buffered Saline	Fischer Scientific	BP3994
Puromycin	Gibco	A1113803
Ssoadvanced Universal SYBR Green Supermix	Bio-Rad	1725272
Trans-Blot Turbo Mini Nitrocellulose Transfer Kit	Bio-Rad	1704158

Table 3.2 Antibodies Used

Antibody	Figure	Vendor	Catalog	Concentration
β-Actin	3.3 B;	LI-COR Bioscience	926-42212	1:1000
CD4 (PE)	3.1 B, C, E	BD Bioscience	5537308	1:50
CD45 (PerCP-Cy5.5)	3.1 B, C, D, E	BioLegend	157208	1:50
Claudin 5	3.1 B	Thermo Fisher	35-2500	1:1000
Ly6G (FITC)	3.1 B, C, D	BD Bioscience	553128	1:50
Occludin	3.3 B	Abcam	ab168986	1:1000
Oncostatin M (AF-647)	3.1 D, E	Bioss	bs-5095R	1:50

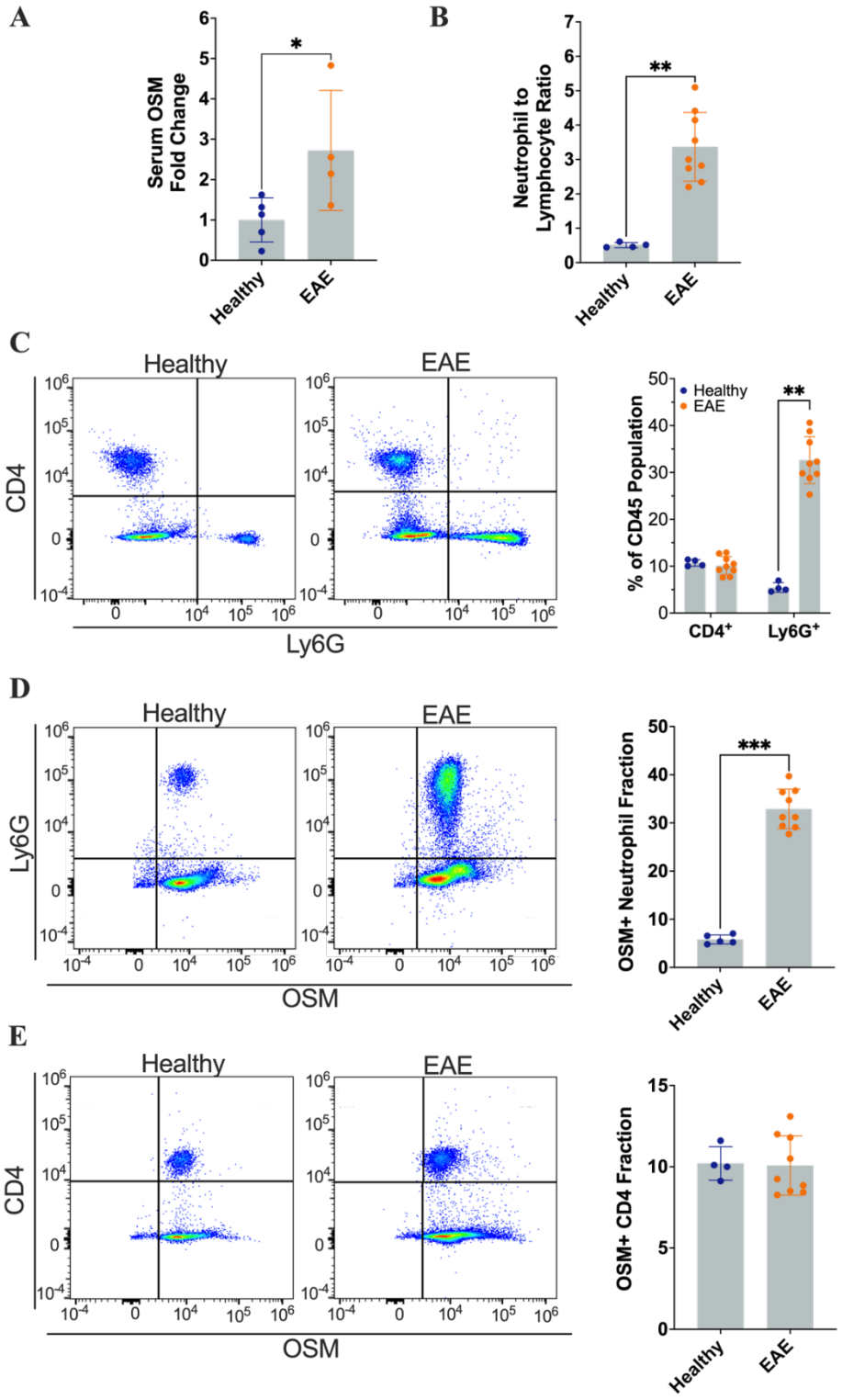

Figure 3.1 Serum Oncostatin M Concentration Increases and Pathogenic Neutrophil-to-Lymphocyte Ratio is Induced During Experimental Autoimmune Encephalomyelitis

A) At day 8 post induction, serum concentration of oncostatin M increases nearly three-fold in EAE-induced mice (orange) compared to healthy controls (blue), as tested by ELISA (Healthy: n=5; EAE: n=4). **(B-E)** Circulating neutrophils increase during the onset of EAE, increasing the neutrophil-to-lymphocyte ratio (NLR) to pathogenic levels. **B)** NLR is significantly increased during the onset of EAE (orange, n=9) compared to healthy controls (blue, n=4). **C)** Representative flow cytometry of circulating CD45+ leukocytes, demonstrates significant increase in Ly6G-positive neutrophils (bottom right quadrant) counts, with no change in CD4 cell counts (top left quadrant) in onset of EAE (orange) compared to healthy (blue) mice. **D)** Additionally, the fraction of OSM+ neutrophils (top right quadrant) increases, with **E)** no change in the fraction of OSM+ CD4 cells (top right quadrant). Dot plots are presented as mean ± standard deviation. Serum data are presented as mean fold change compared to controls. Flow data is presented as a heat map. * = $p < 0.05$; ** = $p < 0.05$; *** = $p < 0.005$ by Mann-Whitney test.

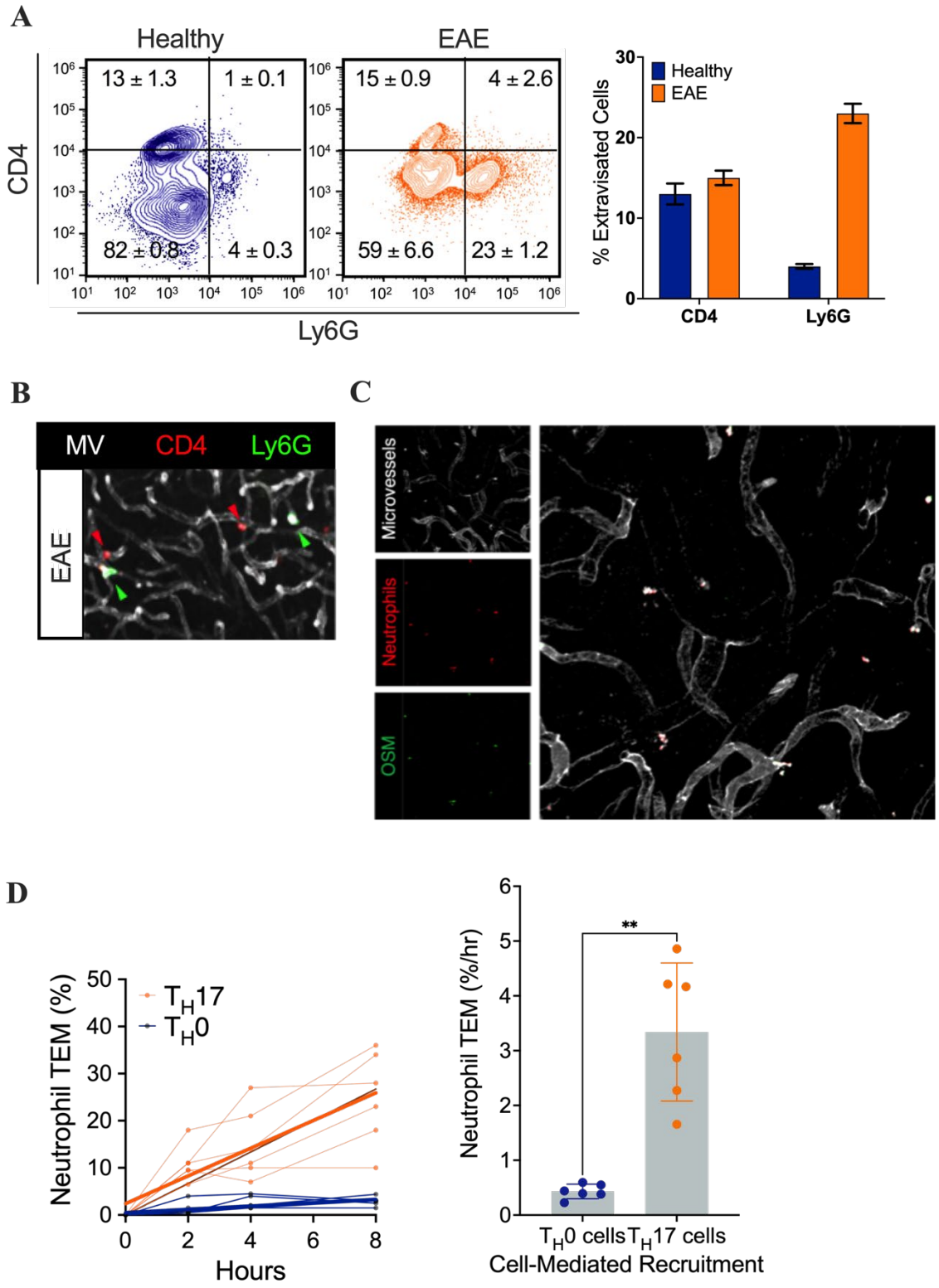

Figure 3.2 OSM+ Neutrophils Migrate Across Blood-Brain Barrier Endothelial Monolayers *In* Vivo and in an *In Vitro* Model of Experimental Autoimmune Encephalomyelitis

Concurrently with increased peripheral neutrophils increases, **A)** flow cytometry of brain homogenates demonstrates an increase in extravasated Ly6G+ neutrophils, with no change in extravasated CD4 populations. **B)** Representative confocal microscopy of brain sections from healthy and EAE mice. Ly6g+ cells (green) are found outside of microvessels (white) in larger populations in mice with EAE compared to healthy mice, with no change in CD4+ cells (red). **C)** Neutrophils (red) found in brain sections via confocal microscopy contain OSM (green). *In vitro*, **D)** neutrophils cross the blood-brain barrier, moving towards encephalitogenic T_H17 (orange, n=6) cells at a higher rate compared to naïve/unstimulated T_H0 (blue, n=6) cells. Flow data represented as topographical map with mean ± standard error of the mean. Transmigration data is presented as individual replicates with mean rate presented in bold, with a dot plot containing mean ± the standard deviation of the individual slopes. * = $p < 0.05$; ** = $p < 0.05$; *** = $p < 0.005$ by Mann-Whitney test.

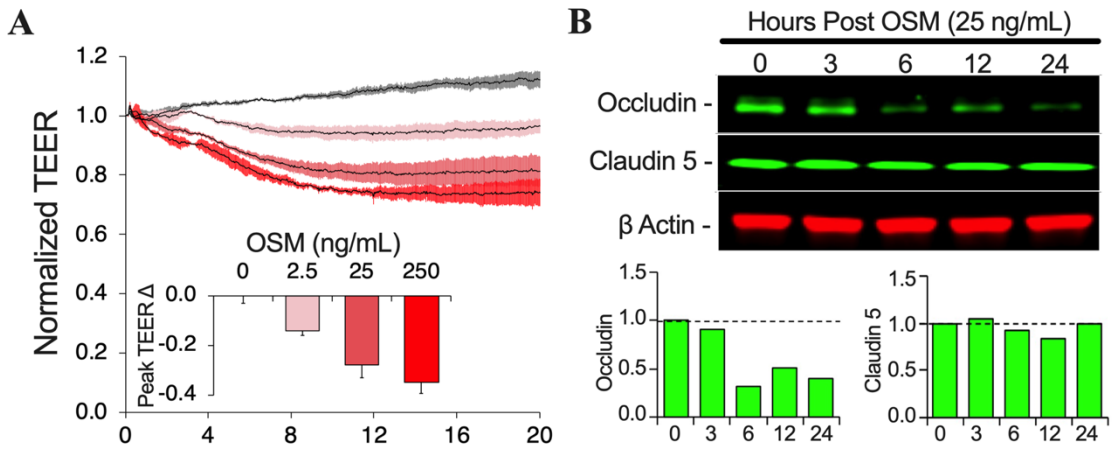

Figure 3.3 Concomitant with Barrier Dysfunction, Occludin, but not Claudin 5 is Lost After Stimulation with Oncostatin M.

In vitro, human BMVEC monolayers were stimulated with oncostatin M. **A)** Trans-endothelial electric resistance (TEER) is lost in a dose- and time- dependent manner over 20 hours, with peak loss at 250 ng/mL. **B)** After stimulation with 25 ng/mL oncostatin M, representative western blot and densitometry analysis for occludin demonstrates loss of protein over 24 hours, with no change in claudin 5 expression.

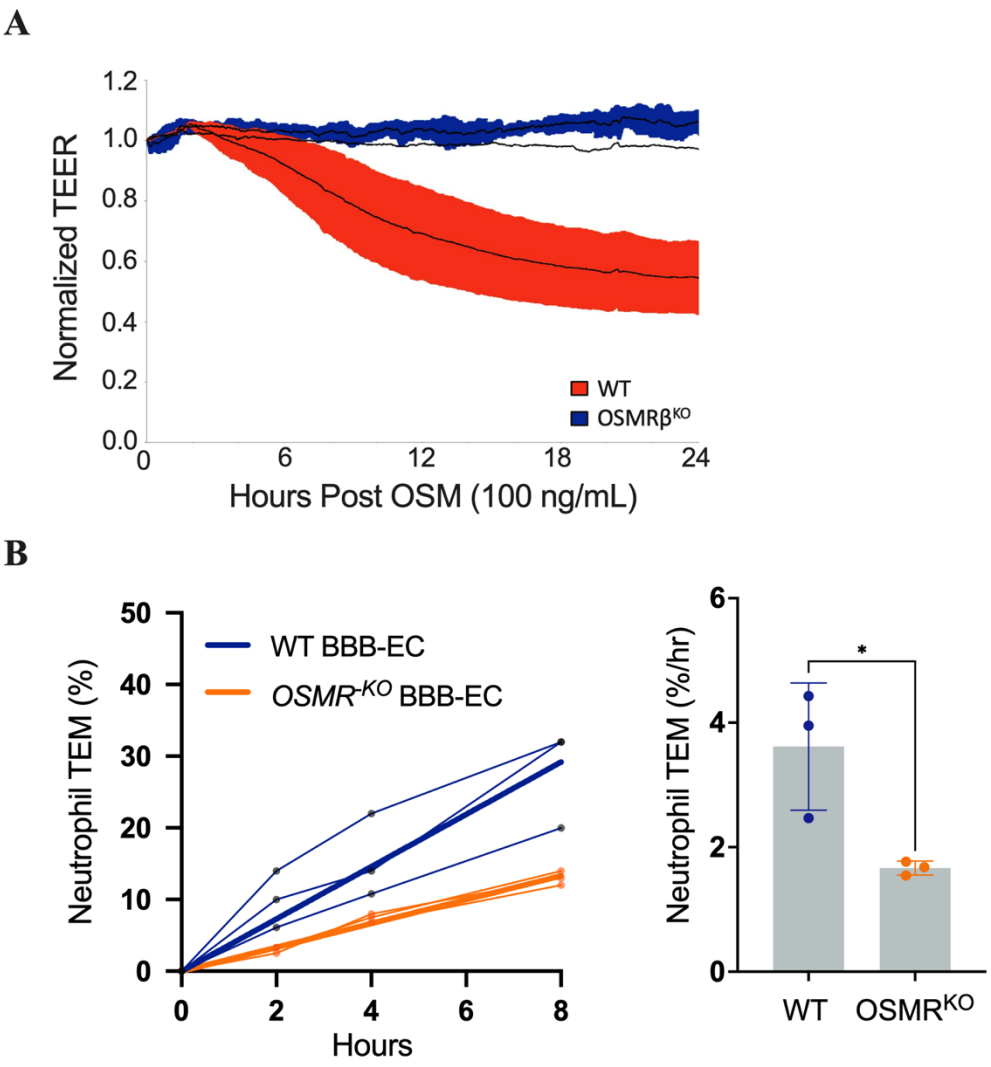

Figure 3.4 Loss of Oncostatin M Signaling Attenuates OSM-Dependent Barrier Dysfunction *in Vitro*.

A) After administration of 100 ng/mL of oncostatin M, trans-endothelial electrical resistance is maintained in $OSMR^{KO}$ blood-brain barrier endothelial cells (blue), while it is significantly decreased in wild type blood-brain barrier endothelial cells (orange). Shaded area indicates standard error of the mean. **B)** Neutrophil transendothelial migration is significantly decreased in $OSMR^{KO}$ (orange) endothelial monolayers compared to wild type (blue). Transmigration data is presented as individual replicates with mean rate presented in bold, with a dot plot containing mean ± the standard

deviation of the individual slopes. ECIS data presented as mean (line) ± standard deviation (highlight). Transmigration data is presented as a dot plot with mean ± standard deviation. * = $p < 0.05$; ** = $p < 0.05$; *** = $p < 0.005$ by Mann-Whitney test.

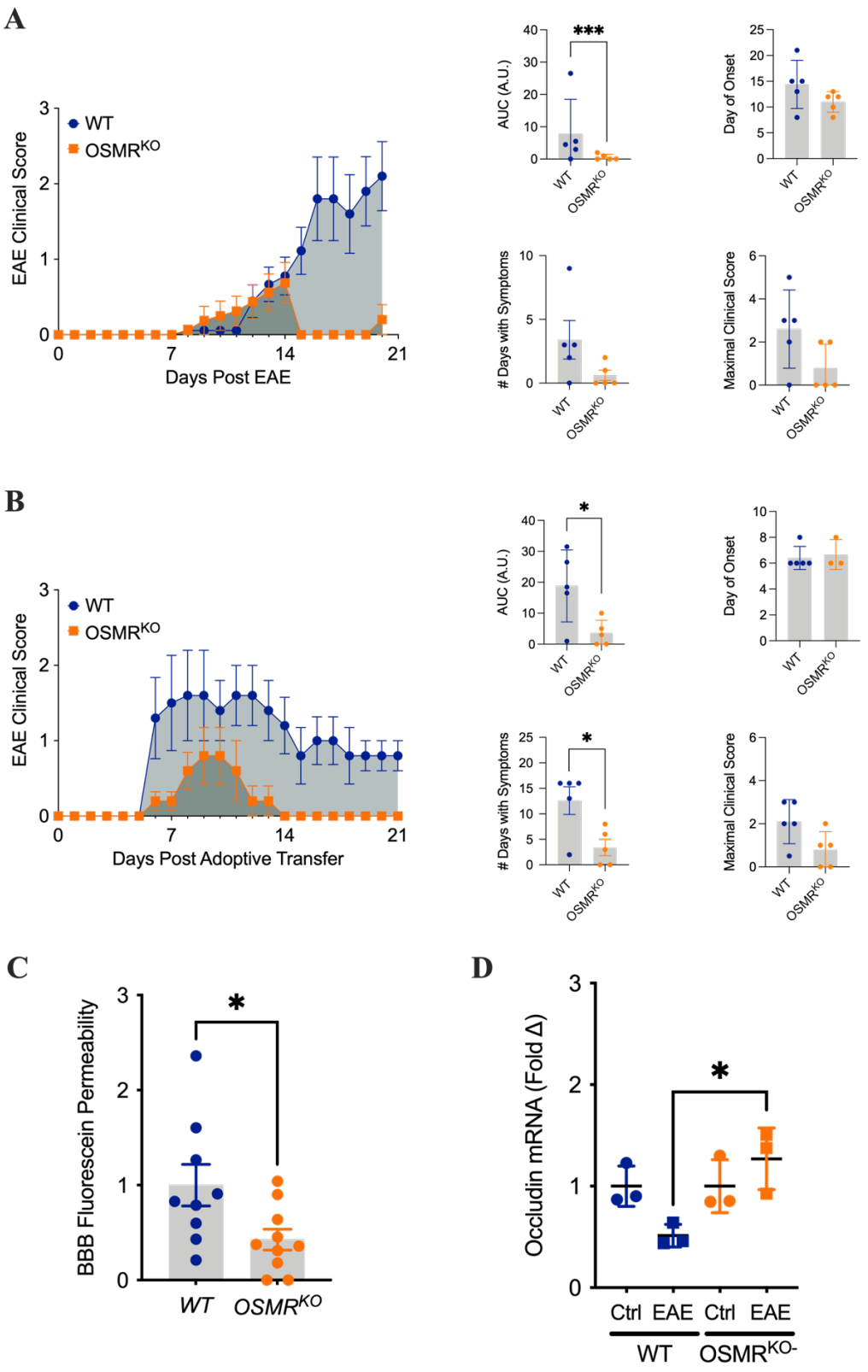

Figure 3.5 Oncostatin M Knockout Attenuates Blood-Brain Barrier Dysfunction in Experimental Autoimmune Encephalomyelitis.

A) Active EAE clinical scores (left) show OSMR-deficient mice (n=5) have a significant decrease in area under the curve, without a difference in day of onset, number of days with symptoms, or maximum clinical score compared to wildtype (n=5). **B)** Adoptive transfer EAE clinical scores (left) show OSMR-deficient (n=5) mice have a significant decrease in both area under the curve and number of days with symptoms, without changing day of onset or max clinical score compared to wildtype (n=5). **C)** Permeability to sodium fluorescein is significantly reduced in OSMR-knockout mice (n=10) during EAE compared to wildtype (n=9). **D)** Occludin expression is rescued in OSMR-knockout mice (n=9, 3 pooled groups of 3) during EAE compared to wildtype (n=9, 3 pooled groups of 3). Clinical scores are represented as mean ± standard error of the mean. Dot plots are presented as mean ± standard deviation; one data point denotes a result from one mouse except for RNA analysis, where each data point is a pool of 3 mice. * = $p < 0.05$; *** = $p < 0.005$ by Mann-Whitney test or one-way ANOVA, where appropriate.

References

Anderson, J. M., & Van Itallie, C. M. (2009). Physiology and Function of the Tight Junction. Cold Spring Harbor Perspectives in Biology, 1(2), a002584. https://doi.org/10/db696x

Bauer, A. T., Bürgers, H. F., Rabie, T., & Marti, H. H. (2010). Matrix metalloproteinase-9 mediates hypoxia-induced vascular leakage in the brain via tight junction rearrangement. Journal of Cerebral Blood Flow and Metabolism: Official Journal of the International Society of Cerebral Blood Flow and Metabolism, 30(4), 837–848. https://doi.org/10/ckmwvp

Beard Jr., R. S., Hoettels, B. A., Meegan, J. E., Wertz, T. S., Cha, B. J., Yang, X., Oxford, J. T., Wu, M. H., & Yuan, S. Y. (2018). AKT2 maintains brain endothelial claudin-5 expression and selective activation of IR/AKT2/FOXO1-signaling reverses barrier dysfunction. Journal of Cerebral Blood Flow & Metabolism, 0271678X1881751. https://doi.org/10.1177/0271678X18817512

Beard, R. S., Haines, R. J., Wu, K. Y., Reynolds, J. J., Davis, S. M., Elliott, J. E., Malinin, N. L., Chatterjee, V., Cha, B. J., Wu, M. H., & Yuan, S. Y. (2014). Non-muscle Mlck is required for -catenin- and FoxO1-dependent downregulation of Cldn5 in IL-1 -mediated barrier dysfunction in brain endothelial cells. Journal of Cell Science, 127(8), 1840–1853. https://doi.org/10.1242/jcs.144550

Bell, R. D., Winkler, E. A., Sagare, A. P., Singh, I., LaRue, B., Deane, R., & Zlokovic, B. V. (2010). Pericytes control key neurovascular functions and neuronal phenotype in the adult brain and during brain aging. Neuron, 68(3), 409–427. https://doi.org/10/c9kwmq

Benson, K., Cramer, S., & Galla, H.-J. (2013). Impedance-based cell monitoring: Barrier properties and beyond. Fluids and Barriers of the CNS, 10(1), 5. https://doi.org/10/f4j8p3

Brown, T. J., Lioubin, M. N., & Marquardt, H. (1987). Purification and characterization of cytostatic lymphokines produced by activated human T lymphocytes. Synergistic antiproliferative activity of transforming growth factor beta 1, interferon-gamma, and oncostatin M for human melanoma cells. Journal of Immunology (Baltimore, Md.: 1950), 139(9), 2977–2983.

Davda, N., Tallantyre, E., & Robertson, N. P. (2019). Early MRI predictors of prognosis in multiple sclerosis. Journal of Neurology, 266(12), 3171–3173. https://doi.org/10/gmz628

De Bondt, M., Hellings, N., Opdenakker, G., & Struyf, S. (2020). Neutrophils: Underestimated Players in the Pathogenesis of Multiple Sclerosis (MS). International Journal of Molecular Sciences, 21(12), 4558. https://doi.org/10/gksp7p

de Vries, H. E., Kuiper, J., Boer, A. G. de, Berkel, T. J. C. V., & Breimer, D. D. (1997). The Blood-Brain Barrier in Neuroinflammatory Diseases. Pharmacological Reviews, 49(2), 143–156.

Duquette, P., Pleines, J., Girard, M., Charest, L., Senecal-Quevillon, M., & Masse, C. (1992). The Increased Susceptibility of Women to Multiple Sclerosis. Canadian Journal of Neurological Sciences, 19(4), 466–471. https://doi.org/10/gmqhtm

Fournier, A. P., Baudron, E., Wagnon, I., Aubert, P., Vivien, D., Neunlist, M., Bardou, I., & Docagne, F. (2020). Environmental enrichment alleviates the deleterious effects of stress in experimental autoimmune encephalomyelitis. Multiple Sclerosis Journal - Experimental, Translational and Clinical, 6(4), 2055217320959806. https://doi.org/10/gmqhsz

Gerrard, B., Singh, V., Babenko, O., Gauthier, I., Wee Yong, V., Kovalchuk, I., Luczak, A., & Metz, G. A. S. (2017). Chronic mild stress exacerbates severity of experimental autoimmune encephalomyelitis in association with altered non-coding RNA and metabolic biomarkers. Neuroscience, 359, 299–307. https://doi.org/10/gbt6t8

Giaever, I., & Keese, C. R. (1991). Micromotion of mammalian cells measured electrically. Proceedings of the National Academy of Sciences, 88(17), 7896–7900. https://doi.org/10/fxgwbx

Grenier, A., Dehoux, M., Boutten, A., Arce-Vicioso, M., Durand, G., Gougerot-Pocidalo, M. A., & Chollet-Martin, S. (1999). Oncostatin M production and regulation by human polymorphonuclear neutrophils. Blood, 93(4), 1413–1421.

Hallmann, R., Savigni, D. L., Morgan, E. H., & Baker, E. (2000). Characterization of iron uptake from transferrin by murine endothelial cells. Endothelium: Journal of Endothelial Cell Research, 7(2), 135–147. https://doi.org/10/gmztzs

Hamilton, K. O., Backstrom, G., Yazdanian, M. A., & Audus, K. L. (2001). P-glycoprotein efflux pump expression and activity in Calu-3 cells. Journal of Pharmaceutical Sciences, 90(5), 647–658. https://doi.org/10/fq82dg

Hurst, S. M., McLoughlin, R. M., Monslow, J., Owens, S., Morgan, L., Fuller, G. M., Topley, N., & Jones, S. A. (2002). Secretion of oncostatin M by infiltrating neutrophils: Regulation of IL-6 and chemokine expression in human mesothelial cells. Journal of Immunology (Baltimore, Md.: 1950), 169(9), 5244–5251. https://doi.org/10/gkm6mb

Kang, Q., Sun, Z., Zou, Z., Wang, M., Li, Q., Hu, X., & Li, N. (2018). Cell-penetrating peptide-driven Cre recombination in porcine primary cells and generation of marker-free pigs. PLOS ONE, 13(1), e0190690. https://doi.org/10/gcsr2j

Khoury, S. J., & Weiner, H. L. (1998). Multiple Sclerosis: What Have We Learned From Magnetic Resonance Imaging Studies? Archives of Internal Medicine, 158(6), 565–573. https://doi.org/10/dc74bh

Lassmann, H. (2018). Multiple Sclerosis Pathology. Cold Spring Harbor Perspectives in Medicine, 8(3), a028936. https://doi.org/10/gcv3hm

Leigh, N. D., Kokolus, K. M., O'Neill, R. E., Du, W., Eng, J. W.-L., Qiu, J., Chen, G. L., McCarthy, P. L., Farrar, J. D., Cao, X., & Repasky, E. A. (2015). Housing Temperature-Induced Stress Is Suppressing Murine Graft-versus-Host Disease through β2-Adrenergic Receptor Signaling. Journal of Immunology (Baltimore, Md.: 1950), 195(10), 5045–5054. https://doi.org/10.4049/jimmunol.1500700

Mackic, J. B., Weiss, M. H., Miao, W., Kirkman, E., Ghiso, J., Calero, M., Bading, J., Frangione, B., & Zlokovic, B. V. (1998). Cerebrovascular Accumulation and Increased Blood-Brain Barrier Permeability to Circulating Alzheimer's Amyloid β Peptide in Aged Squirrel Monkey with Cerebral Amyloid Angiopathy. Journal of Neurochemistry, 70(1), 210–215. https://doi.org/10/c9j93s

Madisen, L., Zwingman, T. A., Sunkin, S. M., Oh, S. W., Zariwala, H. A., Gu, H., Ng, L. L., Palmiter, R. D., Hawrylycz, M. J., Jones, A. R., Lein, E. S., & Zeng, H. (2010). A robust and high-throughput Cre reporting and characterization system for the whole mouse brain. Nature Neuroscience, 13(1), 133–140. https://doi.org/10.1038/nn.2467

Miller, S. D., & Karpus, W. J. (2007). Experimental autoimmune encephalomyelitis in the mouse. Current Protocols in Immunology, Chapter 15, Unit 15.1. https://doi.org/10/b36256

Papenfuss, T. L., Rogers, C. J., Gienapp, I., Yurrita, M., McClain, M., Damico, N., Valo, J., Song, F., & Whitacre, C. C. (2004). Sex differences in experimental autoimmune encephalomyelitis in multiple murine strains. Journal of Neuroimmunology, 150(1–2), 59–69. https://doi.org/10/c4d477

Pérez-Nievas, B. G., García-Bueno, B., Madrigal, J. L., & Leza, J. C. (2010). Chronic immobilisation stress ameliorates clinical score and neuroinflammation in a MOG-induced EAE in Dark Agouti rats: Mechanisms implicated. Journal of Neuroinflammation, 7(1), 60. https://doi.org/10/fnvb8f

Perrière, N., Demeuse, P., Garcia, E., Regina, A., Debray, Andreux, J., Couvreur, P., Scherrmann, J., Temsamani, J., Couraud, P., Deli, M., & Roux, F. (2005). Puromycin-based purification of rat brain capillary endothelial cell cultures. Effect on the expression of blood-brain barrier-specific properties. Journal of Neurochemistry, 93(2). https://doi.org/10.1111/j.1471-4159.2004.03020.x

Popescu, B. F. Gh., Pirko, I., & Lucchinetti, C. F. (2013). Pathology of Multiple Sclerosis: Where Do We Stand? Continuum: Lifelong Learning in Neurology, 19(4 Multiple Sclerosis), 901–921. https://doi.org/10/ggn57t

Puech, C., Hodin, S., Forest, V., He, Z., Mismetti, P., Delavenne, X., & Perek, N. (2018). Assessment of HBEC-5i endothelial cell line cultivated in astrocyte conditioned medium as a human blood-brain barrier model for ABC drug transport studies. International Journal of Pharmaceutics, 551(1–2), 281–289. https://doi.org/10/gfdmz7

Rahn, E. J., Iannitti, T., Donahue, R. R., & Taylor, B. K. (2014). Sex differences in a mouse model of multiple sclerosis: Neuropathic pain behavior in females but not males and protection from neurological deficits during proestrus. Biology of Sex Differences, 5, 4. https://doi.org/10/gb9g3j

Robertson, R. T., Levine, S. T., Haynes, S. M., Gutierrez, P., Baratta, J. L., Tan, Z., & Longmuir, K. J. (2015). Use of labeled tomato lectin for imaging vasculature structures. Histochemistry and Cell Biology, 143(2), 225–234. https://doi.org/10/f6w596

Saunders, N. R., Dziegielewska, K. M., Møllgård, K., & Habgood, M. D. (2015). Markers for blood-brain barrier integrity: How appropriate is Evans blue in the twenty-first century and what are the alternatives? Frontiers in Neuroscience, 9. https://doi.org/10/gj3vq8

Sgolastra, F., Kuksin, C. A., Gonzalez-Perez, G., Minter, L. M., & Tew, G. N. (2018). Enhanced TAT-Cre Protein Transduction for Efficient Gene Recombination in T cells. ACS Applied Bio Materials, 1(2), 444–451. https://doi.org/10/gmzt2s

Stromnes, I. M., & Goverman, J. M. (2006a). Active induction of experimental allergic encephalomyelitis. Nature Protocols, 1(4), 1810–1819. https://doi.org/10/fhgg3p

Stromnes, I. M., & Goverman, J. M. (2006b). Passive induction of experimental allergic encephalomyelitis. Nature Protocols, 1(4), 1952–1960. https://doi.org/10/b48w6x

Szulcek, R., Bogaard, H. J., & van Nieuw Amerongen, G. P. (2014). Electric Cell-substrate Impedance Sensing for the Quantification of Endothelial Proliferation, Barrier Function, and Motility. Journal of Visualized Experiments: JoVE, 85, 51300. https://doi.org/10/gk4qsj

Tanaka, M., Hirabayashi, Y., Sekiguchi, T., Inoue, T., Katsuki, M., & Miyajima, A. (2003). Targeted disruption of oncostatin M receptor results in altered hematopoiesis. Blood, 102(9), 3154–3162. https://doi.org/10.1182/blood-2003-02-0367

Tatsuta, T., Naito, M., Oh-hara, T., Sugawara, I., & Tsuruo, T. (1992). Functional involvement of P-glycoprotein in blood-brain barrier. The Journal of Biological Chemistry, 267(28), 20383–20391.

Thakker, P., Leach, M. W., Kuang, W., Benoit, S. E., Leonard, J. P., & Marusic, S. (2007). IL-23 Is Critical in the Induction but Not in the Effector Phase of Experimental Autoimmune Encephalomyelitis. The Journal of Immunology, 178(4), 2589–2598. https://doi.org/10.4049/jimmunol.178.4.2589

Trip, S. A., & Miller, D. H. (2005). Imaging in multiple sclerosis. Journal of Neurology, Neurosurgery & Psychiatry, 76(suppl 3), iii11–iii18. https://doi.org/10/dtw46f

Truett, G. E., Heeger, P., Mynatt, R. L., Truett, A. A., Walker, J. A., & Warman, M. L. (2000). Preparation of PCR-quality mouse genomic DNA with hot sodium hydroxide and tris (HotSHOT). BioTechniques, 29(1), 52, 54. https://doi.org/10/gfkmx7

van Horssen, J., Brink, B. P., de Vries, H. E., van der Valk, P., & Bø, L. (2007). The blood-brain barrier in cortical multiple sclerosis lesions. Journal of Neuropathology and Experimental Neurology, 66(4), 321–328. https://doi.org/10/bcqxfc

Watson, P. M. D., Paterson, J. C., Thom, G., Ginman, U., Lundquist, S., & Webster, C. I. (2013). Modelling the endothelial blood-CNS barriers: A method for the production of robust in vitro models of the rat blood-brain barrier and blood-spinal cord barrier. BMC Neuroscience, 14, 59. https://doi.org/10/gb5hvd

Wolf, G., Lifschytz, T., Ben-Ari, H., Tatarskyy, P., Merzel, T. K., Lotan, A., & Lerer, B. (2018). Effect of chronic unpredictable stress on mice with developmental under-expression of the Ahi1 gene: Behavioral manifestations and neurobiological correlates. Translational Psychiatry, 8(1), 1–11. https://doi.org/10/gdt8kt

Yuan, S. Y., & Rigor, R. R. (2010). Regulation of Endothelial Barrier Function. Morgan & Claypool Life Sciences. https://doi.org/10.4199/C00025ED1V01Y201101ISP013

Zeini, D., Glover, J. C., Knudsen, K. D., & Nyström, B. (2021). Influence of Lysine and TRITC Conjugation on the Size and Structure of Dextran Nanoconjugates with Potential for Biomolecule Delivery to Neurons. ACS Applied Bio Materials. https://doi.org/10/gms2t5

CHAPTER FOUR: FUTURE DIRECTIONS

Oncostatin M Signaling Pathways

Oncostatin M has a diverse and complex signaling pathway. After binding to the heterodimer of gp130 and OSMR, JAKs (Janus Kinases) are phosphorylated (Thoma et al., 1994). Then, among other potential targets, the Akt or STAT (signal transduction and activator of transcription pathways are triggered; each having a multitude of end effects (Arita et al., 2008; Schaefer et al., 2000; Van Wagoner et al., 2000). Because of the complexity of these cellular underpinnings and the ultimate consequences of OSM signaling in the blood-brain barrier, it is prudent to further investigate this cell-signaling cascade.

STAT and Snail Signaling

After stimulation with OSM, primary human brain endothelial cells show rapid induction of multiple factors. After 15 minutes, STAT3 becomes significantly phosphorylated, with no change in total STAT3 (**Figure 4.1 A**). Because Snail was found to be upregulated at 60 minutes (**Figure 4.1 A**), and is upstream of STAT1, it was assumed that STAT1 signal was not effected by OSM in endothelial cells (de Frutos et al., 2007, p. 1). Similarly, STAT5 is only known to create minor increases in SNAIL, so it has been ruled out (Talati et al., 2015). The STAT family of proteins, however, is very complex, and can involve many combinations of heterodimers and phosphorylation states, so additional research is required (Visan, 2015; J. Yang & Stark, 2008). Finally, in

$OSMR^{KO}$ endothelial cells, STAT3 phosphorylation is lost (**Figure 4.1 B**), indicating a promising target.

AKT Signaling

FoxO1, a common downstream target of AKT phosphorylation, shows no change in activation after OSM stimulation (**Figure 4.1 C**), indicating a decreased likelihood of the Akt pathway being involved in OSM signaling within the BBB (Beard Jr. et al., 2018; Zhang et al., 2011).

SNAIL Knockout Rescues Oncostatin M-Induced Barrier Dysfunction

Following the success of inhibition of STAT3 phosphorylation, we completed an siRNA knockdown of SNAIL, and challenged the cells with OSM. ECIS tracings demonstrate that SNAIL inhibition prevents OSM-mediated blood-brain barrier dysfunction, and potentially increase baseline ECIS-TEER (**Figure 4.1 D**). Interestingly, *Snai1* knockout is embryonically lethal (Murray et al., 2006). To further study the contribution of SNAIL on blood-brain barrier dysfunction, we obtained Snail-floxed mice (B6;129S-$Snai1^{tm2Grid}$/J; Jackson Labs #010686). We have successfully crossed these with BBB^{Cre} mice, and plan on completing both phenotyping and EAE experiments.

Conclusions

The data presented provide initial analysis of potential pathways of oncostatin M within the endothelial blood-brain barrier. Importantly, blocking *Snai1* translation prevents the downstream inflammatory effects of OSM in endothelial cells, providing a rational pathway for future studies. Utilizing BBB-specific *Snai1* knockouts will further clarify the signaling effects of oncostatin M, and potentially reveal therapeutic targets for autoimmune-mediated neuroinflammation.

Table 4.1 Reagents Used

Reagents	Company	Catalog Number
4–20% Mini-PROTEAN TGX Precast Protein Gels	Bio-Rad	4561094
Amaxa Cell Line Nucleofector Transfection Kit V	Lonza	VCA-1003
Bovine Serum Albumin	Sigma-Aldrich	A1470
Collagenase/Dispase	Sigma-Aldrich	11097113001
Control siRNA-A	Santa Cruz Biotechnology	sc-37007
DMEM (phenol free)	Gibco	31-053-028
DNAse I	Spectrum	D348910MG
ECIS Array	Applied Biophysics	8W10E+PC
Human Complete Endothelial Cell Medium	Cell Biologics	H1168
Human Primary Brain Microvascular Endothelial Cells	Cell Biologics	H-6023
Mouse Complete Endothelial Cell Medium	Cell Biologics	M1168
Odyssey Blocking Buffer (TBS)	LI-COR	927-50000
Oncostatin M (recombinant human)	R&D Systems	295-OM-010
Oncostatin M (recombinant mouse)	R&D Systems	495-MO-025
Phosphate Buffered Saline	Fischer Scientific	BP3994
SNAI1 siRNA	Santa Cruz Biotechnology	sc-38399
Trans-Blot Turbo Mini Nitrocellulose Transfer Kit	Bio-Rad	1704158

Table 4.2 Antibodies Used

Antibody	Figure	Vendor	Catalog	Concentration
β-Actin	4.1 A, B, C, D	LI-COR Bioscience	926-42212	1:1000
Active β-Catenin	4.1 C	EMD Millipore	05-665	1:500
Donkey anti-Mouse IgG IRDye 680RD	4.1 A, B, C	LI-COR Bioscience	925-68074	1:20000
Donkey anti-Mouse IgG IRDye 800CW	4.1 A, C	LI-COR Bioscience	926-32212	1:15000
Donkey anti-Rabbit IgG IRDye 800CW	4.1 A, B, C	LI-COR Bioscience	926-32213	1:15000
pFoxO1 (Thr24)	4.1 C	Cell Signaling Technology	2599	1:1000
pSTAT3 (Tyr705)	4.1 A, B	Cell Signaling Technology	9145	1:2000
SNAIL	4.1 A, D	Cell Signaling Technology	3895	1:1000
STAT3	4.1 A	Cell Signaling Technology	9139	1:1000

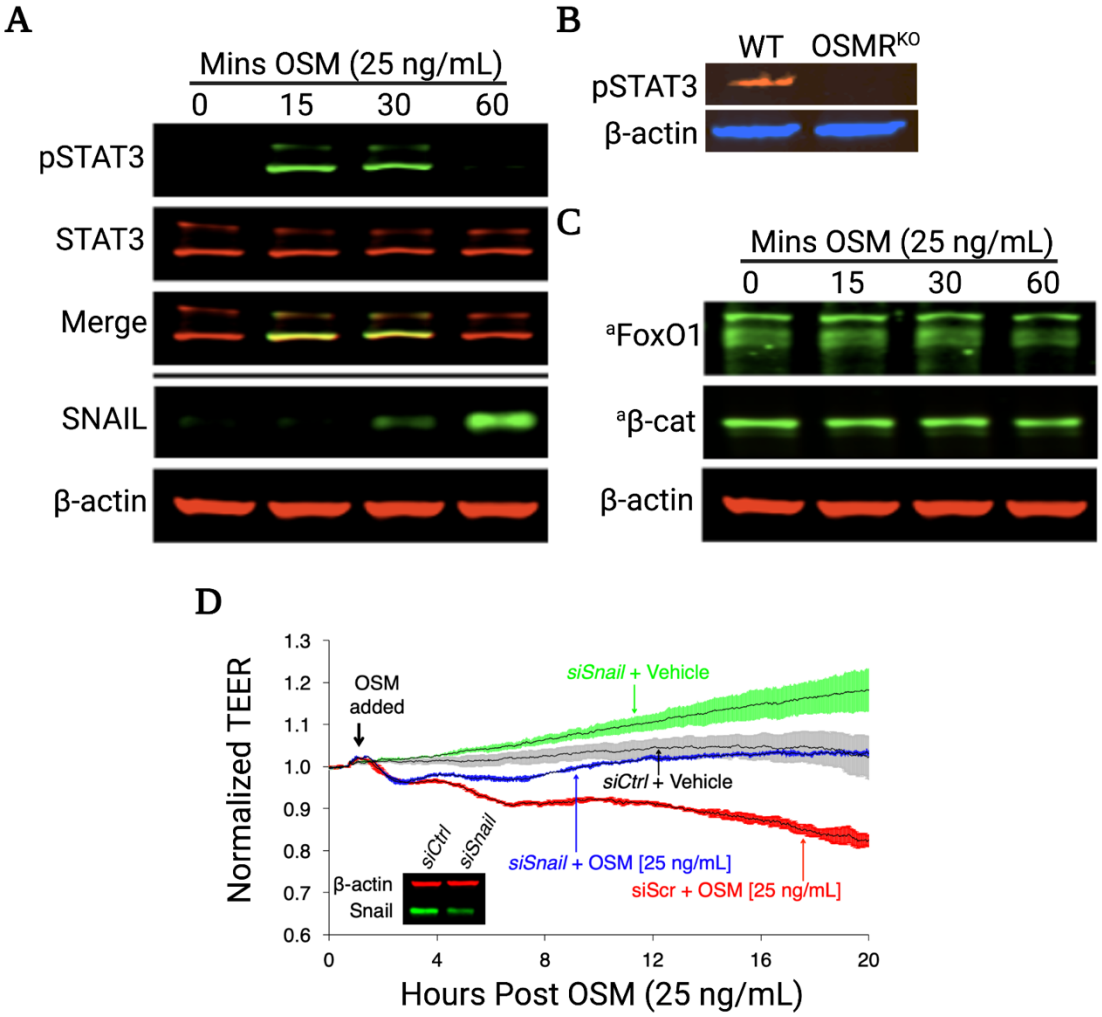

Figure 4.1 Oncostatin M induces increased STAT3 phosphorylation and is Requires SNAIL in the Inflammatory Dysfunction of Brain Microvascular Endothelial Cells.

A) In the 15 minutes following OSM stimulation, human brain microvascular endothelial cells (BMVEC) phosphorylate STAT3, which is returned to normal by 60 minutes. Concomitantly, SNAIL is upregulated at 30 minutes, and remains until at least 60 minutes. **B)** Murine BMVECs similarly show phosphorylation of STAT3. At 30 minutes following OSM stimulation, $OSMR^{KO}$ brain endothelial cells do not show STAT3 phosphorylation as measured by Western blot. **C)** Neither active FoxO1(^{a}FoxO1) nor active β-catenin (^{a}β-cat) change during the first 60 minutes after OSM stimulation. **D)**

Following siRNA-mediated knockdown of SNAIL (blue), brain microvascular endothelial cells are resistant to OSM-mediated barrier dysfunction compared to siRNA scramble control (red). Cells transfected with siSnail maintain higher barrier resistance than cells with control siRNA and vehicle control (green). Inset demonstrates effective knockdown of Snail as measured by Western blot.

References

Arita, Ken, Andrew P. South, Günter Hans-Filho, Thais Harumi Sakuma, Joey Lai-Cheong, Suzanne Clements, Maçanori Odashiro, et al. 2008. "Oncostatin M Receptor-Beta Mutations Underlie Familial Primary Localized Cutaneous Amyloidosis." *American Journal of Human Genetics* 82 (1): 73–80. https://doi.org/10/fwn2q7.

Beard Jr., Richard S, Brian A Hoettels, Jamie E Meegan, Travis S Wertz, Byeong J Cha, Xiaoyuan Yang, Julia T Oxford, Mack H Wu, and Sarah Y Yuan. 2018. "AKT2 Maintains Brain Endothelial Claudin-5 Expression and Selective Activation of IR/AKT2/FOXO1-Signaling Reverses Barrier Dysfunction." *Journal of Cerebral Blood Flow & Metabolism*, December, 0271678X1881751. https://doi.org/10.1177/0271678X18817512.

Frutos, Cristina A. de, Sonia Vega, Miguel Manzanares, Juana M. Flores, Hector Huertas, M. Luisa Martínez-Frías, and M. Angela Nieto. 2007. "Snail1 Is a Transcriptional Effector of FGFR3 Signaling during Chondrogenesis and Achondroplasias." *Developmental Cell* 13 (6): 872–83. https://doi.org/10/cwqsb3.

Murray, Stephen A., Ethan A. Carver, and Thomas Gridley. 2006. "Generation of a Snail1 (Snai1) Conditional Null Allele." *Genesis* 44 (1): 7–11. https://doi.org/10.1002/gene.20178.

Schaefer, L. K., S. Wang, and T. S. Schaefer. 2000. "Oncostatin M Activates Stat DNA Binding and Transcriptional Activity in Primary Human Fetal Astrocytes: Low- and High-Passage Cells Have Distinct Patterns of Stat Activation." *Cytokine* 12 (11): 1647–55. https://doi.org/10/bsvthz.

Talati, Pooja G., Lei Gu, Elyse M. Ellsworth, Melanie A. Girondo, Marco Trerotola, David T. Hoang, Benjamin Leiby, et al. 2015. "Jak2-Stat5a/b Signaling Induces Epithelial-to-Mesenchymal Transition and Stem-Like Cell Properties in Prostate Cancer." *The American Journal of Pathology* 185 (9): 2505–22. https://doi.org/10/gmskfk.

Thoma, B., T. A. Bird, D. J. Friend, D. P. Gearing, and S. K. Dower. 1994. "Oncostatin M and Leukemia Inhibitory Factor Trigger Overlapping and Different Signals through Partially Shared Receptor Complexes." *The Journal of Biological Chemistry* 269 (8): 6215–22.

Van Wagoner, N. J., C. Choi, P. Repovic, and E. N. Benveniste. 2000. "Oncostatin M Regulation of Interleukin-6 Expression in Astrocytes: Biphasic Regulation Involving the Mitogen-Activated Protein Kinases ERK1/2 and P38." *Journal of Neurochemistry* 75 (2): 563–75. https://doi.org/10/cmq26r.

Visan, Ioana. 2015. "About STATs." *Nature Immunology* 16 (7): 688–688. https://doi.org/10/gmskfm.

Yang, Jinbo, and George R. Stark. 2008. "Roles of Unphosphorylated STATs in Signaling." *Cell Research* 18 (4): 443–51. https://doi.org/10/d2zn9h.

Zhang, Xinbo, Naimei Tang, Timothy J. Hadden, and Arun K. Rishi. 2011. "Akt, FoxO and Regulation of Apoptosis." *Biochimica Et Biophysica Acta* 1813 (11): 1978–86. https://doi.org/10/c2q8v5.

APPENDIX A

AKT2 maintains brain endothelial claudin-5 expression and selective activation of IR/AKT2/FOXO1-signaling reverses barrier dysfunction

Citation: Beard Jr., R. S., Hoettels, B. A., Meegan, J. E., Wertz, T. S., Cha, B. J., Yang, X., et al. (2018). AKT2 maintains brain endothelial claudin-5 expression and selective activation of IR/AKT2/FOXO1-signaling reverses barrier dysfunction. Journal of Cerebral Blood Flow & Metabolism, 0271678X1881751. doi:10.1177/0271678X18817512.

Abstract

Inflammation-induced blood–brain barrier (BBB) dysfunction and microvascular leakage are associated with a host of neurological disorders. The tight junction protein claudin-5 (CLDN5) is a crucial protein necessary for BBB integrity and maintenance. CLDN5 is negatively regulated by the transcriptional repressor FOXO1, whose activity increases during impaired insulin/AKT signaling. Owing to an incomplete understanding of the mechanisms that regulate CLDN5 expression in BBB maintenance and dysfunction, therapeutic interventions remain underdeveloped. Here, we show a novel isoform-specific function for AKT2 in maintenance of BBB integrity. We identified that AKT2 during homeostasis specifically regulates CLDN5-dependent barrier integrity in brain microvascular endothelial cells (BMVECs) and that intervention with a selective insulin-receptor (IR) agonist, demethylasterriquinone B1 (DMAQ-B1), rescued IL-1b-induced AKT2 inactivation, FOXO1 nuclear accumulation, and loss of CLDN5-dependent barrier integrity. Moreover, DMAQ-B1 attenuated preclinical CLDN5-dependent BBB dysfunction in mice subjected to experimental autoimmune encephalomyelitis. Taken together, the data suggest a regulatory role for IR/AKT2/FOXO1-signaling in CLDN5 expression and BBB integrity during neuroinflammation.

Introduction

Blood–brain barrier (BBB) dysfunction is a pathological hallmark in inflammation-associated diseases of the central nervous system (CNS), including multiple sclerosis, stroke, dementia, traumatic brain injuries, encephalopathies, and brain metastases.[1–4] Under homeostasis, local cues promote BBB maintenance by fostering highly restrictive brain endothelial cell–cell contacts.[5–7] During an aberrant inflammatory response, however, BBB dysfunction can be triggered by mediators from circulation or the CNS, which act upon endothelial cells (ECs) to reduce their cell–cell adhesive forces. Loss of this adhesion results in barrier hyperpermeability, leading to edema, poor nutrient exchange, neuronal toxicity, and CNS dysfunction.[8,9]

This compromise in BBB integrity is a direct result of inflammatory-mediated disruption of the adherens and tight junction complexes at endothelial cell–cell contacts.[10,11] Although the establishment of the BBB interface requires the involvement of various junctional proteins, the tight junction protein claudin-5 (CLDN5) is known to play an indispensable role in restricting small molecule flux through paracellular passageways.[12–14] In vitro BBB models have demonstrated that CLDN5 is a common target of inflammatory mediators such as interleukin-1β (IL-1β),[15] homocysteine,[16,17] and tumor necrosis factor alpha,[18] while multiple animal models of CNS diseases have shown loss of CLDN5 is a common phenomenon associated with BBB dysfunction.[16,18–23]

Maturation of endothelial tight junctions produced by high levels of CLDN5 is known to require AKT-dependent inactivation and dissociation of the transcription factor FOXO1 from a silencer region within the *Cldn5* promoter.[13,15] Under certain proinflammatory conditions, FOXO1 can re-occupy this silencer, resulting in CLDN5

downregulation and endothelial barrier dysfunction.[15,24,25] Moreover, we have shown in vitro that siRNA-mediated knockdown of *FoxO1* prevents loss of CLDN5 during IL-1β-mediated barrier dysfunction,[15] suggesting that targeting FOXO1 inactivation directly or through upstream regulators, such as AKT, could be an effective means for therapeutic preservation of CLDN5 during inflammation.

Given the complexity and extensiveness of the AKT signaling network, it is not surprising that the outcome of AKT signaling on endothelial barrier maintenance appears to be highly context-dependent. This convolution is, in part, due to AKT isoforms that can have both overlapping and distinct functions,[26] of which both AKT1 and AKT2 have been shown to have unique regulatory roles in vascular endothelium. While much remains undetermined about these isoform-specific functions, AKT1 is known to be involved in the proinflammatory-mediated loss of endothelial barrier integrity, while its deficiency protects against endothelial hyperpermeability in a λ-carrageenan-induced edema model.[27] By way of contrast, AKT2 is known to distinctly regulate endothelial insulin signaling,[28] but it remains largely unknown whether AKT2 is involved in any modulation of barrier integrity.

The role of vascular insulin signaling in endothelial barrier maintenance is even more complicated, as some groups have shown insulin-mediated barrier enhancement, while others have shown negligible effects.[29–31] Although vascular insulin signaling canonically acts through the insulin receptor (IR), insulin is well-known to be cross-reactive with the insulin-like growth factor 1 receptor (IGF1R) and vice versa with insulin-like growth factors (IGFs) cross-reacting with the IR. Despite a high degree of homology between these two receptors, knockout studies have demonstrated that these

pathways mediate very distinct cellular and physiological processes. Namely, the IGF1R primarily mediates mitogenic pathways, while the IR regulates metabolic effects. Due to insulin's receptor promiscuity and conflicting information regarding the effects of insulin on BBB integrity, identifying selective agonists would undoubtedly aid in clarifying the role for IR-specific signaling in endothelial barrier modulation.

Given that FOXO1 inactivation is a known metabolic target for IR signaling,[32] we explored a novel role for IR/AKT/FOXO1-signaling to regulate CLDN5-dependent BBB integrity. First, we establish a pathophysiological relevance for studying this pathway by analyzing brain microvessels isolated from mice with neuroinflammation-induced BBB disruption and demonstrate increased FOXO1 concurrent with decreased CLDN5. We next show that AKT-mediated regulation of CLDN5 and brain microvascular endothelial cell (BMVEC) integrity is distinct to the AKT2 isoform. Furthermore, the selective IR agonist demethylasterriquinone B1 (DMAQ-B1), unlike insulin or IGF-1, preferentially induces IR signaling, decreases FOXO1 nuclear accumulation, upregulates CLDN5, and enhances barrier function in cultured BMVECs. Finally, and most importantly, we demonstrate that DMAQ-B1-dependent IR/AKT2/FOXO1-signaling reverses inflammation-mediated CLDN5 loss and BBB dysfunction. The results from these experiments establish that selective activation of the IR can reverse the aberrant loss of BBB integrity during inflammation. We suggest targeting the IR/AKT2/FOXO1/CLDN5-axis as a potential therapy in CNS diseases associated with BBB dysfunction.

Materials and Methods

Reagents and Supplies

A complete list of reagents and supplies including purchasing information can be found in Supplementary Tables 1 and 2.

Animal Use

Mice used in these studies were C57BL/6 J purchased from Jackson Laboratory. Animals were maintained under a 12-h light/dark schedule with food and water ad libitum. All animal use was approved by the Institutional Animal Care and Use Committees at the University of South Florida and Boise State University and was performed in accordance with the Guide for the Care and Use of Laboratory Animals. All experiments have been reported in compliance with the ARRIVE guidelines.

Experimental Autoimmune Encephalomyelitis and DMAQ-B1 Pharmacotherapy

Ten-week-old male mice were immunized with experimental autoimmune encephalomyelitis (EAE)-inducing kits per the manufacturer's instructions (Hooke Labs, MA) and standardized protocols.[33,34] All analyses and treatments were performed during the preclinical stage at seven to eight days post-induction (d.p.i.), which is a time frame well-established for the onset of EAE-induced BBB dysfunction.[35] For pharmacologic studies, EAE mice (7 d.p.i.) or controls were randomly assigned to receive a single dose of DMAQ-B1 (5 mg/kg) or vehicle (0.5% methylcellulose).[36] Methylcellulose and DMAQ-B1 were prepared fresh daily and administered via oral-gavage with a stainless-steel curved gavage needle (18 G, 5 cm length, 2.4 mm tip; Kent Scientific). Mice were monitored for signs of distress or hypoglycemia for 24 h. Pilot studies revealed that a single-dose of 5 mg/kg did not result in any hypoglycemic episodes.

Analyses of BBB Integrity

As previously described with minor modifications, *Evans blue* (*EB*) *extravasation assays* were used to determine EAE-induced BBB dysfunction.[37,38] Briefly, for EB leakage studies in Figure 1(a), animals ($n = 3$; EAE – 7 d.p.i.) were injected I.P. with 100 µL of 2% EB in PBS, or PBS alone as a 'no EB' control for autofluorescence, 24 h prior to Lactated Ringer's (LR) flushes via transcardial perfusion and perfusion fixation with 4% paraformaldehyde (PFA). Brains were excised and sectioned into 1 mm slices from rostral to caudal using a coronal Adult Mouse Brain Slicer (Zivic Instruments). Slices were arranged and imaged at 700 and 800 nm with a near-infrared imaging system (Odyssey CLx; LI-COR Biosciences). For EB leakage studies in Figure 7(e) and (f) ($n = 5–6$), blood was collected via cardiac puncture and brains were removed after LR flushes and divided into right and left halves. The right half was post-fixed for 24 h in 4% PFA and a sagittal image was obtained with the Odyssey CLx, as shown in Figure 1(a). The left half was homogenized in 1 mL of PBS. EB from the homogenates and plasma was extracted into formamide (2 mL at 60 °C for 24 h) and supernatants (5000 × *g* for 30 min) were compared against an EB standard curve. As an indicator of BBB protein leakage, brain/serum EB concentrations were normalized per brain weight (mg), and values are represented as fold change from control.

In an additional set of experiments (Figure 7(g)), *sodium fluorescein extravasation assays* were used as an indicator of small solute (376 Da; Stokes' radius ≈ 0.45 nm) leakage.[16,39] Mice ($n = 3$; EAE – 8 d.p.i) were injected I.P. with 5 µL/g of 10% sodium fluorescein in saline solution. After 2 h, blood was collected by cardiac puncture, the remaining blood in the cerebrovasculature was flushed with LR, and brains

were rapidly excised. Diluted blood-serum (1:10 in PBS) and supernatants (12,000 × *g* for 15 min at 4°C) from brain homogenates (6 strokes with loose-fitting Dounce homogenizer) were diluted 1:10 in 20% trichloroacetic acid (TCA). After incubation at 4°C for 24 h, supernatants (12,000 × g for 15 min) were removed and diluted with equal volumes of borate buffer (0.05 M, pH 10). Fluorescence (ex. 480 nm, em. 538 nm) from sample supernatants containing solubilized sodium fluorescein in 10% TCA and 0.025 M borate buffer was quantified, brain/serum sodium fluorescein concentration values were normalized per brain weight (mg), and values are represented as fold change from control.

Microvessel Isolation and Characterization

Microvessel isolations were performed as previously described.[40] Whole brains were excised, meninges and pial vessels were carefully removed, and the remaining tissue was homogenized (six strokes with a loose-fitting Dounce homogenizer) in phenol-free DMEM + 2% FBS (DMEM-S). Homogenates were then mixed 1:1 with 36% dextran (~70 kDa; Sigma), and centrifuged for 10 min at 10,000 × *g*. Pellets were resuspended in DMEM-S and sieved through a 70 µm strainer to retain large vessels and allow microvessels to pass through. To reduce RBC contamination, microvessel pellets were layered over Percoll and centrifuged at 1700 × *g* for 10 min. The microvessel enriched pellet was rinsed twice with DMEM and used for further analyses.

For immunostaining and confocal fluorescence microscopy experiments, isolated microvessels from three mice were pooled ($n = 27$; 9 pools of 3), fixed with 4% PFA and permeabilized with 10% donkey serum containing 0.05% Triton X-100. Microvessels were immunostained per standard protocols with appropriate primary and secondary

antibodies in microfuge tubes with end-over-end rotation (see Supplementary Table 2). Stained vessels were adhered to slides via cytocentrifugation (Cytospin, Thermo Shandon), then mounted in Vectashield containing DAPI to coverslips. Confocal micrographs were taken with an Olympus FLUOVIEW FV1000 confocal laser scanning microscope (Olympus), and image stacks were analyzed and processed with Imaris (Bitplane). For Figure 1(b) to ((f),f), Imaris 'Surface' rendering (thresholding) was used to define regions showing positive fluorescence intensity and then the average intensity per voxel in those regions, or volumes of interest (VOI), was determined. For Figure 1(d), nuclei were defined by thresholding and FOXO1 intensities only within these nuclear VOIs were measured.

For Western blotting, microvessels were isolated as above, except that mice were perfused (transcardial) with PBS containing protease and phosphatase inhibitors before excising the brain. Microvessel pellets from three mice were pooled ($n = 9$; 3 pools of 3), resuspended in ice-cold RIPA with protease and phosphatase inhibitors, homogenized (20 strokes with tight-fitting Dounce homogenizer) and incubated on ice for 20 min. Samples were centrifuged at 12,000 × *g* for 10 min at 4°C, supernatants were collected, protein concentrations were determined by BCA assay, and sample protein was normalized in Laemmli sample buffer.

Primary BMVEC Isolation

As we have previously described,[15] primary BMVECs were obtained from isolated microvessels (described above) of C57BL/6 J pups between P7 and P10 (~10 pups for a confluent 25 cm^2 monolayer). The resultant microvessel pellets were resuspended in HBSS with collagenase/dispase, DNase I, and N_a-tosyl-L-lysine

chloromethyl ketone (TLCK) for 40 min at 37°C. BMVECs were pelleted, washed with DMEM-S, seeded at confluence, and grown on collagen type IV-coated plates in endothelial growth medium (Cell Biologics) at 37°C with 5% CO_2 in a humidified incubator. Unless otherwise stated in figure legends, only initially plated cells (P0) or cells passaged once (P1) at a 1:1 ratio were used in these experiments. Additionally, before use in experiments, BMVECs were grown for two to seven days post-confluence (P.C.) to allow for proper maturation of tight junctions.

BMVEC Barrier Function Assays

Endothelial cell barrier functional assays were conducted as we have previously demonstrated.[15] *For solute permeability and transwell transendothelial electrical resistance (TEER) assays*, BMVEC monolayers were grown seven days P.C. in collagen type IV-coated, 0.4 μm PTFE transwell inserts prior to inflammatory injury and/or treatment with pharmacologic and molecular interventions. Before adding sodium fluorescein (0.5 mg/mL) to the luminal chamber, stable measurements of TEER ($\Omega \times cm^2$) were obtained with a Millicell-ERS voltohmmeter (EMD Millipore). Then, 30 min after luminal addition of sodium fluorescein, samples were collected from both the upper (luminal) and lower (abluminal) chambers for fluorescence analyses. Sodium fluorescein concentrations were determined using a standard curve and the sodium fluorescein permeability coefficient (P_s) was calculated as follows: $P_S = [A]/t \times 1/A \times V/[L]$ where $[A]$ is the abluminal concentration; t is the time in seconds; A is the area of the membrane in cm^2; V is the volume of the abluminal chamber; and $[L]$ is the luminal concentration. *For electric cell-substrate impedance (ECIS)-based TEER assays*, an indicator of cell-cell adhesive barrier resistance, the barrier function of cultured BMVEC

monolayers was determined by measuring real-time TEER using an ECIS sensor (ECIS Zθ, Applied BioPhysics). ECIS tracings are presented as normalized TEER, and peak changes are quantified for statistical analyses.

Gene Silencing

Introduction of siRNA duplexes was achieved using a Nucleofector® Kit from Amaxa Biosystems (MD, USA), as we have previously described.[15] BMVECs (1×10^6) were resuspended in 100 µL of transfection solution, mixed to final concentration of 2 µM siRNA, and transfected with program T-011 on the Nucleofector IIb™ device. Cells were plated onto collagen type IV-coated ECIS arrays, transwell inserts and/or culture flasks.

BMVEC Immunocytochemistry

Tight junction proteins were immunostained in BMVEC monolayers per standard immunohistochemistry (ICC) protocols and as we have shown before.[15,41,42] BMVECs were grown to 48 h P.C. on glass coverslips and treated with various doses of DMAQ-B1 for 6 h. Cell monolayers were fixed with 4% PFA, permeabilized with 0.05% Triton X-100, blocked with 2% BSA in PBS, and probed with anti-CLDN5 (AF 488) and anti-ZO-1 (AF 594) primary conjugated antibodies overnight at 4°C. Coverslips were mounted with Vectashield containing DAPI, confocal micrographs were obtained with Olympus FLUOVIEW FV1000 confocal laser-scanning microscope, and images were analyzed and processed with Imaris (Bitplane). For Figure 5, ZO-1^+ areas at endothelial cell–cell borders were defined by thresholding with Surface rendering in Imaris software. Then the total CLDN5 intensity in these ZO-1^+ areas was measured and divided by ZO-1^+ areas to provide average CLDN5. For representative 3D images, a 3D-colocalization channel

(yellow) was used to highlight the increased density of CLDN5 in tight junction complexes.

Sandwich FLISAs

Three separate sandwich fluorescent-linked immunosorbent assays (FLISAs) were used per standard protocols and adapted for detection with the Odyssey CLx. Briefly, microtiter plates were coated with capture antibodies (5 µg/mL) in carbonate/bicarbonate buffer (pH 9.6) overnight at 4°C, and blocked at RT for 1 h. Protein concentrations of BMVEC lysates were normalized (BCA assay) and incubated in capture antibody-coated wells for 90 min at 37°C. Plates were washed with TBS + 0.05% Tween-20 (TBST) and then incubated with detection antibodies for 2 h at RT. Plates were either imaged immediately on Odyssey CLx (IRDye® 800CW-conjugated primary antibodies) or incubated with IRDye® 800CW-conjugated secondary antibody for 1 h at RT before imaging. As an indicator of IR and IGFR1 activity, a sandwich FLISA was developed to determine tyrosine phosphorylation on insulin receptor substrate 1 (IRS-1). A mouse anti-IRS-1 antibody was used as the capture antibody, and a primary rabbit anti-phosphotyrosine followed by a secondary IRDye® 800CW-conjugated donkey anti-rabbit was used as the detection antibody. In order to identify the isoform-specificity of AKT activation loop phosphorylation at T308 (pT308 on AKT), isoform-specific rabbit monoclonal antibodies against either AKT1 or AKT2 were used as capture antibodies and an IRDye® 800CW-conjugated rabbit anti-pAKT(T308) was used as the detection antibody. An IRDye® 800CW Labeling Kit (LI-COR Biosciences) was used for primary conjugation to the rabbit anti-pAKT(T308), as per the manufacturer's instructions.

High-salt Nuclear Extraction

Nuclear isolation and protein extraction was performed as previously described.[15] Following treatments, BMVECs were collected into non-nuclear extraction buffer (Buffer A: 10 mM HEPES, 1.5 mM $MgCl_2$, 10 mM KCl, 0.5 mM DTT, 0.05% NP40, pH 7.9) with protease and phosphatase inhibitors. Nuclei were pelleted and washed. Pellets were resuspended in Buffer B (5 mM HEPES, 1.5 mM $MgCl_2$, 0.2 mM EDTA, 0.5 mM DTT, 26% glycerol (v/v), 300 mM NaCl, pH 7.9). Samples were homogenized (20 strokes tight-fitting Dounce homogenizer), incubated on ice for 30 min, centrifuged at 24,000 $\times g$ for 20 min at 4°C, and the supernatant was collected as nuclear extract. Protein from nuclear extract was quantified (BCA assay) and normalized in Laemmli sample buffer.

mRNA and Protein Analyses

For real-time quantitative PCR (qPCR) assays, mRNA was isolated from BMVEC monolayers with RNAzol® following manufacturer's procedures. RNA was normalized, and reverse transcription was completed with iScript™ cDNA Synthesis Kit according to the manufacturer's procedures. Quantification cycle (Cq) values were determined with quantitative real-time PCR in accordance with the PrimePCR™ assay. The $2^{-\Delta\Delta Cq}$ method was used as a relative quantification strategy with the results presented as the fold change of target gene expression in a target sample relative to a control sample, normalized to β-actin as the reference gene. *For Western blotting*, two-color near-finrared immunoblotting was completed per standardized protocols and imaged with an Odyssey CLx scanner.

Statistical Analyses

All statistical analyses were performed with Prism (Version 7.0 e; Graphpad Software, Inc.). α was set at 0.05 a priori for statistical significance. No specific blinding was performed in these studies. A detailed list of statistical analyses is provided in Supplementary Table 3.

Results

Endothelial FOXO1 is Activated and CLDN5 is Downregulated During Neuroinflammation

EAE-induced BBB dysfunction precedes the onset of CNS damage, demyelination, and paralysis.[43] Accordingly, CLDN5 loss from BBB has also been reported during EAE.[20,35,45] Using this model, we analyzed EB leakage to confirm neuroinflammatory-mediated BBB dysfunction (Figure 1(a)). Given the knowledge, albeit primarily based on cell culture studies, that CLDN5 is regulated by FOXO1-mediated transcriptional repression,[13,15,25] we then sought out evidence for this mechanism in microvessels isolated from mice with EAE-induced BBB dysfunction. As hypothesized, microvessels from EAE mice have significantly total and nuclear-localized FOXO1 (tFOXO1 and nFOXO1, respectively) staining (Figure 1(b) to (d)). At BBB tight junctions, ZO-1 expression remained unchanged and served as a volume of interest (VOI) to analyze changes in CLDN5 density (Figure 1(b), ((e)e) and ((f)).f)). Expressional changes were also confirmed by immunoblotting microvessel homogenates (Figure 1(g) and ((hh)).

BMVEC Regulation of CLDN5 by AKT is Isoform-Specific

Next, we investigated AKT isoform-specific regulation of CLDN5-dependent BMVEC barrier function. We tested several conditions where CLDN5 expression is known to change and evaluated relative differences in the most likely AKT isoforms to be involved in CLDN5 regulation, AKT1 and AKT2 (Figure 2). BBB endothelial cells are known to lose their barrier properties in culture, especially with subsequent passaging. Here we demonstrate by immunoblotting BMVEC lysates that CLDN5 and AKT2, but not AKT1, are significantly decreased after passaging freshly isolated BMVECs (P0) (Figure 2(a)). Knowing that BMVEC CLDN5 expression levels continue to incrementally increase for several days after confluence, we compared the daily changes in expression levels of *Akt1*, *Akt2*, and *Cldn5* in BMVEC monolayers relative to the levels in subconfluent BMVECs (Figure 2(b)). While relative mRNA for all of these genes increased after confluence (1 day P.C.), only *Akt2* and *Cldn5* continued over the following days. To determine the direct isoform-specific effect of AKT on CLDN5, we silenced *Akt1* and *Akt2* with siRNA and evaluated CLDN5 expression and TEER. Knockdown efficiency was ~50% for both AKT1 and AKT2. However, immunoblotting the same lysates for CLDN5 revealed that only knockdown of AKT2 had any detectable effect on CLDN5 expression (Figure 2(c) and ((d)).d)). Simultaneously, the effects of *Akt1* and *Akt2* silencing on BMVEC monolayers revealed that loss of AKT2 causes significant barrier dysfunction (Figure 2(e)). Interestingly, AKT1 knockdown produced a nominal increase in barrier integrity, which is consistent with the findings that suggest AKT1 activation may be involved in hyperpermeability.[27]

We previously reported that exposing BMVECs to elevated IL-1β for 1.5 h causes AKT inactivation (decreased pT308 on AKT), FOXO1 activation (increased pT24 on FOXO1, nuclear accumulation, and occupancy on *Cldn5* silencer), and CLDN5 loss (decreased mRNA and protein) sustained for at least 24 h.[15] Here, we found that exposing BMVECs to IL-1β for 24 h also leads to loss of AKT2 expression, but not AKT1 (Figure 2(f)). Since we have shown in this work that nuclear accumulation of FOXO1 and downregulation of CLDN5 are present in brain microvessels of EAE mice (Figure 1), we immunoblotted those same lysates for expression levels of AKT1 and AKT2 (Figure 2(g)). As with IL-1β-mediated loss of AKT2, microvessels from EAE mice have decreased AKT2 with no loss of AKT1.

Selective activation of IR signaling in BMVECs enhances barrier integrity

While the role of AKT1 in endothelial cells has been well-studied, the only known function in endothelium for which AKT2 may be the predominant mediator is insulin signaling. Although the insulin signaling pathway is well-known to regulate FOXO transcription factors,[46] there is a scarcity of knowledge regarding insulin signaling in the regulation of CLDN5-dependent BBB integrity. This lack of information is likely because of multiple confounders that make it difficult to study insulin-receptor signaling, such as receptor promiscuity and overlapping functions of insulin and IGFs, heterogeneous IR and IGFR expression, heterodimerization of the IR and IGFR subunits, insulin resistance, and multiple intracellular targets. Thus, in these studies, we used the IR-selective agonist DMAQ-B1 and compared it to insulin- and IGF-signaling in BMVECs. Since IRS-1 can be a common substrate for both IR and IGFR tyrosine kinases[47] and may be upstream of AKT2/FOXO1-signaling,[46] we used sandwich FLISAs

to identify the EC_{50} of insulin (Figure 3(a)), IGF-1 (Figure 3(b)), and DMAQ-B1 (Figure 3(c)), on tyrosine phosphorylation of IRS-1. The EC_{50} for insulin and IGF-1 was within the physiological response ranges,[48] and the EC_{50} for DMAQ-B1 was similar to previous reports.[36]

As one of several small-molecule IR agonists that have been tested for their utility as oral anti-diabetics, DMAQ-B1 was discovered to preferentially trigger IR-dependent activation of PI3K/AKT signaling at low concentrations, without activating the IGF1R or its canonical downstream ERK1/2 pathway.[53] Using the EC_{50} for pIRS-1, we found that treating BMVECs with insulin [2 nM], IGF-1 [20 nM], and DMAQ-B1 [5 μM] all led to a similar increase in active AKT; however, only insulin and IGF-1 increased ERK activity (Figure 3(d)). Interestingly, even though all three agonists induced comparable phosphorylation of IRS-1 and AKT phosphorylation, only DMAQ-B1 led to decreased nuclear localization of FOXO1, upregulation of CLDN5, and enhancement of BMVEC barrier function (Figure 3(e) to ((h)).h)). To confirm that the presence of DMAQ-B1 had no confounding impact on BMVEC proliferation or viability in our cell culture studies, a stain-based cell cycle assay (DAPI) and a stain-based viability assay (calcein AM and propidium iodide) were conducted on BMVEC monolayers (P3; two days P.C.) following 6 h of incubation with DMAQ-B1 [5 μM] or a vehicle control and no differences were observed in either cell cycle distribution or ratio of viable to nonviable cells (Figure S1).

<u>DMAQ-B1 promotes AKT2/FOXO1-signaling and increases Cldn5 mRNA upregulation</u>

Further analyses of DMAQ-B1 revealed that DMAQ-B1 dose-dependently promotes AKT2-specific activation (pT308 on AKT2; Figure 4(a) and ((b)),b)), FOXO1 inactivation (decreased nuclear accumulation; Figure 4(c)), and transcriptional-mediated

upregulation of *Cldn5* (qRT-PCR/mRNA – Figure 4(d); ICC/protein – Figure 5; and WB/protein – Figure S2). Compared to vehicle (0 μM), treating BMVECs with 2.5, 5, and 10 μM of DMAQ-B1 increased total active AKT (pT308) after 45 min. However, sandwich FLISAs revealed that DMAQ-B1 [10 μM] significantly increased pT308 on AKT2, but not AKT1 (Figure 4(b)). Additionally, we found that *Cldn5* mRNA is increased concurrently with decreased ^{n}FOXO1 following 45 min of treatment with DMAQ-B1. DMAQ-B1 also dose-dependently increased CLDN5 protein levels after 6 h (WB – Figure S1; ICC – Figure 5). Confocal analysis of fixed BMVECs demonstrated that increased CLDN5 levels were indeed localized to the EC–EC tight junctions demarcated by ZO-1, which was unchanged with DMAQ-B1 treatment. Furthermore, 3D rendering of a CLDN5 at ZO-1 colocalization channel highlights how upregulation of CLDN5 does not just increase its turnover, but significantly increases its density at EC–EC junctions (Figure 5).

DMAQ-B1-Mediated BMVEC Barrier Enhancement is Dependent upon CLDN5 Upregulation

Using three separate techniques to measure BMVEC barrier function, we found in all cases that DMAQ-B1 dose-dependently increases ECIS-TEER (Figure 6(a)), transwell-fluorescein permeability (Figure 6(b)), and transwell-TEER (Figure 6(c)). To determine a causal role for CLDN5 in DMAQ-B1-mediated BMVEC barrier enhancement, we silenced *Cldn5* with siRNA (Figure 6(d)) and analyzed TEER (Figure 6(e)) or transwell permeability assays (Figure 6(f)). Efficiency of CLDN5 knockdown was determined by immunoblotting 24 h after transfection (Figure 6(d)). *Cldn5*-silenced

monolayers abrogated the barrier-enhancing effects of DMAQ-B1 [5 μM; 6 h] compared to controls (Figure 6(e) and ((f)).f)).

DMAQ-B1 Reverses Inflammation-Induced BMVEC Barrier Disruption In Vitro and In Vivo

Given that inflammation is well known to mediate insulin resistance,[49,71] we sought to determine if DMAQ-B1 could attenuate inflammation-mediated BMVEC barrier dysfunction in vitro and in vivo. We first found that DMAQ-B1 can attenuate IL-1β-mediated AKT activation, FOXO1 inactivation, and CLDN5 downregulation (Figure 7(a)). Next, we treated IL-1β-stimulated [100 ng/mL] BMVECs on ECIS after 1 h with DMAQ-B1 and followed TEER tracings for an additional 5 h. DMAQ-B1 [5 μM] not only increased baseline TEER, but also increased TEER of IL-1β-treated BMVECs (Figure 7(b) and ((c)).c)). Additionally, IL-1β-mediated sodium fluorescein hyperpermeability was rescued with co-treatment of DMAQ-B1 (Figure 7(d)). Since we have observed significant BBB dysfunction eight days post-induction of EAE mice, 24 h prior (7 d.p.i.) we gave one single dose of DMAQ-B1 [5 mg/kg; via oral gavage] to both control and EAE mice. Both EB and sodium fluorescein extravasation assays revealed significantly less leakage from brain microvessels in EAE mice treated with DMAQ-B1 compared to those untreated (Fig. 7F--G).G). Concomitantly, EAE-induced loss of CLDN5 was abrogated with DMAQ-B1 (Figure 7(h)).

Discussion

The key finding presented in this study is that isoform-specific activation of AKT2 by the selective IR agonist, DMAQ-B1, rescued loss of CLDN5-dependent BBB integrity. We applied a step-wise approach to demonstrate the involvement of the

AKT2/FOXO1-signaling pathway in maintaining high CLDN5 expression, and determined the potential of DMAQ-B1 to reverse diminished CLDN5 levels. First, we detected significant nuclear accumulation of FOXO1 and loss of CLDN5 in microvessels isolated from mice with EAE-induced BBB dysfunction. Second, by determining the correlation of AKT2 and CLDN5 expression and conducting AKT2-specific knockdown experiments, we identified the importance of AKT2 in maintaining high levels of CLDN5. Third, by evaluating the canonical IR/AKT2/FOXO1 signaling pathway, we determined the novel capacity of DMAQ-B1 to reduce FOXO1 nuclear accumulation, increase CLDN5 density at tight junctions, and strengthen barrier function of primary BMVEC monolayers. Fourth, siRNA-mediated silencing of BMVEC *Cldn5* confirmed that CLDN5 is necessary for enhanced barrier function induced by DMAQ-B1. Lastly, DMAQ-B1 reversed BMVEC barrier dysfunction in vitro and in vivo following inflammatory challenge.

Contemporaneous with inflammation-induced microvascular leakage, a quantitative loss of CLDN5 from the BBB has been reported in multiple neurological diseases, which at least in part suggests that CLDN5 is transcriptionally downregulated. Hence, preventing or reversing this downregulation is key to therapeutic preservation of BBB integrity. FOXO1-mediated transcriptional repression of *Cldn5* was first identified in cell culture studies for its role in AJ-dependent upregulation of CLDN5 following endothelial confluency,[13] and Morini et al.[25] recently extended their findings to include that FOXO1 also recruits a polycomb repressor complex to the same *Cldn5* silencer occupied by FOXO1 in subconfluent endothelial cells. We recapitulate this data as a proof-of-principle for our culture model, but also demonstrate that *Cldn5* mRNA levels

continue to increase beyond endothelial confluency. Elevated levels of FOXO1, along with the loss of CLDN5, were also observed in an acrolein-induced lung injury model.[24] Our results here extend our previous in vitro findings to an in vivo model of neuroinflammatory-mediated CNS injury. In this model, BBB dysfunction precedes EAE-induced paralysis,and CLDN5 downregulation concomitant with BBB dysfunction has been reported multiple times.[20,35,45] However, the precise onset and regulatory mechanisms governing CLDN5 downregulation during EAE was not well-resolved, and to the best of our knowledge, this is the first report of EAE-induced FOXO1 activation in brain microvessels associated with a loss of CLDN5-dependent BBB integrity.

Most literature devoted to FOXO1 in endothelial cells has been focused on angiogenesis and postnatal neovascularization.[31,50–53] However, the role of FOXO1 in highly mature endothelial cells, such as those of the BBB, remains unclear. Our studies, therefore, were intentionally conducted on adult mice in vivo (> 90 d.p.n.), and mature BMVEC monolayers. In addition to our previous FOXO1 knockdown studies,[15] we found enhanced barrier properties of BMVEC monolayers with no signs of overgrowth or apparent problems. Similarly, Park et al.[54] demonstrated inactive FOXO1 in the blood–retinal barrier (BRB) of adult mice, which was reactivated in diabetic retinopathy leading to loss of BRB integrity.[54] Our finding of inflammation-mediated FOXO1 activation and diminished endothelial cell–cell integrity is in line with this finding, as well as another in vivo study demonstrating the atheroprotective effects of endothelial-specific FOXO1 depletion from aortic endothelial cells.[55] Interestingly, this study also reported that upregulation of ICAM-1 and increased monocyte-endothelial adhesion is dependent on FOXO1 activation. Taken as a whole, it would appear that FOXO1 lies dormant in

mature endothelium, especially at the BBB, yet serves as an inflammatory response element that may couple leukocyte transmigration with disassembly of endothelial cell–cell junctional complexes.

FOXO1 inactivation by AKT is a canonical target of insulin signaling in endothelial cells, which is well-known to be impaired during inflammation.[56] Nevertheless, tightly controlled insulin therapy to maintain normoglycemia has been shown to counteract inflammation-mediated endothelial dysfunction,[57–59] suggesting that at least some level of IR activation is intact. A role for insulin-signaling in BBB function remains controversial, as some have shown insulin-mediated barrier enhancement and others have shown no effect.[29–31,60–63] Our results demonstrate that exposing BMVECs to physiologically relevant concentrations of insulin and IGF-1 produced equal levels of IRS-1 phosphorylation compared with DMAQ-B1, but unlike DMAQ-B1-mediated IR agonism they did not reduce nuclear accumulation of FOXO1, alter CLDN5 expression, or enhance BMVEC barrier function. How then do we explain the barrier-enhancing effects of DMAQ-B1, given that all three agonists produced equal levels of not just IRS-1, but AKT phosphorylation too? AKT is well-known to simultaneously both proangiogenic and antiangiogenic, which may be related to isoform-specificity. Thus, one plausible explanation is that insulin and IGF-1 trigger IRS-1 and AKT1 phosphorylation through the IGF1R or hybrid IR/IGF1R receptors,[63] whereas DMAQ-B1 is selective for IR agonism that is known to result in phosphorylation of AKT2. This is additionally supported by our finding that insulin and IGF-1 uniquely trigger the canonical IGF1R target, ERK1/2, which is also known for its proangiogenic and hyperpermeability-inducing roles in microvessels. Indeed, we did find a nominal decrease in barrier function

following IGF-1, but we did not observe the same for insulin. This discrepancy may be due to insulin promiscuity counterbalancing both the positive and negative effects on barrier regulation.

While certain aspects of endothelial AKT remain poorly elucidated, there is consensus that specificity of these isozymes is highly context-dependent owing to factors such as tissue distribution, cellular localization, temporal regulation, and different signaling pathways.[64–67] Based upon gene ablation studies, only AKT1 and AKT2 appear to have physiological relevance in endothelial cells, although their roles appear to be markedly different with minor functional compensations. For example, deletion of endothelial *Akt1* in *Akt2*$^{-/-}$ mice displays either impaired proliferation and aberrant angiogenesis if excised during development,[65] or loss of mural cell coverage and organ failure if deleted in adult mice.[68] Conversely, AKT2 function is known to promote cell cycle exit through p21 binding[69] and is the primary isoform responsible for endothelial IR-signaling,[28,65] which is consistent with our work supporting an isoform-specific role of AKT2-activity to maintain barrier function of highly quiescent BBB endothelial cells.

It is well-known that the BBB requires additional establishment and maintenance of TJ proteins to maintain the highly restrictive paracellular clefts of BBB endothelial cells. Our observation of passaging-induced loss of AKT2 and CLDN5 may partially explain why elevated TJ protein expression and BMVEC integrity are diminished in cultured ECs.[70,71] It is also well-described that TJ expression continues to increase following monolayer formation of brain endothelial cells, and a major step in endothelial barrier formation requires AKT1-dependent inactivation of FOXO1 and increased *Cldn5* transcriptional upregulation.[13,25] Consistently, peripheral vessels of *Akt1*-null mice have

baseline vascular leakage.[66] Until now, a role for AKT2 in endothelial barrier regulation had not been established. Recently, however, Zhang et al. showed *Akt2* upregulation was a target of β-catenin/Tcf transcriptional regulation,[72] which is known to be necessary for development and maintenance of the BBB.[38,73–76] Additionally, Frisa et al. have demonstrated in aortic endothelial cells an AKT1-to-AKT2 switch model which was Notch-induced and dependent upon AKT2 upregulation, inhibition of GSK-3β phosphorylation, and FOXO1 inactivation. Our work agrees with all these observations, suggesting that AKT1 drives initial barrier development and that AKT2 expression regulates barrier maintenance. Interestingly, it was recently shown in brain endothelial cells that inhibition of GSK-3β increases the half-life of Cldn5 protein.[77] Thus, coupled with our findings, this places AKT2 upstream of both maximal transcriptional regulation and protein stabilization of CLDN5.

Significant progress has been made in the past decade to understand the contributions of isoform-specific AKT activity during various diseases.[78] In accordance with AKT-mediated regulation of FOXO1, reports defining a role of AKT isoforms in vascular disease are largely limited to aberrant vascular remodeling and macrovascular disease.[79] Consistent with the angiogenic role of endothelial AKT1, several reports have described pro-inflammatory roles for AKT1 in endothelial cells. Though global AKT1 deletion was shown to increase baseline vascular permeability, AKT1-deficient mice are resistant to acute histamine- and λ-carrageenan-induced microvascular leakage, as well as infiltration of neutrophils and monocytes.[27,65] Much less is known about the contribution of AKT activity to BBB function and neuroinflammatory disease, especially as it pertains to isoform-specificity. Several reports show that loss of BBB integrity involves

impairment of AKT signaling[80–82]; however, to the best of our ability, we were unable to find any reports describing a role for AKT2 in BBB endothelial cells. Here, we have identified a novel isoform-specific role for AKT2 in the maintenance of CLDN5-dependent endothelial barrier integrity, which is impaired following inflammatory insult. In similar samples used to obtain our results of brain endothelial cell FOXO1 activation by IL-1β in vitro,[15] and EAE in vivo, we identified a significant decrease in expression of AKT2 concomitant with CLDN5, but no changes in AKT1. Similarly, inflammation-mediated changes in AKT2 expression have been reported in other insulin-sensitive tissues, such as the liver and muscles.[83] We never observed complete loss of AKT2 in the inflammatory models employed here and our results show that activating the remaining AKT2 with DMAQ-B1 to promote restoration of CLDN5 is still possible.

Given the complexity of insulin signaling during inflammation, and the mixed results pertaining to insulin therapy for endothelial dysfunction, we were unsure if DMAQ-B1 could attenuate or reverse inflammatory-mediated BBB integrity. Coupled with our in vitro findings, however, a model of sepsis-induced insulin resistance and brain injury was attenuated with metformin administration. While this rescue was associated with increased global AKT phosphorylation and diminished edema, the cellular origin of this AKT-dependent neuroprotective effect was not addressed as only whole tissue homogenates were analyzed.[84] Therefore, we chose the primary focus of our culminating in vivo work to be whether DMAQ-B1 could rescue CLDN5 expression and CLDN5-dependent barrier integrity. For the underlying intracellular signaling mechanisms, we tested the IR/AKT2/FOXO1/CLDN5 pathway in endothelial monolayers and while it would have been ideal to quantitatively measure the signaling

activity of these proteins in vivo or within intact microvessels, such experiments were hindered by several technical limitations. In particular, the abundance of AKT2 and FOXO1 expressed within brain microvessels is very low and there exist no commercially available pAKT2 isoform-specific antibodies, thereby making it challenging to quantitatively compare the levels of their expression or isoform-specific AKT2 activity under basal and EAE conditions following administration of DMAQ-B1. Nevertheless, the profound rescue in BBB integrity we observed following DMAQ-B1 treatment, suggests that during neuroinflammation the AKT2/FOXO1/CLDN5 signaling axis remains responsive to pharmacologic intervention and, therefore, might be a viable therapeutic strategy for restoration of BBB function.

In summary, our current findings define a regulatory role for IR/AKT2/FOXO1-mediated regulation of CLDN5 which can be selectively triggered by the IR agonist, DMAQ-B1, to restore submaximal CLDN5 expression and barrier integrity back to the BBB during neuroinflammation.

Acknowledgments

We thank the Advanced Microscopy and Cell Imaging core at University of South Florida and the Biomolecular Research Center at Boise State University. We acknowledge Jonathan Overstreet, Kristina Chapman, Desiree Self and Ofeira Faapouli for their technical support with animal experiments and endothelial cell isolations and Laura Bond for statistical support.

Funding

The author(s) disclosed receipt of the following financial support for the research, authorship, and/or publication of this article: This work was supported by funding from

the National Institutes of Health grants GM097270 (S.Y.Y.), HL070752 (S.Y.Y.), HL126646 (S.Y.Y.), HL120954 (M.H.W.), GM109095 (J.T.O.), and a Veterans Administration Merit Review BX000799 (M.H.W.). R.S.B.J. was supported by career development funding from the National Institutes of Health (GM109095 and GM103408) and the American Heart Association (16POST27060005 and 17SDG33660381).

Declaration of conflicting interests

The author(s) declared no potential conflicts of interest with respect to the research, authorship, and/or publication of this article.

Authors' contributions

RSBJ performed, analyzed and interpreted most of the experiments. BAH participated in cell culture, gene silencing, and Western blotting experiments. JEM participated in cell culture, mRNA isolation and RT-PCR. TSW participated in animal maintenance and microvessel isolations. BJC assisted with confocal imaging and analyses. JTO contributed to the design and analyses of sandwich FLISAs. XY and MHW contributed to the design and data analyses of in vivo experiments. SYY initiated, directed and sponsored the work through all levels of development. All the authors discussed the results and approved the manuscript.

References

1. Hawkins BT and Davis TP. The blood-brain barrier/neu- rovascular unit in health and disease. Pharmacol Rev 2005; 57: 173–85.

2. Muldoon LL, Alvarez JI, Begley DJ, et al. Immunologic privilege in the central nervous system and the blood- brain barrier. J Cereb Blood Flow Metab 2013; 33: 13–21.

3. Rosenberg GA. Neurological diseases in relation to the blood-brain barrier. J Cereb Blood Flow Metab 2012; 32: 1139–1151.

4. Sweeney MD, Sagare AP and Zlokovic BV. Blood-brain barrier breakdown in Alzheimer disease and other neuro- degenerative disorders. Nat Rev Neurol 2018; 14: 133–150.

5. Armulik A, Genove G, Mae M, et al. Pericytes regulate the blood-brain barrier. Nature 2010; 468: 557–561.

6. Abbott NJ, Ronnback L and Hansson E. Astrocyte- endothelial interactions at the blood-brain barrier. Nat Rev Neurosci 2006; 7: 41–53.

7. Thomsen MS, Routhe LJ and Moos T. The vascular basement membrane in the healthy and pathological brain. J Cereb Blood Flow Metab 2017; 37: 3300–3317.

8. Obermeier B, Daneman R and Ransohoff RM. Development, maintenance and disruption of the blood- brain barrier. Nat Med 2013; 19: 1584–1596.

9. Liebner S, Dijkhuizen RM, Reiss Y, et al. Functional morphology of the blood-brain barrier in health and dis- ease. Acta Neuropathol 2018; 135: 311–336.

10. Yuan SY and Rigor RR. Regulation of endothelial barrier function. San Rafael (CA): Morgan & Claypool Life Sciences, 2010.

11. Luissint AC, Artus C, Glacial F, et al. Tight junctions at the blood brain barrier: physiological architecture and disease-associated dysregulation. Fluids Barriers CNS 2012; 9: 23.

12. Morita K, Sasaki H, Furuse M, et al. Endothelial clau- din: claudin-5/TMVCF constitutes tight junction strands in endothelial cells. J Cell Biol 1999; 147: 185–194.

13. Taddei A, Giampietro C, Conti A, et al. Endothelial adherens junctions control tight junctions by VE- cadherin-mediated upregulation of claudin-5. Nat Cell Biol 2008; 10: 923–934.

14. Nitta T, Hata M, Gotoh S, et al. Size-selective loosening of the blood-brain barrier in claudin-5-deficient mice. J Cell Biol 2003; 161: 653–660.

15. Beard RS Jr, Haines RJ, Wu KY, et al. Non-muscle Mlck is required for beta-catenin- and FoxO1-dependent downregulation of Cldn5 in IL-1beta-mediated barrier dysfunction in brain endothelial cells. J Cell Sci 2014; 127: 1840–1853.

16. Beard RS Jr, Reynolds JJ and Bearden SE. Hyperhomocysteinemia increases permeability of the blood-brain barrier by NMDA receptor-dependent regu- lation of adherens and tight junctions. Blood 2011; 118: 2007–2014.

17. Beard RS Jr, Reynolds JJ and Bearden SE. Metabotropic glutamate receptor 5 mediates phosphorylation of vascu- lar endothelial cadherin and nuclear localization of beta- catenin in response to homocysteine. Vascul Pharmacol 2012; 56: 159–167.

18. Aveleira CA, Lin CM, Abcouwer SF, et al. TNF-alpha signals through PKCzeta/NF-kappaB to alter the tight junction complex and increase retinal endothelial cell per- meability. Diabetes 2010; 59: 2872–2882.

19. McColl BW, Rothwell NJ and Allan SM. Systemic inflammation alters the kinetics of cerebrovascular tight junction disruption after experimental stroke in mice. J Neurosci 2008; 28: 9451–9462.

20. Argaw AT, Gurfein BT, Zhang Y, et al. VEGF-mediated disruption of endothelial CLN-5 promotes blood-brain barrier breakdown. Proc Natl Acad Sci U S A 2009; 106: 1977–1982.

21. D'Agnillo F, Williams MC, Moayeri M, et al. Anthrax lethal toxin downregulates claudin-5 expression in human endothelial tight junctions. PLoS One 2013; 8: e62576.

22. Ma X, Zhang H, Pan Q, et al. Hypoxia/Aglycemia- induced endothelial barrier dysfunction and tight junc- tion protein downregulation can be ameliorated by citico- line. PLoS One 2013; 8: e82604.

23. Greene C, Kealy J, Humphries MM, et al. Dose-depen- dent expression of claudin-5 is a modifying factor in schizophrenia. Mol Psychiatry 2017; 1–11.

24. Jang AS, Concel VJ, Bein K, et al. Endothelial dysfunc- tion and claudin 5 regulation during acrolein-induced lung injury. Am J Respir Cell Mol Biol 2011; 44: 483–490.

25. Morini MF, Giampietro C, Corada M, et al. VE-cad- herin-mediated epigenetic regulation of endothelial gene expression. Circ Res 2018; 122: 231–245.

26. Konishi H, Kuroda S, Tanaka M, et al. Molecular clon- ing and characterization of a new member of the RAC protein kinase family: association of the pleckstrin hom- ology domain of three types of RAC protein kinase with protein kinase C subspecies and beta gamma subunits of G proteins. Biochem Biophys Res Commun 1995; 216: 526–534.

27. Di Lorenzo A, Fernandez-Hernando C, Cirino G, et al. Akt1 is critical for acute inflammation and histamine- mediated vascular leakage. Proc Natl Acad Sci U S A 2009; 106: 14552–14557.

28. Rask-Madsen C, Li Q, Freund B, et al. Loss of insulin signaling in vascular endothelial cells accelerates athero- sclerosis in apolipoprotein E null mice. Cell Metab 2010; 11: 379–389.

29. Hasselbalch SG, Knudsen GM, Videbaek C, et al. No effect of insulin on glucose blood-brain barrier transport and cerebral metabolism in humans. Diabetes 1999; 48: 1915–1921.

30. Kondo T, Hafezi-Moghadam A, Thomas K, et al. Mice lacking insulin or insulin-like growth factor 1 receptors in vascular endothelial cells maintain normal blood-brain barrier. Biochem Biophys Res Commun 2004; 317: 315–320.

31. Liu H, Liu X, Jia L, et al. Insulin therapy restores impaired function and expression of P-glycoprotein in blood-brain barrier of experimental diabetes. Biochem Pharmacol 2008; 75: 1649–1658.

32. Cai W, Sakaguchi M, Kleinridders A, et al. Domain- dependent effects of insulin and IGF-1 receptors on sig- nalling and gene expression. Nat Commun 2017; 8: 14892.

33. Wilhelm K, Happel K, Eelen G, et al. FOXO1 couples metabolic activity and growth state in the vascular endo- thelium. Nature 2016; 529: 216–220.

34. Mendel I, Kerlero de Rosbo N and Ben-Nun A. A myelin oligodendrocyte glycoprotein peptide induces typical chronic experimental autoimmune encephalomyelitis in H-2b mice: fine specificity and T cell receptor V beta expression of encephalitogenic T cells. Eur J Immunol 1995; 25: 1951–1959.

35. Thakker P, Leach MW, Kuang W, et al. IL-23 is critical in the induction but not in the effector phase of experi- mental autoimmune encephalomyelitis. J Immunol 2007; 178: 2589–2598.

36. Lutz SE, Smith JR, Kim DH, et al. Caveolin1 is required for Th1 cell infiltration, but not tight junction remodel- ing, at the blood-brain barrier in autoimmune neuroin- flammation. Cell Rep 2017; 21: 2104–2117.

37. Zhang B, Salituro G, Szalkowski D, et al. Discovery of a small molecule insulin mimetic with antidiabetic activity in mice. Science 1999; 284: 974–977.

38. Beard RS Jr, Yang X, Meegan JE, et al. Palmitoyl acyl- transferase DHHC21 mediates endothelial dysfunction in systemic inflammatory response syndrome. Nat Commun 2016; 7: 12823.

39. Zhou Y, Wang Y, Tischfield M, et al. Canonical WNT signaling components in vascular development and bar- rier formation. J Clin Invest 2014; 124: 3825–3846.

40. Gulati A, Nath C, Shanker K, et al. Fluorescein spectro- photofluorometry: a sensitive quantitative method for evaluating the blood brain barrier. Pharmacol Res Commun 1982; 14: 649–661.

41. Bell RD, Winkler EA, Sagare AP, et al. Pericytes control key neurovascular functions and neuronal phenotype in the adult brain and during brain aging. Neuron2010 68: 409–427.

42. Rigor RR, Beard RS Jr, Litovka OP, et al. Interleukin- 1beta-induced barrier dysfunction is signaled through PKC-theta in human brain microvascular endothelium. Am J Physiol Cell Physiol 2012; 302: C1513–C1522.

43. Mayo JN, Beard RS Jr, Price TO, et al. Nitrative stress in cerebral endothelium is mediated by mGluR5 in hyper- homocysteinemia. J Cereb Blood Flow Metab 2012; 32: 825–834.

44. Roukos V, Pegoraro G, Voss TC, et al. Cell cycle staging of individual cells by fluorescence microscopy. Nat Protoc 2015; 10: 334–348.

45. Aube B, Levesque SA, Pare A, et al. Neutrophils mediate blood-spinal cord barrier disruption in demyelinating neuroinflammatory diseases. J Immunol 2014; 193: 2438–2454.

46. Paul D, Cowan AE, Ge S, et al. Novel 3D analysis of Claudin-5 reveals significant endothelial heterogeneity among CNS microvessels. Microvasc Res 2013; 86: 1–10.

47. Cheng Z, Guo S, Copps K, et al. Foxo1 integrates insulin signaling with mitochondrial function in the liver. Nat Med 2009; 15: 1307–1311.

48. Kleinridders A. Deciphering brain insulin receptor and insulin-like growth factor 1 receptor signalling. J Neuroendocrinol 2016; 28: 1–13.

49. Mastick CC, Kato H, Roberts CT Jr, et al. Insulin and insulin-like growth factor-I receptors similarly stimulate deoxyribonucleic acid synthesis despite differences in cel- lular protein tyrosine phosphorylation. Endocrinology 1994; 135: 214–222.

50. de Luca C and Olefsky JM. Inflammation and insulin resistance. FEBS Lett 2008; 582: 97–105.

51. Potente M, Urbich C, Sasaki K, et al. Involvement of Foxo transcription factors in angiogenesis and postnatal neovascularization. J Clin Invest 2005; 115: 2382–2392.

52. Dharaneeswaran H, Abid MR, Yuan L, et al. FOXO1- mediated activation of Akt plays a critical role in vascular homeostasis. Circ Res 2014; 115: 238–251.

53. Nwadozi E, Roudier E, Rullman E, et al. Endothelial FoxO proteins impair insulin sensitivity and restrain muscle angiogenesis in response to a high-fat diet. FASEB J 2016; 30: 3039–3052.

54. Paik JH, Kollipara R, Chu G, et al. FoxOs are lineage- restricted redundant tumor suppressors and regulate endothelial cell homeostasis. Cell 2007; 128: 309–323.

55. Park DY, Lee J, Kim J, et al. Plastic roles of pericytes in the blood-retinal barrier. Nat Commun 2017; 8: 15296.

56. Tsuchiya K, Tanaka J, Shuiqing Y, et al. FoxOs integrate pleiotropic actions of insulin in vascular endothelium to protect mice from atherosclerosis. Cell Metab 2012; 15: 372–381.

57. Shoelson SE, Lee J and Goldfine AB. Inflammation and insulin resistance. J Clin Invest 2006; 116: 1793–1801. 58. Franklin VL, Khan F, Kennedy G, et al. Intensive insulin therapy improves endothelial function and microvascular reactivity in young people with type 1 diabetes. Diabetologia 2008; 51: 353–360.

59. Tian J, Wang J, Li Y, et al. Endothelial function in patients with newly diagnosed type 2 diabetes receiving early intensive insulin therapy. Am J Hypertens 2012; 25: 1242–1248.

60. Zhang WF, Zhu XX, Hu DH, et al. Intensive insulin treatment attenuates burn-initiated acute lung injury in rats: role of the protective endothelium. J Burn Care Res 2011; 32: e51–e58.

61. Woods SC, Seeley RJ, Baskin DG, et al. Insulin and the blood-brain barrier. Curr Pharm Des 2003; 9: 795–800.

62. Hoheisel D, Nitz T, Franke H, et al. Hydrocortisone reinforces the blood-brain barrier properties in a serum free cell culture system. Biochem Biophys Res Commun 1998; 244: 312–316.

63. Ito S, Yanai M, Yamaguchi S, et al. Regulation of tight- junction integrity by insulin in an in vitro model of human blood-brain barrier. J Pharm Sci 2017; 106: 2599–2605.

64. Nitert MD, Chisalita SI, Olsson K, et al. IGF-I/insulin hybrid receptors in humanendothelial cells. Mol Cell Endocrinol 2005; 229: 31–37.

65. Ackah E, Yu J, Zoellner S, et al. Akt1/protein kinase Balpha is critical for ischemic and VEGF-mediated angiogenesis. J Clin Invest 2005; 115: 2119–2127.

66. Lee MY, Luciano AK, Ackah E, et al. Endothelial Akt1 mediates angiogenesis by phosphorylating multiple angiogenic substrates. Proc Natl Acad Sci U S A 2014; 111: 12865–12870.

67. Chen J, Somanath PR, Razorenova O, et al. Akt1 regu- lates pathological angiogenesis, vascular maturation and permeability in vivo. Nat Med 2005; 11: 1188–1196.

68. Somanath PR, Chen J and Byzova TV. Akt1 is necessary for the vascular maturation and angiogenesis during cutaneous wound healing. Angiogenesis 2008; 11: 277–288.

69. Kerr BA, West XZ, Kim YW, et al. Stability and function of adult vasculature is sustained by Akt/Jagged1 signal- ling axis in endothelium. Nat Commun 2016; 7: 10960.

70. Heron-Milhavet L, Franckhauser C, Rana V, et al. Only Akt1 is required for proliferation, while Akt2 promotes cell cycle exit through p21 binding. Mol Cell Biol 2006; 26: 8267–8280.

71. Liebner S, Kniesel U, Kalbacher H, et al. Correlation of tight junction morphology with the expression of tight junction proteins in blood-brain barrier endothelial cells. Eur J Cell Biol 2000; 79: 707–717.

72. Deli MA, Abraham CS, Kataoka Y, et al. Permeability studies on in vitro blood-brain barrier models: physi- ology, pathology, and pharmacology. Cell Mol Neurobiol 2005; 25: 59–127.

73. Zhang J, Huang K, Shi Z, et al. High beta-catenin/Tcf-4 activity confers glioma progression via direct regulation of AKT2 gene expression. Neuro Oncol 2011; 13: 600–609.

74. Tran KA, Zhang X, Predescu D, et al. Endothelial beta- catenin signaling is required for maintaining adult blood- brain barrier integrity and central nervous system homeo- stasis. Circulation 2016; 133: 177–186.

75. Liebner S, Corada M, Bangsow T, et al. Wnt/beta-cate- nin signaling controls development of the blood-brain barrier. J Cell Biol 2008; 183: 409–417.

76. Daneman R, Agalliu D, Zhou L, et al. Wnt/beta-catenin signaling is required for CNS, but not non-CNS, angio- genesis. Proc Natl Acad Sci U S A 2009; 106: 641–646.

77. Engelhardt B and Liebner S. Novel insights into the development and maintenance of the blood-brain barrier. Cell Tissue Res 2014; 355: 687–699.

78. Ramirez SH, Fan S, Dykstra H, et al. Inhibition of glyco- gen synthase kinase 3beta promotes tight junction stabil- ity in brain endothelial cells by half-life extension of occludin and claudin-5. PLoS One 2013; 8: e55972.

79. Hers I, Vincent EE and Tavare JM. Akt signalling in health and disease. Cell Signal. 2011; 23: 1515–27.

80. Yu H, Littlewood T and Bennett M. Akt isoforms in vascular disease. Vascul Pharmacol 2015; 71: 57–64.

81. Wang ZG, Cheng Y, Yu XC, et al. bFGF Protects Against blood-brain barrier damage through junction protein regulation via PI3K-Akt-Rac1 pathway following traumatic brain injury. Mol Neurobiol 2016; 53: 7298–7311.

82. Wu F, Chen Z, Tang C, et al. Acid fibroblast growth factor preserves blood-brain barrier integrity by activat- ing the PI3K-Akt-Rac1 pathway and inhibiting RhoA following traumatic brain injury. Am J Transl Res 2017; 9: 910–925.

83. Li L, McBride DW, Doycheva D, et al. G-CSF attenuates neuroinflammation and stabilizes the blood-brain barrier via the PI3K/Akt/GSK-3beta signaling pathway follow- ing neonatal hypoxia-ischemia in rats. Exp Neurol 2015; 272: 135–144.

84. Kim YB, Peroni OD, Franke TF, et al. Divergent regu- lation of Akt1 and Akt2 isoforms in insulin target tissues of obese Zucker rats. Diabetes 2000; 49: 847–856.

85. Tang G, Yang H, Chen J, et al. Metformin ameliorates sepsis-induced brain injury by inhibiting apoptosis, oxi- dative stress and neuroinflammation via the PI3K/Akt signaling pathway. Oncotarget 2017; 8: 97977–97989.

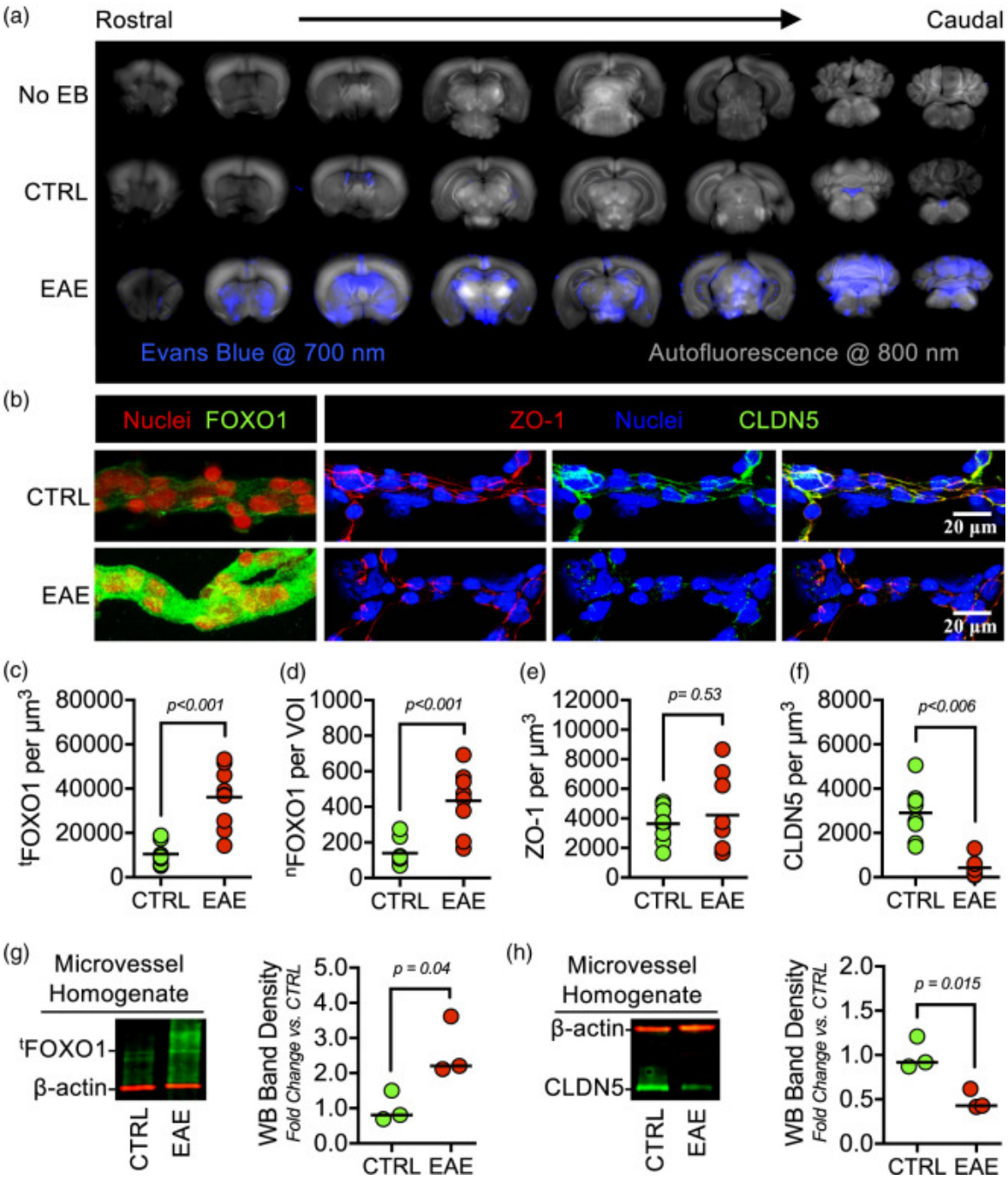

Figure A.1 Brain microvessels from mice with EAE-induced BBB dysfunction have increased nuclear FOXO1 and decreased tight junctional expression of CLDN5. EAE or mock-EAE (Ctrl) were induced per standard protocols and analyzed for BBB dysfunction eight days post-induction (d.p.i.).

(a) Proof-of-principle that EAE mice 8 d.p.i. have BBB dysfunction. Qualitative plasma protein leakage into the mouse brains was determined by imaging Evans blue (EB) extravasation. Representative images of 1 mm coronal brain slices (olfactory bulbs

not included) showing EB leakage captured at 700 nm (pseudo-colored blue) and brain autofluorescence at 800 nm (pseudo-colored grayscale) with a near-infrared imaging scanner. **(b)** Representative confocal micrographs of isolated brain microvessels (those ≤ 30 μm in diameter) immunostained for either FOXO1, ZO-1, and/or CLDN5, then counterstained with DAPI to demarcate nuclei. In total, 27 mice per group were used and microvessel pellets were pooled together from 3 mice each for a total of 9 pools per group. **(c–f)** Imaris 3D visualization software was used to analyze confocal micrographs and quantify: **(c)** total FOXO1 (^{t}FOXO1) density; **(d)** nuclear-localized FOXO1 (^{n}FOXO1) per uniform spherical volume of interest (VOI) centered within each nucleus; and 3D density of ZO-1 **(e)** and CLDN5 (f) at endothelial cell–cell contacts. Data are represented as aligned dot plots, where each dot represents a microvessel pool. **(g–h)** Representative Western blots and densitometry analysis for ^{t}FOXO1 **(g)** and CLDN5 **(h)**. In total, nine mice per group were used and microvessel pellets were pooled together from three mice each for a total of three pools per group. Data are represented as scatter dot plots overlaid with mean fold change compared to control group plus corresponding p-value reported above each comparison.

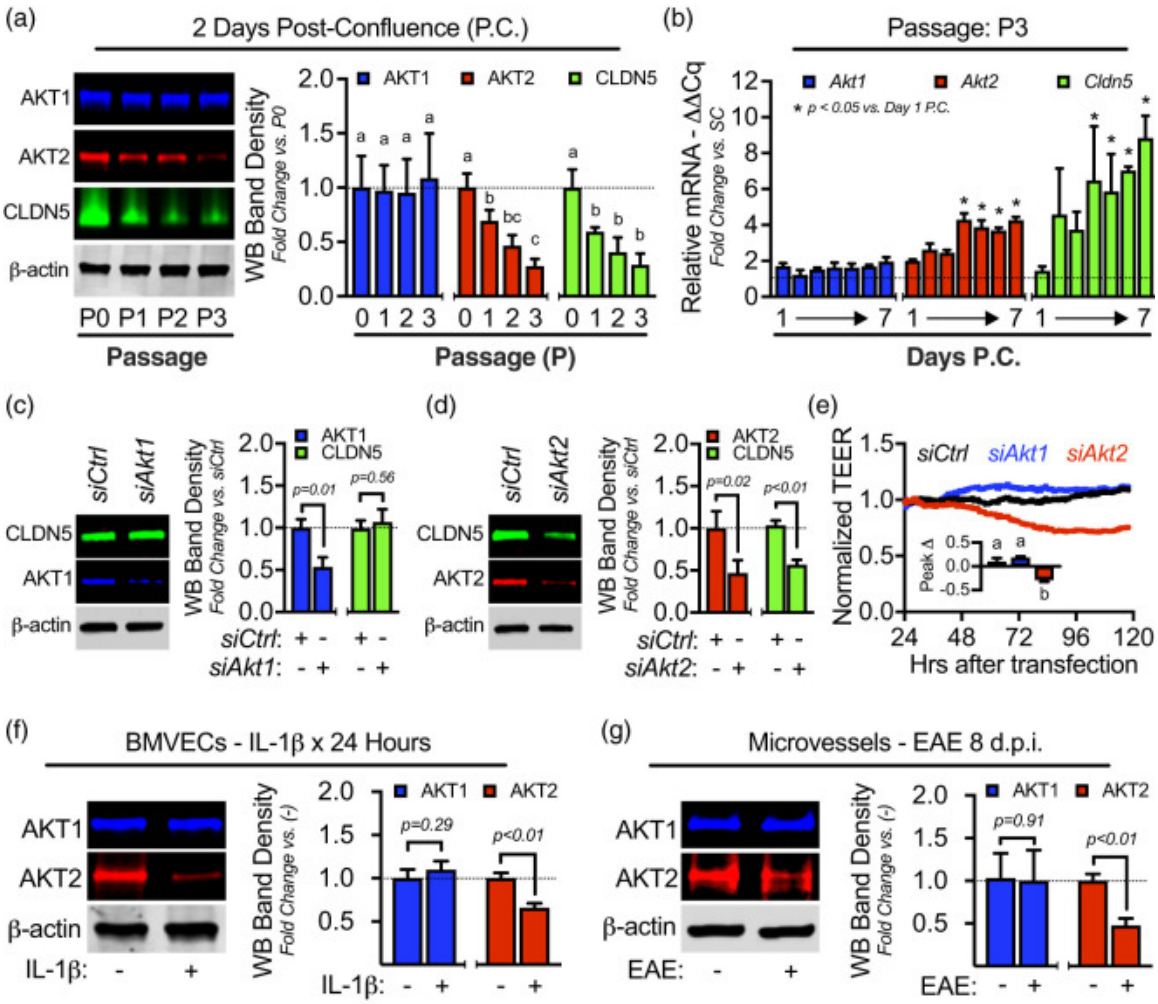

Figure A.2 The AKT2 isoform is distinctly correlated with primary BMVEC barrier integrity and changes in CLDN5 expression.

(a) Freshly isolated BMVECs were seeded at confluence in cultureware (P0). Additional cells were passaged three times (P1–P3). BMVECs from each passage were allowed to mature for two days post-confluence (P.C.). Lysates were collected and expression levels of AKT1, AKT2, and CLDN5 were determined by Western blotting. Bar graphs are divided into individual datasets for each protein target and represent the mean ± S.D. Groups with the same symbol within each individual dataset are not significant from each other ($p \geq 0.05$). **(b)** Conversely, total mRNA from P3 BMVECs was collected from sub-confluent (SC) cells and confluent monolayers each day through

seven days P.C. Relative mRNA expression (ΔΔCq; fold change relative to SC samples normalized to β-actin as the reference gene) for *Akt1*, *Akt2,* and *Cldn5* was determined by qRT-PCR. Bar graphs are divided into individual datasets for each mRNA target and represent the mean ± S.D. Asterisks indicate $p < 0.05$ versus 1 day P.C. for each target mRNA. **(c–e)** AKT1 and AKT2 were silenced in BMVECs by siRNA (*siAkt1* or *siAkt2*). Confirmation of knockdown and the effect on CLDN5 expression was determined by Western blotting **(c–d)**. Bar graphs are divided into individual datasets for each protein target and are represented as mean fold change compared to the *siCtrl* group plus corresponding *p*-value reported above each comparison. **(e)** Representative ECIS tracings demonstrating the impact of AKT1 or AKT2 knockdown on BMVEC barrier integrity from 24 to 120 h post-transfection. At least three independent experiments for each transfection were performed with cells from three separate BMVEC isolations. Each tracing was normalized to the first time point and the peak change in TEER was determined. Embedded bar graphs represent mean normalized peak change ± S.D. and groups with the same symbol are not significant from each other ($p \geq 0.05$). (f–g) Comparison of inflammatory-mediated changes in AKT isoform expression levels in vitro and in vivo. **(f)** In vitro, mature BMVECs (P1; 7 days P.C.) were stimulated with IL-1β [100 ng/mL] or vehicle control (−) for 24 h and expression levels of AKT1 and AKT2 were compared by Western blotting. Bar graphs are divided into individual datasets for each protein target and are represented as mean fold change compared to the control group plus corresponding *p*-value reported above each comparison. **(g)** In vivo, EAE was induced in mice and compared to mock controls. After 8 d.p.i., brain microvessels were isolated from both groups and AKT1-2 expression was determined by

Western blotting. Bar graphs are divided into individual datasets for each protein target and are represented as mean fold change compared to the control group plus corresponding *p*-value reported above each comparison.

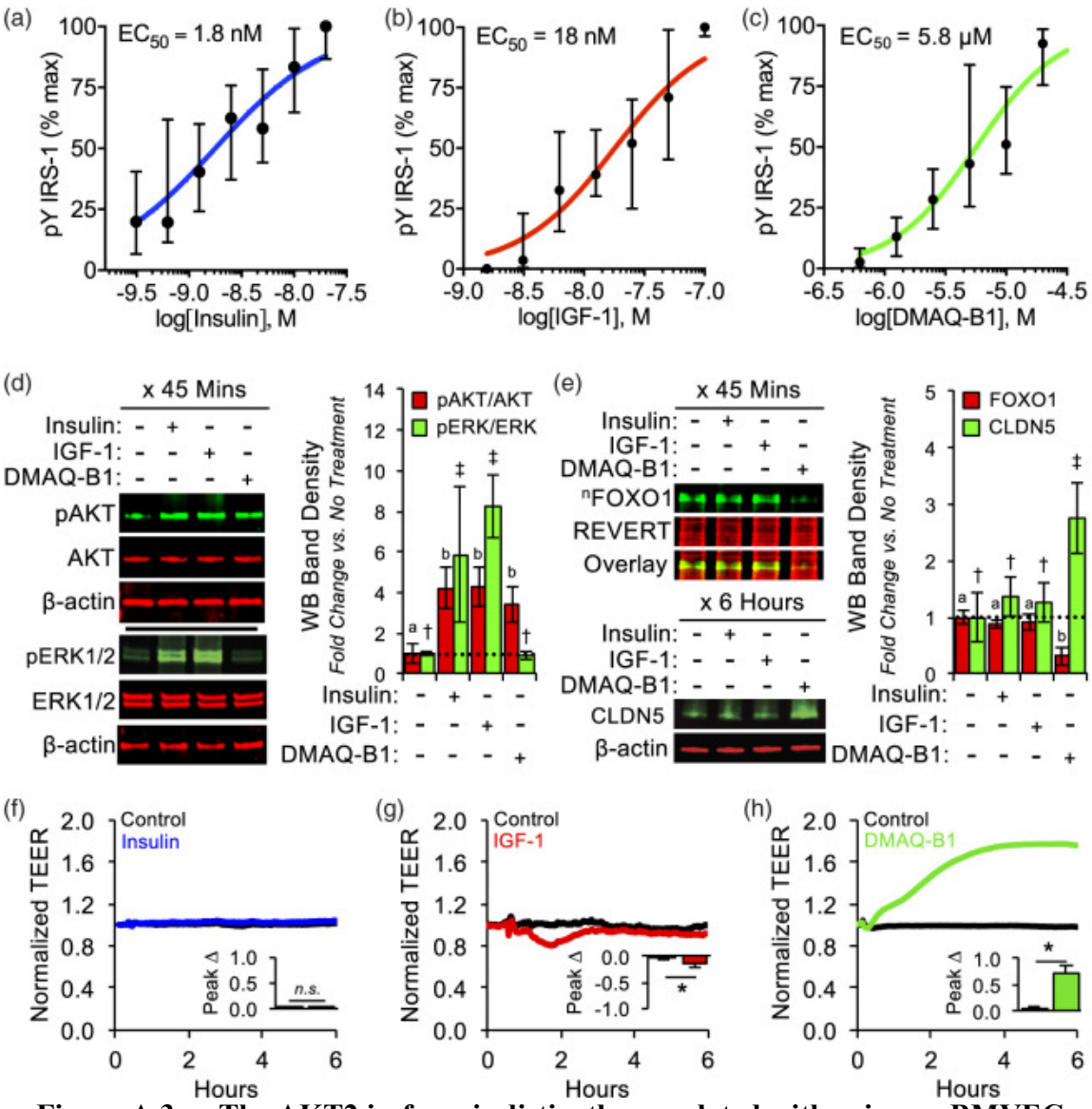

Figure A.3 The AKT2 isoform is distinctly correlated with primary BMVEC barrier integrity and changes in CLDN5 expression.

BMVECs were allowed to mature for 48 h P.C. and then treated with varying concentrations of insulin, IGF-1, or DMAQ-B1. **(a–c)** After 45 min, cell lysates were analyzed with a sandwich FLISA (capture Ab = anti-IRS-1, detection Ab = anti-pY) to determine total tyrosine phosphorylation on IRS-1 (pY IRS-1). Dots represent median percentage of maximal dose-response ± IQR and EC50 values were obtained from dose-response curves. **(d–e)** Representative Western blots and densitometry analyses for active

AKT (pT308), active Erk1/2 (pT202/pY204), and nFOXO1 (blotting nuclear lysates for FOXO1) were determined after treating BMVECs for 45 min with insulin [2 nM], IGF-1 [20 nM], or DMAQ-B1 [5 μM]. Subsequent changes in CLDN5 expression 6 hours after treatment were also determined by Western blotting and densitometry **(e)**. Data for each protein target are represented as mean fold change compared to the no treatment group ± S.D. Within each individual protein target dataset, groups with the same symbol are not significant from each other ($p \geq 0.05$). Target proteins were not compared against each other. **(f–h)** Changes in BMVEC barrier resistance to insulin, IGF-1, or DMAQ-B1 were evaluated for 6 h after treatment. At least three independent ECIS experiments were performed with cells from three separate BMVEC isolations. Each tracing was normalized to its baseline and peak change in TEER was determined. Representative tracings for treatment groups are depicted by colored lines and untreated controls are depicted by black lines. Embedded bar graphs represent mean normalized peak changes in TEER ± S.D. Asterisks indicate $p < 0.05$ versus untreated controls and n.s. indicates no significance.

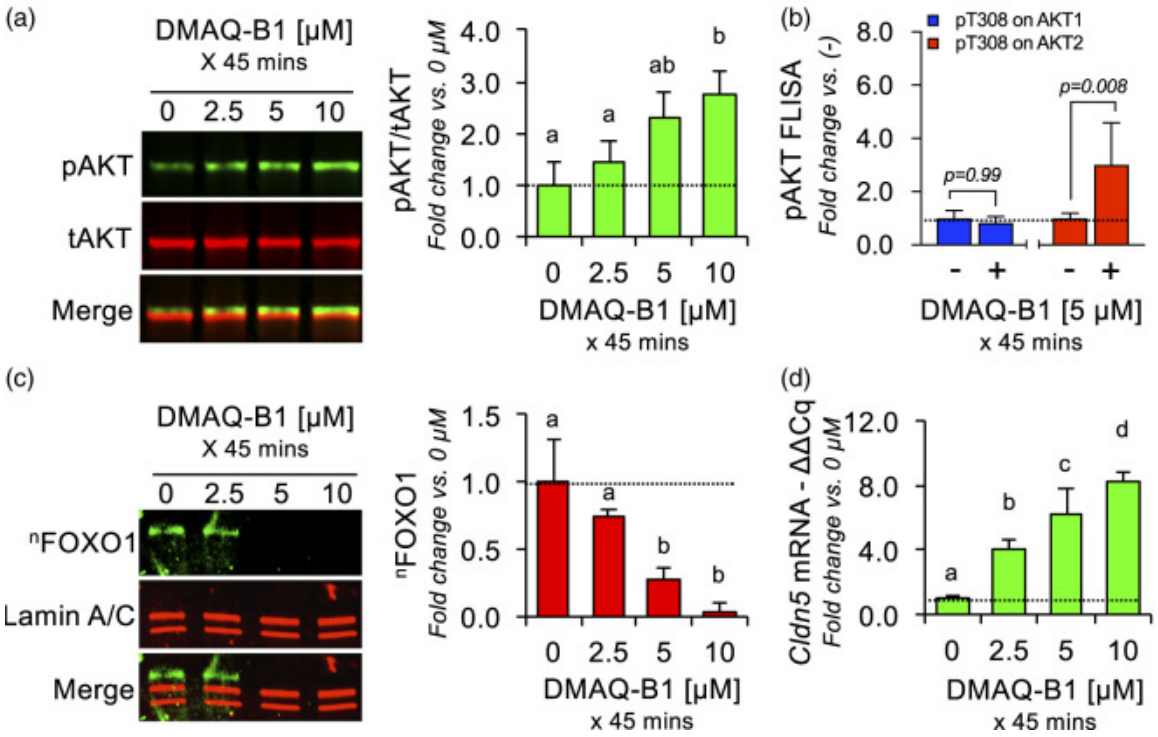

Figure A.4 DMAQ-B1 dose-dependently increases AKT2 activity, decreases FOXO1 nuclear accumulation, and upregulates *Cldn5* mRNA.

(a–d) BMVECs (P3; two days P.C.) were treated with DMAQ-B1 [0, 2.5, 5, or 10 μM] for 45 min and lysates were analyzed for AKT2 activity, ^{n}FOXO1 levels, and Cldn5 mRNA levels. **(a)** AKT activity was determined by Western blotting for pT308 on AKT (pAKT; not isoform-specific) and normalizing against total AKT (tAKT; not isoform-specific). Data are represented as mean fold change compared to the no treatment group ± S.D. Groups with the same symbol are not significant from each other ($p \geq 0.05$). **(b)** AKT isoform-specific phosphorylation in response to DMAQ-B1 was determined by FLISAs using AKT1- or AKT2-specific antibodies as capture antibodies and pT308-AKT as the detection antibody. Bar graphs are divided into individual datasets for each protein target and are represented as mean fold change compared to the vehicle control (−) group ± S.D. and corresponding p-values reported above each comparison. **(c)** FOXO1 levels in BMVEC nuclear lysates were determined by Western

blotting with lamin A/C used as a nuclear loading control. Data are represented as mean fold change compared to the vehicle control (0 μM) group ± S.D. Groups with the same symbol are not significant from each other ($p \geq 0.05$). **(d)** Relative Cldn5 mRNA was determined by qRT-PCR. Data are represented as mean fold change compared to the no treatment group ± S.D. Groups with the same symbol are not significant from each other ($p \geq 0.05$).

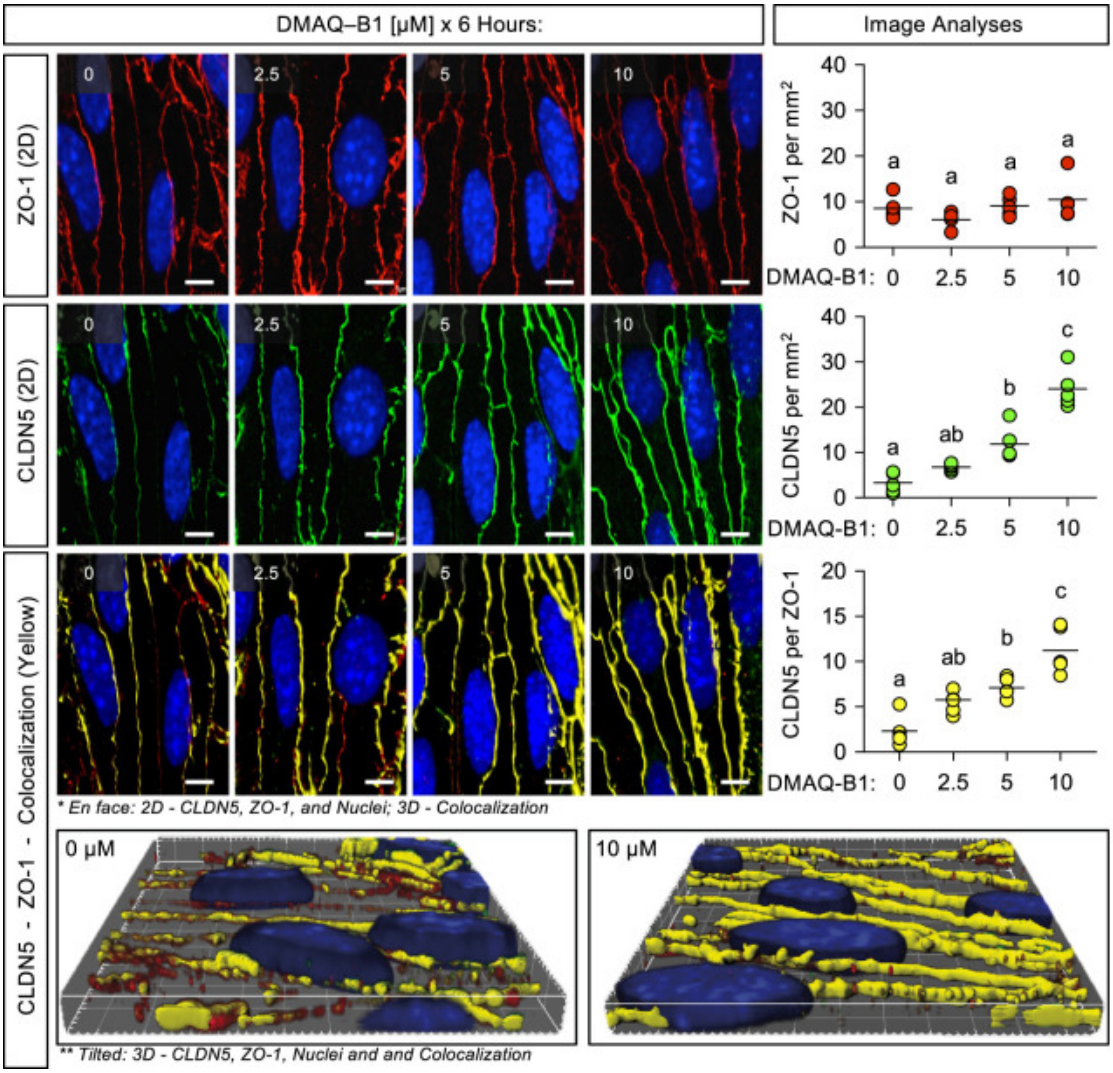

Figure A.5 DMAQ-B1-mediated upregulation of CLDN5 increases the density of CLDN5 protein at BMVEC tight junctions.

BMVECs (P3; two days P.C.) were grown on glass coverslips and treated with DMAQ-B1 [0, 2.5, 5, or 10 μM] for 6 h. BMVEC monolayers (n = 5) were fixed and immunostained for ZO-1 and CLDN5, then counterstained with DAPI to demarcate nuclei (Blue). Confocal micrographs were obtained and Imaris software was used for image analyses and 3D rendering. Representative 2D images of ZO-1 (Red) and CLDN5 (Green) and corresponding graphs of intensity analyses are displayed in the top two rows. ZO-1 at BMVEC cell–cell contacts was used to establish a VOI at tight junctions and a

3D colocalization channel (Yellow; ZO-1+ and CLDN5+ voxels) was established for visual evaluation of CLDN5 expression at BMVEC tight junctions. Representative 2D merged images with 3D rendering of the colocalization channel displayed en face, and graph of CLDN5 intensity per VOI are displayed in the third row. The last row is the same 3D image area as those shown for 0 and 10 μM DMAQ-B1, but expanded and tilted to enhance visual representation. All graphs are represented as aligned dot plots overlaid with mean value (black line) and groups with the same symbol within each plot are not significant from each other ($p \geq 0.05$).

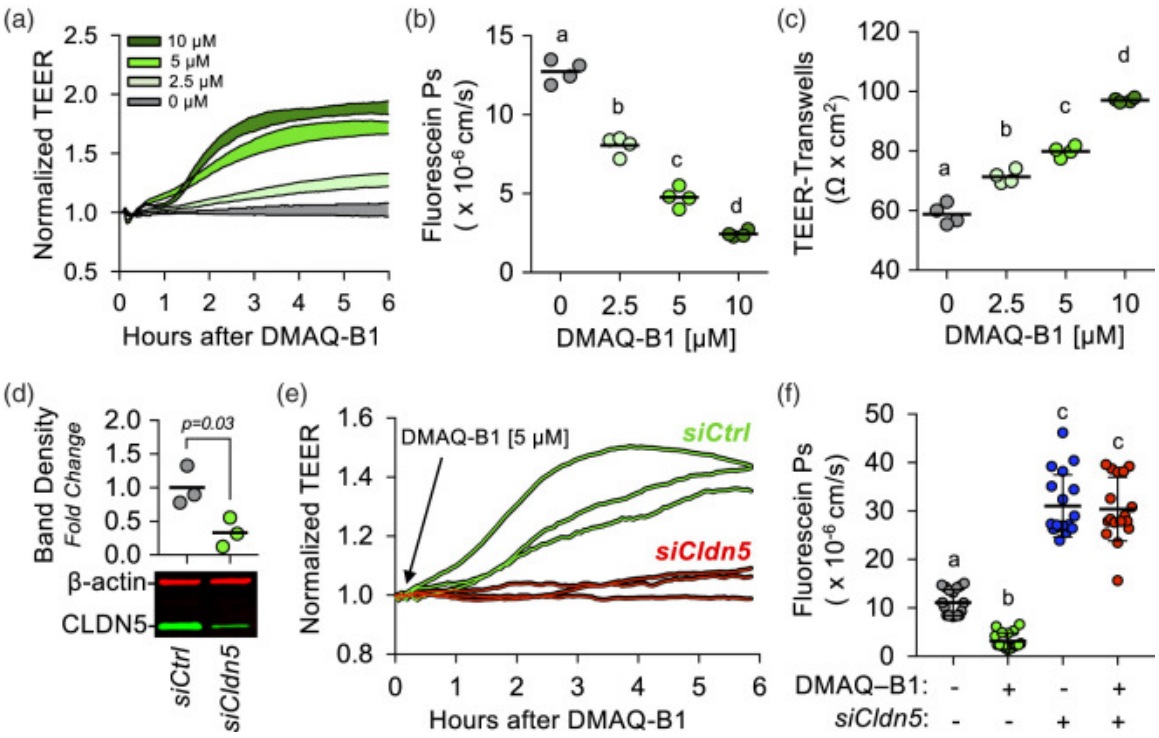

Figure A.6 CLDN5 upregulation is necessary for DMAQ-B1-mediated BMVEC barrier enhancement.

(a–c) DMAQ-B1 dose-dependently enhances BMVEC barrier function. **(a)** Representative ECIS tracings in response to DMAQ-B1 [0, 2.5, 5, or 10 µM]. At least three independent experiments for each treatment were performed with cells from three separate BMVEC isolations. Each tracing was normalized to the first time point and the filled area for each group represents mean change in TEER ± S.D. Alternatively, after 6 h of treating BMVEC monolayers grown in transwell inserts (P3; two days P.C.) with DMAQ-B1, sodium fluorescein permeability coefficients (Ps) were obtained **(b)** and transwell-TEER was measured **(c)**. Data are represented as scatter dot plots overlaid with mean value (black line) and groups with the same symbol within each plot are not significant from each other ($p \geq 0.05$). **(d–f)** The effects of CLDN5 knockdown on DMAQ-B1-mediated BMVEC barrier enhancement were determined with ECIS and transwell permeability assays. **(d)** Knockdown efficiency of CLDN5 in BMVECs as

verified by Western blotting. Data are represented as scatter dot plots overlaid with mean value (black line) plus corresponding p-value reported above. **(e)** Representative spaghetti plots of individual ECIS tracings of BMVECs transfected with siCldn5 or siCtrl and then treated 24 h later with DMAQ-B1 [5 μM]. Each tracing was normalized to the first time point. **(f)** The effects of CLDN5 knockdown on BMVEC monolayer permeability to sodium fluorescein with or without DMAQ-B1 were measured. DMAQ-B1 [5 μM] was applied to BMVEC monolayers for 6 h, and permeability was calculated based on sodium fluorescein transendothelial diffusion rate. Data are represented as scatter dot plots overlaid with mean ± S.D. lines. Groups with the same symbol are not significant from each other ($p \geq 0.05$).

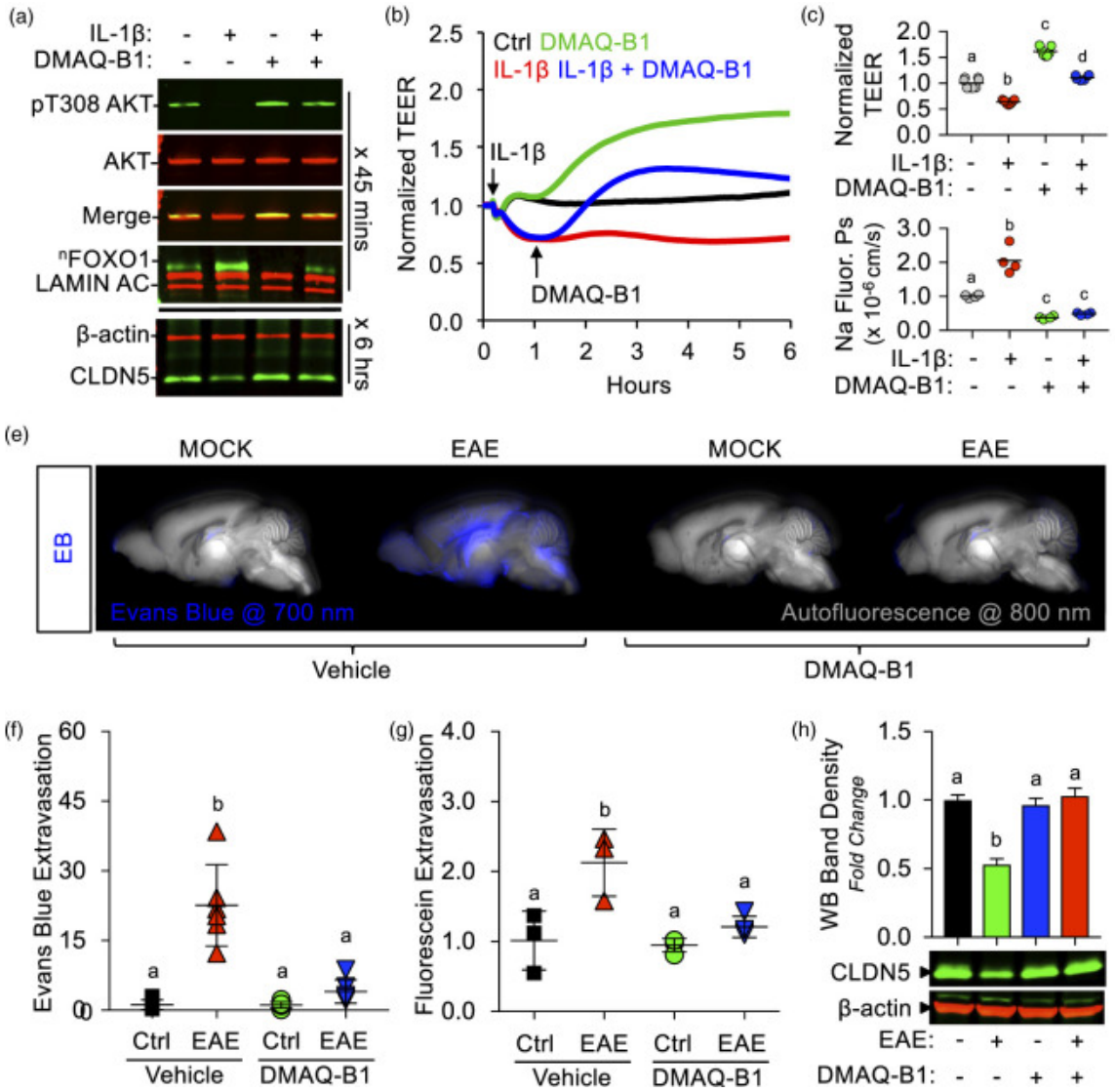

Figure A.7 DMAQ-B1 reverses inflammation-mediated brain endothelial barrier dysfunction in vitro and in vivo.

(a-d) BMVEC monolayers (P3; two days P.C.) were divided into four groups: (1) vehicle control (Ctrl), (2) IL-1β [100 ng/mL], (3) DMAQ-B1 [5 μM], or (4) DMAQ-B1 + IL-1β. **(a)** The ability of DMAQ-B1 to attenuate IL-1β-mediated AKT inactivation, FOXO1 nuclear accumulation, and CLDN5 downregulation was determined by Western blotting. Representative Western blots from three independent experiments are shown **(b–d)** The ability of DMAQ-B1 to reverse IL-1β-mediated BMVEC barrier dysfunction was tested with ECIS-TEER measurements or transwell permeability assays. DMAQ-B1

was added 1 h after IL-1β challenge. **(b)** Representative normalized ECIS tracings, **(c)** normalized peak TEER changes, and **(d)** sodium fluorescein permeability coefficients. All values were obtained from at least 3 independent experiments. Data for **(c)** and **(d)** are represented as scatter dot plots overlaid with mean value (black line) and groups with the same symbol within each plot are not significant from each other ($p \geq 0.05$). **(e–h)** EAE or mock-EAE (Ctrl) were induced and analyzed 8 d.p.i. for BBB dysfunction and CLDN5 expression changes. 24 h prior to harvest (7 d.p.i.), mice from each group were split into two additional groups that received DMAQ-B1 [5 mg/kg] or vehicle (0.5% methylcellulose) via oral gavage. In total, 8–10 mice per group were used and harvested brains were split by hemisphere to allow for simultaneous determination of BBB dysfunction and CLDN5 expression. **(e–g)** Plasma protein and solute leakage into the mouse brains were determined by EB ($n = 5–6$) and sodium fluorescein ($n = 3–4$) extravasation assays. **(e)** Representative images from EB extravasation assay showing plasma protein leakage into the right hemisphere. Images were captured at 700 nm (pseudo-colored blue) and brain autofluorescence at 800 nm (pseudo-colored grayscale). Quantitative results from EB **(f)** and sodium fluorescein **(g)** permeability assays. **(h)** CLDN5 expression from left hemisphere brain homogenates was determined by Western blotting. All in vivo values were normalized to the vehicle-treated group subjected to mock EAE (Ctrl) and graphs are represented as dot plots or bar graphs overlaid with mean ± S.D. lines. Groups with the same symbol within each graph are not significant from each other ($p \geq 0.05$).

Supplementary Material

Supplementary Methods

Cell-cycle analysis and viability assay

Imaging-based cell-cycle analysis was performed as described elsewhere with some minor modifications.[44] Briefly, after DMAQ-B1 treatments, BMVEC monolayers from four independent isolations were fixed, stained with DAPI and imaged (n = 20; 5 micrographs per isolation and treatment group) with an EVOS FL Imaging System (ThermoFisher Scientific). To determine the total number of BMVECs within each monolayer and generate cell-cycle histograms, micrographs were processed with ImageJ (NIH; Version: 2.0.0.rc-65/1.51s) and image analysis–based quantification of integrated nuclear (DAPI) intensity was performed. Relative frequency (%) distributions of nuclear areas were created with Prism (Version 7.0e; Graphpad Software, Inc.) to generate cell cycle profiles, and cell cycle phases (G1/G0, S, and G2/M) were identified by applying visually selected cutoffs. To assess whether DMAQ-B1 may affect BMVEC viability, BMVEC monolayers (P3; 2 days P.C.) were incubated with either a vehicle control, DMAQ-B1 [5 μM], or doxorubicin [0.4 μM] (as a positive control) for 6 hours (n = 15; 5 micrographs per isolation and treatment group), then a commercial live/dead viability/cytotoxicity kit was used according to manufacturer's instructions. Fluorescent micrographs were acquired with an EVOS FL Imaging System using light cubes appropriate for the kit (GFP for calcein AM and RFP for propidium iodide) and the number of positive cells for each stain were tabulated to calculate the ratio of viable to nonviable cells for each group.

Supplementary Tables and Figures

Table A.S1 List of reagents used in these studies.

Reagents	Company	Catalog Number
Amaxa® Cell Line Nucleofector® Kit V	Lonza	VCA-1003
Boric Acid	Sigma	B6768
cOmplete™ protease/phosphatase inhibitor	Sigma	5892970001
Collagen Type IV	Advanced BioMatrix	5022
Dextran ~70 kD	Sigma	31390
DNAse I	ThermoFisher	EN0521
DMAQ-B1	Tocris	LM22B 10
DMEM	Gibco	31053028
Donkey serum	Sigma	D9663
Doxorubicin	Sigma	D1515
EAE Induction Kit	Hooke Labs	EK-2110
Endothelial Growth Medium	Cell Biologics	M116
Evans blue	Sigma	E2129
Formamide	Sigma	F9037
Laemmli sample buffer	LI-COR	928-40004

Reagents	Company	Catalog Number
LIVE/DEAD viability/cytotoxicity kit, for mammalian cells	ThermoFisher	L3224
Nα-Tosyl-L-lysine chloromethyl ketone hydrochloride	Sigma	90182
Paraformaldehyde	Sigma	P6148
Percoll	Sigma	GE17-0891
RIPA lysis buffer	Sigma	20-188
siControl	SCBT	sc-37007
siAkt1	SCBT	sc-29196
siAkt2	SCBT	sc-38910
siCldn5	SCBT	sc-43045
Sodium fluorescein	Sigma	F6377
Trichloroacetic acid	Sigma	T6399
Vectashield with DAPI	Vector Laboratories	H-1200

Table A.S2 List of antibodies used in each experiment.

Antibody	Fig.	Company	Catalog #
α-catenin	S2A	SCBT	sc-7894
β-actin	1G,H; 2A,C,D,F,G; 3D; 6D; 7A,H; S2A	LI-COR	926-42214
β-catenin	S2A	CST	2677
δ-catenin	S2A	SCBT	sc-81793
γ-catenin	S2A	SCBT	sc-514115
AKT	3D; 4A; 7A	CST	2966
AKT1	2A,C,F,G; 4B	CST	3063
AKT2	2A,D,F,G; 4B	CST	2938
Claudin-3	S2A	ThermoFisher	34-1700
Claudin-5	1B,H; 2A,C,D,F,G; 6D; 7A,H; S2A	Invitrogen	35-2500
Claudin-5 (AF 488)	5	ThermoFisher	352588
Claudin-12	S2A	Invitrogen	38-8200
ERK 1/2	3D	CellSciences	CPE201
FoxO1	1B,G; 3E; 4C; 7A	EMD Millipore	05-1075
Lamin A/C	4C; 7A	CST	4777

Antibody	Fig.	Company	Catalog #
Occludin	S2A	Invitrogen	33-1500
pAKT(T308)	3D; 4A,B; 7A	CST	4056
pERK 1/2	3D	CST	4695
IRS-1	3A,B,C	CST	2382
Phosphotyrosine (pY)	3A,B,C	Millipore-Sigma	05-321
VE-Cadherin	S2A	SCBT	sc-52751
ZO-1	1B; S2A	Invitrogen	40-2200
ZO-1 (AF 594)	5	ThermoFisher	339194

Table A.S3 Statistical analyses used in each experiment.

Fig. #	Summary Statistics	Statistical Test	Post-Hoc Test
Fig. 1C-F	Aligned dot plots - mean - no error bars	Unpaired t-test	N/A
Fig. 1G,H	Scattered dot plots – normalized mean - no error bars	Unpaired t-test	N/A
Fig. 2A	Bar graphs – normalized mean for each protein ± S.D.	One-way ANOVA	Tukey's
Fig. 2B	Bar graphs – normalized mean for each mRNA ± S.D.	One-way ANOVA	Dunnett's
Fig. 2C,D	Bar graphs – normalized mean for each protein ± S.D.	Unpaired t-test	N/A
Fig. 2E	Representative ECIS tracings – normalized mean – bar graphs of normalized mean peak changes in TEER ± S.D.	One-way ANOVA	Tukey's
Fig. 2F,G	Bar graphs – normalized mean ± S.D.	Unpaired t-test	N/A
Fig. 3A-C	Dose-response curves - median ± IQR	Variable slope	N/A
Fig. 3D,E	Bar graphs – normalized mean ± S.D.	One-way ANOVA	Tukey's
Fig. 3F-H	Representative ECIS tracings – normalized mean – bar graphs of normalized mean peak changes in TEER ± S.D.	Unpaired t-test	N/A
Fig. 4A	Bar graphs – normalized mean ± S.D.	One-way ANOVA	Tukey's
Fig. 4B	Bar graphs – normalized mean for each protein ± S.D.	Unpaired t-test	N/A

Fig. #	Summary Statistics	Statistical Test	Post-Hoc Test
Fig. 4C,D	Bar graphs – normalized mean ± S.D. One-way	One-way ANOVA	Tukey's
Fig. 5	Aligned dot plots - mean - no error bars	One-way ANOVA	Tukey's
Fig. 6B-C	Scattered dot plots - mean - no error bars	One-way ANOVA	Tukey's
Fig. 6D	Scattered dot plots - normalized mean - no error bars	Unpaired t-test	N/A
Fig. 6F	Scattered dot plots - normalized mean ± S.D.	One-way ANOVA	Tukey's
Fig. 7C,D	Scattered dot plots – normalized mean - no error bars	One-way ANOVA	Tukey's
Fig. 7F,G	Scattered dot plots - normalized mean ± S.D.	One-way ANOVA	Tukey's
Fig. 7H	Bar graphs - normalized mean ± S.D.	One-way ANOVA	Tukey's
Fig. S1A	Scattered dot plot – normalized mean ± S.D.	Unpaired t-test	N/A
Fig. S1D	Scattered dot plot – normalized mean ± S.D.	One-way ANOVA	Tukey's
Fig. S2B	Bar graphs – normalized mean ± S.D.	One-way ANOVA	Tukey's

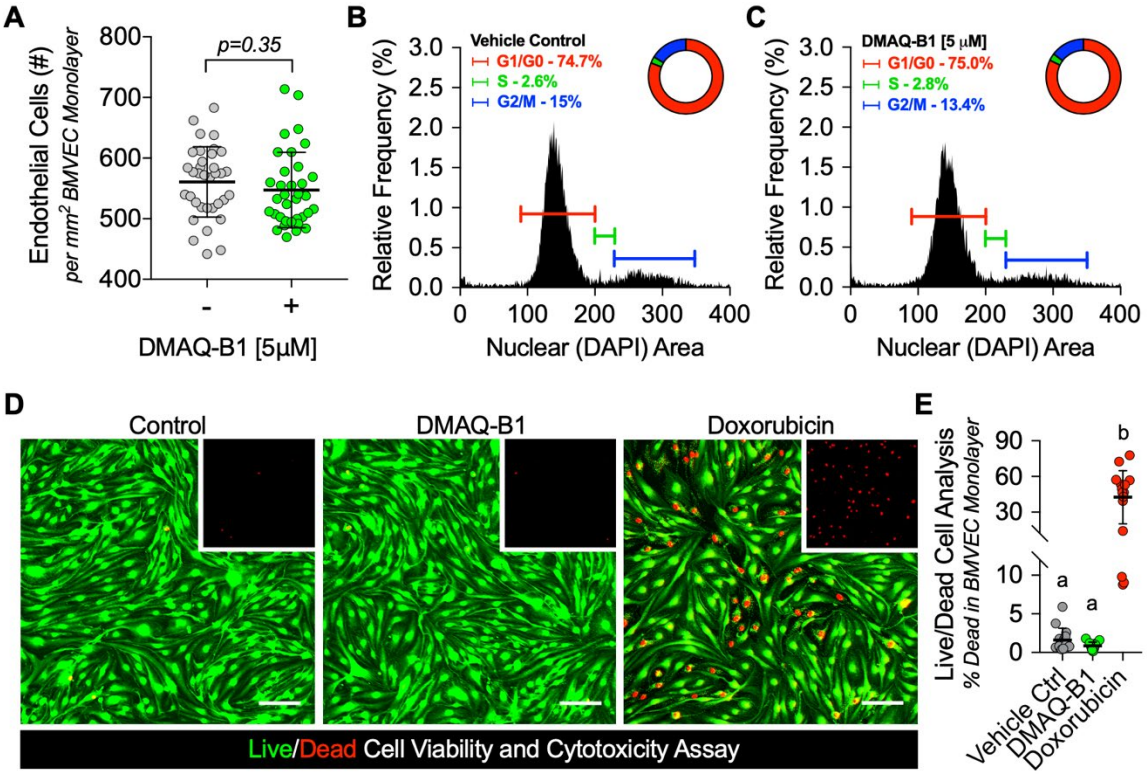

Figure S1. DMAQ-B1 does not alter BMVEC proliferation, viability, or cytotoxicity.

BMVEC monolayers (P3; 2 days P.C.) were treated with DMAQ-B1 [5 μM] for 6 hours and two different assays were used to determine the effect of DMAQ-B1 on BMVEC proliferation, viability, and cytotoxicity. **(A-C)** Following DMAQ-B1 treatment, BMVEC monolayers from four independent isolations and experiments were stained with DAPI and fluorescence micrographs (n = 20) were used to: **(A)** determine the total number of endothelial cells within each imaged monolayer, which are presented as scatter dot plots overlaid with mean ± S.D. lines plus corresponding p-value reported above; or, **(B,C)** generate cell-cycle histograms to determine the percentage of BMVECs in G1/G0, S, or G2/M phases which are provided as percentages and as 'parts of a whole' in donut charts. **(D,E)** In a separate set of experiments (n = 3), the number of viable ('live') and non-viable ('dead') cells in each BMVEC monolayer was determined by using a

live/dead cell viability and cytotoxicity assay. Doxorubicin – [0.4 μM] for the same time frame – was used as a positive control for cell death and/or cytotoxicity. **(D)** Representative fluorescence micrographs of BMVEC monolayers with live cells (green) and dead cells (red), and insets displaying only the red channel. Scale bars = 0.1 mm. **(E)** Quantification of the percentage of non-viable, or 'dead' cells, within each BMVEC monolayer. Percentages are presented as scatter dot plots overlaid with mean ± S.D. lines and groups with the same symbol are not significant from each other ($p \geq 0.05$).

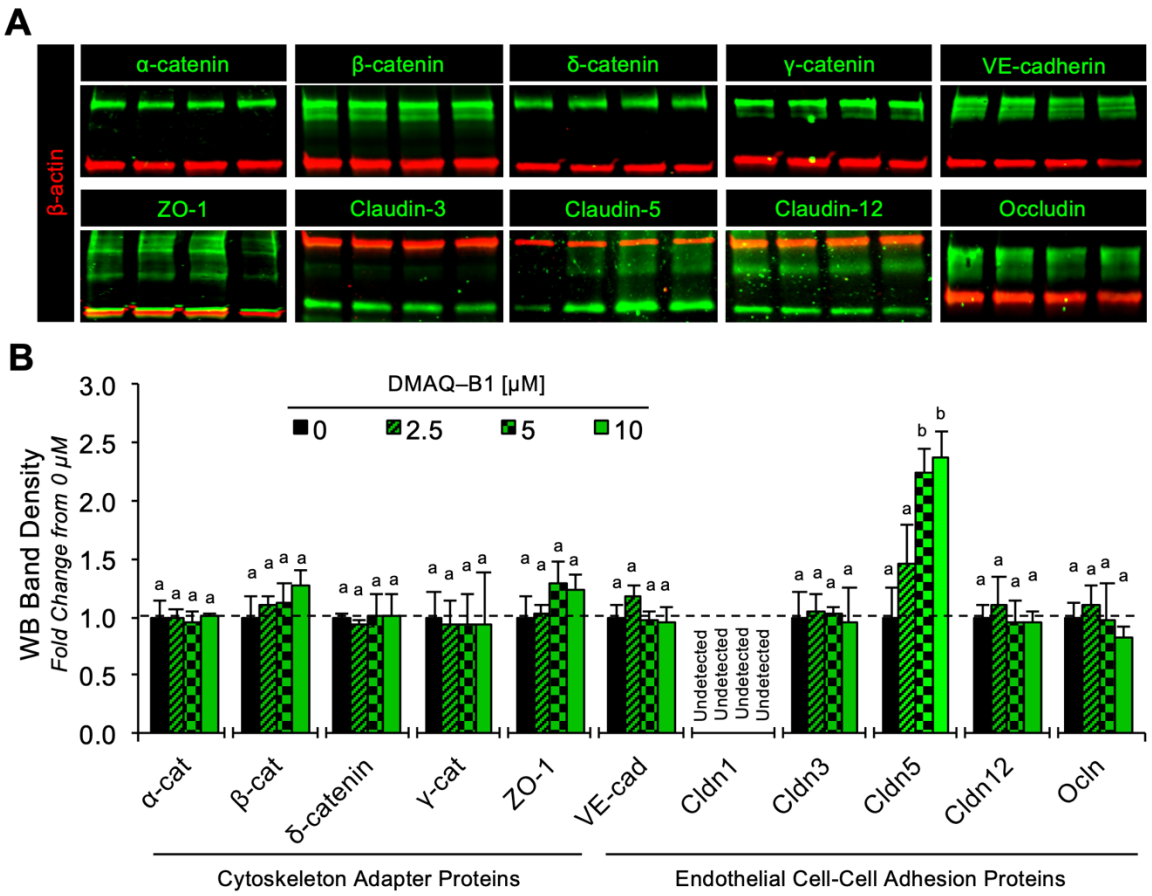

Figure S2. Compared with other common adherens and tight junctional proteins DMAQ-B1 uniquely upregulates CLDN5.

(A-B) BMVECs (P3; 2 days P.C.) were treated with DMAQ-B1 [0, 2.5, 5, or 10 μM] for 6 hours and adherens and tight junction proteins (adherens junction proteins = α-, β-, δ-, γ-catenin and VE-cadherin; tight junction proteins = ZO-1, claudin-1, -3, -5, -12, and occludin) expression levels were determined by two-color near- infrared western blotting for each protein (pseudo-colored green) and β-actin (pseudo-colored red). Representative western blots are provided **(A)**, and densitometry results **(B)** are reported as normalized fold changes compared to vehicle control (0 μM) treated BMVECs. Bar graphs are divided into individual data sets for each protein target and represent the mean ± S.D. Groups with the same symbol within each individual target protein data set are not significant from each other ($p \geq 0.05$).